Ideal Magnetohydrodynamic Spectra of Static and Flowing Plasmas

Tomoya Tatsuno

November, 2001

Abstract

One dimensional linear spectral properties for incompressible ideal magnetohydrodynamic (MHD) plasmas are explored for various situations. The non-triviality of the problem mainly consists of two aspects. One is that the infinite dimensionality of the generator induces continuous spectra. The other is that the generator in case of finite shear flow becomes non-Hermitian (non-selfadjoint), which is not yet solved even in modern mathematics. In addition to the viewpoint of mathematical physics, it is also deeply related to a future energy development, magnetic fusion. For long sustainment of a fusion plasma, at least the linear stability of the equilibrium configuration is necessary. Such stability analyses are accomplished by studying spectra of linearized MHD equations. The spectral analyses are given for point spectra and continuous spectra for Hermitian operators (static equilibria). Also, non-Hermitian problems due to the shear flow in magnetized plasmas are analyzed. Point spectra and continuous spectra related to MHD modes are discussed, respectively, then the resonance between point and continuous spectra is investigated.

The main results are as follows. Firstly, for static magnetized cylindrical plasmas, it is shown that the marginal stability is not described by the local criterion when pressure gradient disappears at the mode resonant surface. Then the beta (ratio of plasma pressure to magnetic pressure) limit may increase for a stair-like pressure profile for a stellarator even with a magnetic hill. For static magnetized slab plasmas with sharp density gradients, the rate of the shear Alfvén continuum damping has been analytically calculated. The result was compared with magnetic fluctuations observed in the pellet injection experiment of Heliotron-E. Next, for a magnetized cylindrical plasma with a rigid plasma flow, the destabilizing mechanism of external kink mode has been clarified when the plasma is surrounded by a resistive wall. Here, the closest position of the resistive wall to the plasma edge for the stabilization of resistive wall mode is proposed. For a magnetized slab plasma with a linear flow and an ambient homogeneous magnetic field, complex behavior originating from the non-Hermiticity introduced by the shear flow has been shown for an interchange instability. All linear instabilities will be suppressed asymptotically by the combined effect of Alfvén wave propagation and linear flow profile with constant velocity shear. Finally, for a slab plasma with a sheared flow, an exact spectral theory for a particular non-Hermitian flow profile has been constructed. The mechanism of Kelvin-Helmholtz instability is clarified, and the eigenvalue problem is shown to be an incomplete approach.

Contents

Chapter 1

Introduction

One dimensional linear spectral properties in single fluid magnetohydrodynamics (MHD) were explored in this thesis by considering plasmas with and without mass flows. Electromagnetic field equations in vacuum are linear systems. However, by introducing magnetofluids in the system, MHD equations become highly nonlinear due to coupling between the electromagnetic and fluid properties of plasmas. In such nonlinear systems, a lot of fascinating collective phenomena will appear; chaotic motions, self-organizations, nonlinear waves, and so on. It should be stressed that even the linear problems, which describe the dynamics of small amplitude motion around an equilibrium state, also contain much more interesting behavior than a simple system of point mass, or that governed by the linear Schrödinger equation. The infinite dimensionality of the generator induces continuous spectra, and moreover, as well as neutral fluids, the generator in case of finite shear flow equilibrium becomes non-Hermitian (non-selfadjoint), which is still an unresolved problem in modern mathematics.

In addition to the above mentioned significance from mathematical physics, spectral analysis of MHD is also related to an energy research for future human lives; it is magnetic fusion. A fundamental requirement for realizing a fusion reactor is to confine a high density and high temperature[1] plasma for sufficiently long time. In order to obtain such a plasma, magnetic confinement systems have been studied, which basically utilize cyclotron motion of charged particle in a toroidal magnetic field. For the sustainment of plasma as a whole, at least the linear stability of the confined plasma is indispensable in the time scale of the plasma dynamics. Studies of such stability properties are accomplished by the spectral analysis.

[1] Actually, the highest temperature was achieved at JT-60U in 1998 at more than five hundred million degrees of centigrade, which is considered to be a few tens times higher than the core temperature of the Sun [13].

The practical magnetic confinement configurations for aiming at fusion reactors are mainly toroidal. Thus, multi-dimensional analyses of MHD stability are required. Multi-dimensional spectral properties for static plasmas are recently discussed in many literatures, e.g. for 2D [56, 150] and 3D [59]. However, the multi-dimensional stability analysis is much more difficult for the magnetized plasmas with shear flows.

In this thesis, one dimensional spectral properties are discussed rather deeply including discrete and continuous spectra in non-Hermitian operators. First, we will treat point spectra in Chap. 3 and continuous spectra in Chap. 4 for Hermitian operators (static plasmas). Although there are still many unresolved problems of MHD stability in static equilibria, recently MHD stability of equilibria with plasma flows are investigated intensively, because of the spontaneous formation of zonal flows from electrostatic turbulence [82]. Another reason is the rotational stabilization of MHD instabilities, e.g. resistive wall modes [122]. Recently, a confinement system which actively uses the flow shear for the improved confinement is even proposed [101]. Thus, the latter half of the thesis is devoted to non-Hermitian problems of sheared plasma flow. Point spectra and continuous spectra are discussed in Chap. 5 and in Chap. 6, respectively. Finally, the resonance between point spectra and continuous spectra is mathematically investigated in Chap. 7.

Let us describe the main results in each chapter with an emphasis on physics. We will firstly introduce the MHD system of equations in Chap. 2. Usually, pre-Maxwell equations for electromagnetic field, which comes from the neglect of the displacement current, are used in ideal MHD. We will discuss in detail why and how the displacement current will be omitted. We will also introduce the spectral method for the analysis of linearized MHD equations. The boundary condition is well known to affect the spectra of differential equations. Here, it is explicitly shown that the 'norm' (or scalar product) also plays an essential role for especially Hermiticity of the operator. The construction of general solution is guaranteed if the generating operator is shown to be Hermitian under any norm. Mathematically, boundary condition and norm are considered in the definition of the Hilbert space in which the formal differential operators are embedded. After all description of the mathematical background, we will summarize the spectra of incompressible MHD equations, on which the rest part of the thesis is based.

In Chap. 3, some unusual properties of the unstable point spectra are investigated [133, 45, 88, 47]. The Mercier (Suydam) criterion for localized interchange modes in stellarators does not predict instability in cases where global modes are unstable. One case is non-resonant pressure driven instabilities with low mode numbers, which become unstable even if the mode resonant surface does not exist inside the plasma column. The other case is interchange instabilities when the pressure gradi-

ent vanishes at the mode resonant surface. If the pressure becomes flat in a narrow region around the mode resonant surface, high mode number instabilities may be eliminated and the beta (ratio of plasma pressure to magnetic pressure) limit at the particular resonant surface increases. Also radial mode structure at nearly marginal beta changes significantly. Resonant unstable modes have a sequence of eigenvalues which converges to the edge of the Alfvén continuum, and the corresponding eigenfunctions tend to localize around the resonant surface. However, non-resonant unstable modes show the global structure and have a step like structure around the resonant surface even in the limit of marginal beta value. Property of the non-resonant mode and transition from the resonant to the non-resonant one are clarified with a cylindrical plasma model for a low shear stellarator with a magnetic hill.

In Chap. 4, Alfvén continuous spectrum is picked up [132]. The MHD wave is studied when two steep density gradient regions exist at surfaces of slab plasma. In such a case, it is shown that the surface Alfvén wave has two branches with nearly the same damping rates, since the steep density gradients are located closely each other. However, for the sharp boundary plasma, the surface Alfvén wave does not damp. As the density profile is relaxed, the damping rates become larger, pass via extremum, and again they become small when the scale length of the density gradients becomes extremely large. These damping rates seem consistent with behavior of magnetic fluctuations observed in the Heliotron-E pellet injection experiment.

As an example of non-Hermitian operators, we will first analyze the effect of the outer resistive conducting wall and the rigid flow of the plasma on external kink instabilities in Chap. 5 [153]. Rigid plasma flow itself will not introduce non-Hermiticity, however, the finite difference of the velocity between the resistive wall and the plasma will be regarded as a kind of discontinuous shear of the flow. We will firstly show the physical mechanism of Kelvin-Helmholtz instability in the neutral fluids, then show the correspondence of external kink mode in the cylindrical plasma with a surrounding resistive wall and a rigid plasma flow to the Kelvin-Helmholtz instability. It is shown that the resistive wall does not only affect to push back the plasma surface wave, but also pull to destabilize the external kink modes.

In Chap. 6, transient and secular behavior of interchange fluctuations is analyzed in an ambient shear flow by invoking Kelvin's method of shearing modes [143, 131]. Because of its non-Hermiticity, complex transient phenomena can occur in a shear flow system. It is shown that, for each mode, the combined effect of shear flow stretching and Alfvén wave propagation overcomes the instability driving force at sufficiently long time, and damps fluctuations of the magnetic flux for all wave numbers. On the other hand, electrostatic perturbations can be destabilized for sufficiently strong interchange drive. The time asymptotic behavior in both cases is

algebraic (non-exponential).

In Chap. 7, we will construct an exact mathematical formulation of neutral fluids which contains the resonance of point spectra (diocotron modes) and continuous ones (entropy waves) [152]. It is easily understood by the finite dimensional spectral theory that the simple resonance among point spectra will cause secular growth of the modes. However, by introducing a new definition of the Hilbert space, it is shown that the resonance, which contains the energy flow from continuous spectra to point ones, may not cause secular behavior of the perturbed quantities. By considering another model, e.g. parallel dynamics, it is also shown in Ref. [84] that such secular behavior will be realized due to the inclusion of the resonance between two different continuous spectra. It means that, even if the system has no unstable eigenvalue [91], growth of the algebraic type is possible, which may cause linear instability of the system. It is pointed out in Appendix C that such kind of resonance (between continuum and point spectra) is also found in the kinetic treatment of the electrostatic oscillations (plasma oscillations).

Chapter 2

Single fluid magnetohydrodynamics

2.1 Magnetohydrodynamic equations

At first, we will introduce non-relativistic, single fluid, ideal magnetohydrodynamic (MHD) equations in SI units. Their derivation and validity are given in many books (see for example, Refs. [1, 3, 10, 19, 23]). Continuity equation and equation of motion are written as

$$\partial_t \rho + \nabla \cdot (\rho \boldsymbol{v}) = 0, \tag{2.1}$$

$$\rho(\partial_t \boldsymbol{v} + \boldsymbol{v} \cdot \nabla \boldsymbol{v}) = \boldsymbol{j} \times \boldsymbol{B} - \nabla p, \tag{2.2}$$

where ρ, $\boldsymbol{v}$, $\boldsymbol{j}$, $\boldsymbol{B}$ and p are fluid mass density, velocity, current density, magnetic field and pressure, respectively. Since the time scale of plasma dynamics is considerably faster than the heat conduction, we may assume that the each fluid element is insulated against heat exchange with its surroundings and locally in thermodynamic equilibrium. Consider the plasma as an ideal gas which follows the thermodynamical equation of state $p = nT$, where n and T denote the particle number density and the temperature in units of energy (J), respectively. Then the time evolution of pressure is shown as,

$$\partial_t p + \boldsymbol{v} \cdot \nabla p + \gamma p \nabla \cdot \boldsymbol{v} = 0, \tag{2.3}$$

where γ denotes the specific heat ratio. It is noted that, when we do not treat the plasma as an ideal gas, e.g. incompressible fluid, we need another equation of state. These set of equations describe the dynamics of the plasma. We do not consider non-ideal kinetic effects including viscosity or resistivity of the plasma in this thesis.

For the magnetic field $\boldsymbol{B}$ and the electric field $\boldsymbol{E}$, we use the Maxwell equations.

One of them is Faraday's law,

$$\nabla \times \boldsymbol{E} = -\partial_t \boldsymbol{B}, \tag{2.4}$$

and another is Ampère's law,

$$\nabla \times \boldsymbol{B} = \mu_0 \boldsymbol{j} \left(+ \frac{1}{c^2} \partial_t \boldsymbol{E} \right), \tag{2.5}$$

where μ_0 is the vacuum permeability, and c is the speed of the light, respectively. Here we note that Maxwell's displacement current (in the bracket) will often be neglected due to the smallness of its correction on MHD dynamics in non-relativistic regime. It is also related to the Galilei invariance of the equations, which we discuss in the next section. Since the plasma is assumed to be a perfectly conducting medium, the plasma resistivity is neglected and Ohm's law becomes

$$\boldsymbol{E} + \boldsymbol{v} \times \boldsymbol{B} = \boldsymbol{0}, \tag{2.6}$$

which merely implies that the electric field will not appear in the rest frame of the plasma.

These equations consist a closed set of ideal MHD: i.e. for fourteen independent variables ρ, $\boldsymbol{v}$, $\boldsymbol{j}$, $\boldsymbol{B}$, p and $\boldsymbol{E}$, we have fourteen independent equations. In MHD equations, the Gauss' law for the electric field is not necessary since each fluid element is considered to be neutralized and charge separation is not treated. It is also noted that the Gauss' law for the magnetic field is considered as an initial condition. If it is initially satisfied, it will be kept forever as we can see by taking the divergence of Eq. (2.4)[1].

For later applications, let us further manipulate the above equations. Substituting Ohm's law (2.6) into Faraday's law (2.4) leads to the magnetic field induction equation

$$\partial_t \boldsymbol{B} - \nabla \times (\boldsymbol{v} \times \boldsymbol{B}) = \boldsymbol{0}, \tag{2.7}$$

which enables us to eliminate the electric field from the governing equations. Moreover, by substituting Ampère's law (2.5) into the equation of motion (2.2), we can eliminate the plasma current from governing equations as

$$\rho(\partial_t \boldsymbol{v} + \boldsymbol{v} \cdot \nabla \boldsymbol{v}) = \frac{1}{\mu_0} (\nabla \times \boldsymbol{B}) \times \boldsymbol{B} - \nabla p, \tag{2.8}$$

where we have neglected the displacement current in Ampère's law.

[1] In two fluid theory, the former Gauss' law can be also understood as an initial condition. It is shown by taking the divergence of Eq. (2.5), denoting the electric charge as $\sigma = e(Zn_\mathrm{i} - n_\mathrm{e})$, and using continuity equations for electrons and ions.

In summary, the single fluid MHD equations are shown as

$$\partial_t \rho + \nabla \cdot (\rho \boldsymbol{v}) = 0, \tag{2.9}$$

$$\partial_t \boldsymbol{v} + \boldsymbol{v} \cdot \nabla \boldsymbol{v} = \frac{1}{\mu_0 \rho} \boldsymbol{B} \cdot \nabla \boldsymbol{B} - \frac{1}{\rho} \nabla \Big(p + \frac{B^2}{2\mu_0} \Big), \tag{2.10}$$

$$\partial_t p + \boldsymbol{v} \cdot \nabla p + \gamma p \nabla \cdot \boldsymbol{v} = 0, \tag{2.11}$$

$$\partial_t \boldsymbol{B} + \boldsymbol{v} \cdot \nabla \boldsymbol{B} = -\boldsymbol{B}(\nabla \cdot \boldsymbol{v}) + \boldsymbol{B} \cdot \nabla \boldsymbol{v}. \tag{2.12}$$

There are eight independent variables ρ, $\boldsymbol{v}$, $\boldsymbol{B}$, and p, and corresponding eight independent evolution equations.

It is noted that the ideal MHD system has no characteristic scale length in general. They have two characteristic velocities, namely the Alfvén velocity and the sound velocity; however, there is no other typical scale. By taking any spatial scale with proportional to the time scale, we can write the equations into normalized form in any size. However, if we introduce a certain non-ideal effect, this property will be broken. For example, the Hall MHD system and the resistive MHD system contain the ion cyclotron frequency and the resistive diffusion time, respectively. They introduce the characteristic spatial scale when combined with the velocity one, namely the ion skin depth and the resistive skin depth.

2.2 Galilei invariance of Maxwell equations

Galilean transformation is defined as a small velocity limit of the Lorentz transformation [5]. It is clear that the non-relativistic fluid equations are Galilei invariant. However, the knowledge of relativity theory [25] is useful to show how the electromagnetic fields will be Galilean transformed. The Lorentz transformations of the electromagnetic fields in Gaussian units are given in Ref. [20]. Transformations of those expressions from Gaussian units to SI units can be done by means of the table in Ref. [17].

Let the inertial system K^* be moving with the relative velocity $\boldsymbol{V}$ with respect to the reference frame K. Then, the electromagnetic fields in the system K^* will be expressed in terms of that in the system K as

$$\boldsymbol{E}^*_\perp = \Gamma(\boldsymbol{E}_\perp + \boldsymbol{V} \times \boldsymbol{B}_\perp) \tag{2.13}$$

$$\boldsymbol{B}^*_\perp = \Gamma\Big(\boldsymbol{B}_\perp - \frac{1}{c^2} \boldsymbol{V} \times \boldsymbol{E}_\perp\Big), \tag{2.14}$$

where $\perp$ denotes the direction perpendicular to the relative velocity $\boldsymbol{V}$ between two systems. The parallel component of the field will not be changed. Here $\Gamma = (1 - V^2/c^2)^{-1/2}$ denotes the Lorentz factor. Charge density σ will be combined with

the current density $\boldsymbol{j}$ to give a four-vector, therefore, they will be transformed as

$$\sigma^* = \Gamma\Big(\sigma - \frac{1}{c^2}\boldsymbol{j}\cdot\boldsymbol{V}\Big) \tag{2.15}$$

$$\boldsymbol{j}^* = \Gamma(\boldsymbol{j} - \sigma\boldsymbol{V}). \tag{2.16}$$

Of course, this combination of the transformation will not change Maxwell equations (including displacement current). With the relativistic equation of motion, they constitute the Lorentz invariant set of governing equations.

If we take the limit $|\boldsymbol{V}/c| \ll 1$, we obtain the following set of Galilean transformation relationships;

$$\boldsymbol{E}^* = \boldsymbol{E} + \boldsymbol{V}\times\boldsymbol{B}, \tag{2.17}$$

$$\boldsymbol{B}^* = \boldsymbol{B}, \tag{2.18}$$

$$\sigma^* = \sigma, \tag{2.19}$$

$$\boldsymbol{j}^* = \boldsymbol{j} - \sigma\boldsymbol{V}. \tag{2.20}$$

In the single fluid MHD equations, however, we have no charge separation which always give $\sigma = 0$ in the non-relativistic limit. Therefore, the current density will not be changed by the Galilean transformation. From these relations, it is readily shown that the pre-Maxwell equations (without displacement current) will not change their forms by the Galilean transformations (2.17)-(2.20). Thus, it is justified that the displacement current is neglected in the *non-relativistic* MHD model.

2.3 Conservation of energy

2.3.1 Nonlinear form

We will review the energy conservation relation and consider the effect of neglecting the displacement current again. Taking the scalar product of Eq. (2.2) with $\boldsymbol{v}$, the left hand side leads to

$$\begin{aligned}\rho\boldsymbol{v}\cdot(\partial_t\boldsymbol{v} + \boldsymbol{v}\cdot\nabla\boldsymbol{v}) &= \rho\partial_t\Big(\frac{1}{2}v^2\Big) + \rho\boldsymbol{v}\cdot(\boldsymbol{v}\cdot\nabla\boldsymbol{v}) + \frac{v^2}{2}[\partial_t\rho + \nabla\cdot(\rho\boldsymbol{v})] \\ &= \partial_t\Big(\frac{1}{2}\rho v^2\Big) + \nabla\cdot\Big(\frac{1}{2}\rho v^2\boldsymbol{v}\Big).\end{aligned} \tag{2.21}$$

Here, in the first equality, we have added the left hand side of continuity equation Eq. (2.1) multiplied by $v^2/2$. In the second equality, we have used the vector relation $\boldsymbol{v}\cdot\nabla\boldsymbol{v} = \nabla(v^2/2) - \boldsymbol{v}\times(\nabla\times\boldsymbol{v})$. The second term of the right hand side of Eq. (2.2) will be evaluated as

$$\boldsymbol{v}\cdot\nabla p = \frac{1}{\gamma-1}\partial_t p + \frac{\gamma}{\gamma-1}\nabla\cdot(p\boldsymbol{v}), \tag{2.22}$$

with the adiabatic equation of state (2.3).

The first term of the right hand side of Eq. (2.2) will be evaluated by means of Maxwell equations. By taking scalar products of Eq. (2.4) with $\boldsymbol{B}/\mu_0$ and Eq. (2.5) with $\epsilon_0\boldsymbol{E}$ and adding each other, we obtain

$$\partial_t\Big[\Big(\frac{\epsilon_0}{2}E^2\Big)+\frac{1}{2\mu_0}B^2\Big]=-\frac{1}{\mu_0}\nabla\cdot(\boldsymbol{E}\times\boldsymbol{B})-\boldsymbol{j}\cdot\boldsymbol{E}, \tag{2.23}$$

where the first term of the right hand side denotes the Poynting vector, and the second term denotes Joule heat. The first term in the right hand side of equation of motion (2.2), therefore, will give

$$\begin{aligned}\boldsymbol{v}\cdot(\boldsymbol{j}\times\boldsymbol{B})&=-\boldsymbol{j}\cdot(\boldsymbol{v}\times\boldsymbol{B})=\boldsymbol{j}\cdot\boldsymbol{E}\\&=-\partial_t\Big[\Big(\frac{\epsilon_0}{2}E^2\Big)+\frac{1}{2\mu_0}B^2\Big]-\frac{1}{\mu_0}\nabla\cdot(\boldsymbol{E}\times\boldsymbol{B}),\end{aligned} \tag{2.24}$$

where we have used Ohm's law (2.6) in the second equality, and Eq. (2.23) in the last.

Adding up equalities (2.21), (2.22), and (2.24), we obtain the following local energy conservation relation:

$$\begin{aligned}&\partial_t\Big[\frac{1}{2}\rho v^2+\frac{1}{\gamma-1}p+\Big(\frac{\epsilon_0}{2}E^2\Big)+\frac{1}{2\mu_0}B^2\Big]\\&\qquad=-\nabla\cdot\Big[\frac{1}{2}\rho v^2\boldsymbol{v}+\frac{1}{\mu_0}\boldsymbol{E}\times\boldsymbol{B}+\frac{\gamma}{\gamma-1}p\boldsymbol{v}\Big],\end{aligned} \tag{2.25}$$

where the round bracket denotes the contribution of the displacement current. It is noted that the neglect of the displacement current leads to the exclusion of electric field energy from the conservation law. This may explain why the governing equations without displacement current are called 'magnetofluid' or 'magnetohydrodynamic' system of equations.

2.3.2 Linearized form and energy principle for static equilibria

Firstly, the physical quantities are divided into the equilibrium and the perturbation parts as

$$\psi=\psi_0+\psi_1, \tag{2.26}$$

where subscripts 0 and 1 denote the equilibrium and perturbed quantities, respectively. Magnetohydrodynamic equilibria are defined by stationary class of solutions of the governing equations given by $\partial_t=0$. These are expressed by the solutions of

equations:

$$\nabla \cdot (\rho_0 \boldsymbol{v}_0) = 0, \tag{2.27}$$

$$\rho_0 \boldsymbol{v}_0 \cdot \nabla \boldsymbol{v}_0 = \boldsymbol{j}_0 \times \boldsymbol{B}_0 - \nabla p_0, \tag{2.28}$$

$$\boldsymbol{v}_0 \cdot \nabla p_0 + \gamma p_0 \nabla \cdot \boldsymbol{v}_0 = \boldsymbol{0}, \tag{2.29}$$

$$\nabla \times (\boldsymbol{v}_0 \times \boldsymbol{B}_0) = \boldsymbol{0}, \tag{2.30}$$

$$\nabla \times \boldsymbol{B}_0 = \mu_0 \boldsymbol{j}_0. \tag{2.31}$$

It is noted that the magnetic field must also satisfy the divergence free condition ($\nabla \cdot \boldsymbol{B}_0 = 0$). In the case of static ($\boldsymbol{v}_0 = \boldsymbol{0}$) plasma, they can be very much simplified and give

$$\boldsymbol{j}_0 \times \boldsymbol{B}_0 = \nabla p_0, \tag{2.32}$$

which reduces to Grad-Shafranov equation in the toroidal axisymmetric case. General analyses of the equilibria with flows become a very profound problems even in the two dimensional case (see e.g. Ref. [31]); however, it is not the subject of this thesis. Later, we will discuss the linear spectral analyses for only simplified one dimensional model equilibria which satisfy the above equations almost trivially.

Suppose that such a static ($\boldsymbol{v}_0 = \boldsymbol{0}$) equilibrium is obtained, and let us introduce the displacement vector $\boldsymbol{\xi}$ for describing perturbations by

$$\partial_t \boldsymbol{\xi}(\boldsymbol{x}, t) = \boldsymbol{v}_1(\boldsymbol{x}, t), \quad \boldsymbol{\xi}(\boldsymbol{x}, 0) = \boldsymbol{0}. \tag{2.33}$$

Then, we can derive the evolution equation for $\boldsymbol{\xi}$ as

$$\begin{aligned} \partial_t^2 \boldsymbol{\xi} &= \mathcal{F}\boldsymbol{\xi} \\ &= \frac{1}{\rho_0}\Big[\nabla(\gamma p_0 \nabla \cdot \boldsymbol{\xi} + \boldsymbol{\xi} \cdot \nabla p_0) \\ &\quad + \frac{1}{\mu_0}(\nabla \times \boldsymbol{B}_0) \times [\nabla \times (\boldsymbol{\xi} \times \boldsymbol{B}_0)] \\ &\quad + \frac{1}{\mu_0}[\nabla \times (\nabla \times (\boldsymbol{\xi} \times \boldsymbol{B}_0))] \times \boldsymbol{B}_0\Big]. \end{aligned} \tag{2.34}$$

After some tedious manipulations, it can be shown that the force operator $\mathcal{F}$ is Hermitian [10, 21] with respect to the scalar product

$$\langle \boldsymbol{\eta} \,|\, \boldsymbol{\xi} \rangle \equiv \frac{1}{2} \int_\Omega \rho_0 \bar{\boldsymbol{\eta}} \cdot \boldsymbol{\xi} \, \mathrm{d}V, \tag{2.35}$$

where the bar denotes the complex conjugate, and Ω denotes the plasma volume surrounded by a perfectly conducting wall. It is noted that this scalar product leads to the energy norm which plays a very important role in the later sections.

Hermiticity of the force operator $\mathcal{F}$ allows us to apply the spectral resolution due to von Neumann theorem [28]. Moreover, we can show the conservation of the perturbed energy

$$W = \frac{1}{2}\int_\Omega \rho_0 \left(|\partial_t \boldsymbol{\xi}|^2 - \bar{\boldsymbol{\xi}} \cdot \mathcal{F}\boldsymbol{\xi}\right) \mathrm{d}V, \tag{2.36}$$

by multiplying $\partial_t \bar{\boldsymbol{\xi}}$ on both sides of Eq. (2.34), $\partial_t \boldsymbol{\xi}$ on that of the complex conjugate of Eq. (2.34), and adding each side of equations. The conservation of W may also be shown with the triangular bracket defined by Eq. (2.35) as

$$\begin{aligned}
\frac{\mathrm{d}W}{\mathrm{d}t} &= \frac{\mathrm{d}}{\mathrm{d}t}\left(\langle \partial_t \boldsymbol{\xi} \,|\, \partial_t \boldsymbol{\xi}\rangle - \langle \boldsymbol{\xi} \,|\, \mathcal{F}\boldsymbol{\xi}\rangle\right) \\
&= \langle \partial_t^2 \boldsymbol{\xi} \,|\, \partial_t \boldsymbol{\xi}\rangle + \langle \partial_t \boldsymbol{\xi} \,|\, \partial_t^2 \boldsymbol{\xi}\rangle - \langle \partial_t \boldsymbol{\xi} \,|\, \mathcal{F}\boldsymbol{\xi}\rangle - \langle \boldsymbol{\xi} \,|\, \mathcal{F}\partial_t \boldsymbol{\xi}\rangle \\
&= \langle \partial_t^2 \boldsymbol{\xi} - \mathcal{F}\boldsymbol{\xi} \,|\, \partial_t \boldsymbol{\xi}\rangle + \langle \partial_t \boldsymbol{\xi} \,|\, \partial_t^2 \boldsymbol{\xi} - \mathcal{F}\boldsymbol{\xi}\rangle \\
&= 0,
\end{aligned} \tag{2.37}$$

where we have used the Hermiticity of the force operator $\mathcal{F}$ in the third equality. Another important consequence of the Hermiticity is the energy principle [40, 96, 10, 21] which describes the necessary and sufficient condition for the MHD stability of static equilibria;

$$\delta W(\boldsymbol{\xi}, \boldsymbol{\xi}) \equiv -\langle \boldsymbol{\xi} \,|\, \mathcal{F}\boldsymbol{\xi}\rangle \geq 0 \quad (\text{for any } \boldsymbol{\xi}) \quad \longleftrightarrow \quad \text{stable}. \tag{2.38}$$

However, it is noted that the Hermiticity does not hold for shear flow plasmas as well as neutral fluids. Thus, these advantages for the linear stability theory will be lost in shear flow systems.

2.4 Magnetohydrodynamic waves in homogeneous plasmas

Let us review the small amplitude waves in the ideal MHD system for homogeneous plasmas. If the plasma is flowing with a homogeneous velocity, it generates just a uniform Doppler shift of wave frequencies. Thus, we consider static plasma here without loss of generality. Consider the equilibrium magnetic field to be in the z direction of the Cartesian coordinates as

$$\boldsymbol{B}_0 = (0, 0, B_{0z}). \tag{2.39}$$

Physical quantities are linearized with respect to perturbations as

$$\psi = \psi_0 + \psi_1, \tag{2.40}$$

where subscripts 0 and 1 denote the equilibrium and perturbed quantities, respectively. Assume $e^{\mathrm{i}(\boldsymbol{k}\cdot\boldsymbol{x}-\omega t)}$ dependence for perturbed fields, where $\boldsymbol{k} = (0, k_\perp, k_\parallel)$ in the Cartesian coordinates. Then, Eqs. (2.9)-(2.12) will be combined and written after linearization as

$$-\mathrm{i}\omega \begin{pmatrix} \rho \\ p \\ v_x \\ v_y \\ v_z \\ B_x \\ B_y \\ B_z \end{pmatrix} = \mathcal{A} \begin{pmatrix} \rho \\ p \\ v_x \\ v_y \\ v_z \\ B_x \\ B_y \\ B_z \end{pmatrix}, \tag{2.41}$$

where the matrix $\mathcal{A}$ is given by

$$\mathcal{A} = \begin{pmatrix} 0 & 0 & 0 & \mathrm{i}k_\perp\rho_0 & \mathrm{i}k_\parallel\rho_0 & 0 & 0 & 0 \\ 0 & 0 & 0 & -\mathrm{i}k_\perp\gamma p_0 & -\mathrm{i}k_\parallel\gamma p_0 & 0 & 0 & 0 \\ 0 & 0 & 0 & 0 & 0 & \frac{\mathrm{i}k_\parallel B_{0z}}{\mu_0\rho_0} & 0 & 0 \\ 0 & -\frac{\mathrm{i}k_\perp}{\rho_0} & 0 & 0 & 0 & 0 & \frac{\mathrm{i}k_\parallel B_{0z}}{\mu_0\rho_0} & -\frac{\mathrm{i}k_\perp B_{0z}}{\mu_0\rho_0} \\ 0 & -\frac{\mathrm{i}k_\parallel}{\rho_0} & 0 & 0 & 0 & 0 & 0 & 0 \\ 0 & 0 & \mathrm{i}k_\parallel B_{0z} & 0 & 0 & 0 & 0 & 0 \\ 0 & 0 & 0 & \mathrm{i}k_\parallel B_{0z} & 0 & 0 & 0 & 0 \\ 0 & 0 & 0 & -\mathrm{i}k_\perp B_{0z} & 0 & 0 & 0 & 0 \end{pmatrix}. \tag{2.42}$$

Here, we have omitted the subscript 1 denoting perturbed quantities for simplicity. The matrix $\mathcal{A}$ may not seem to be anti-Hermitian due to the asymmetry of the components $\mathcal{A}_{14,15}$ and $\mathcal{A}_{41,51}$, however, it can be removable due to the vacancy of the first column. It is also noted that the first and the second row is parallel with each other. Physically it means that the time evolution equations which show the continuity and the adiabatic state are not purely independent. One of the two equations (and thus, one of two physical quantities, namely density or pressure) can be removable from the system by means of the relation

$$p = c_{\mathrm{s}}^2 \rho^\gamma, \tag{2.43}$$

where c_{s} denotes the local phase velocity of the sound wave. After the reduction of the physical quantities, we can transform the matrix $\mathcal{A}$ into anti-Hermitian one by introducing the appropriate normalizations. Reduced 7×7 anti-Hermitian matrix contains the seven orthogonal eigenvectors and the corresponding eigenvalues. All eigenvalues of the anti-Hermitian matrix give pure imaginary numbers, namely real ω's. Thus, there are seven types of small amplitude waves in the ideal MHD system.

Alfvén waves Since the v_x and B_x components can be easily decoupled from others in Eq. (2.41), we can readily obtain the Alfvén wave dispersion relation as

$$\omega = \pm k_\parallel v_{\rm A}, \tag{2.44}$$

where the corresponding eigenvectors are written as

$$(v_x, B_x) = (\mp 1, \sqrt{\mu_0 \rho_0}), \quad \rho = p = v_y = v_z = B_y = B_z = 0. \tag{2.45}$$

Here the phase velocity of the Alfvén wave is introduced as $v_{\rm A} = B_{0z}/\sqrt{\mu_0\rho_0}$. It is noted that, since $\boldsymbol{k} \cdot \boldsymbol{v} = 0$, Alfvén wave shows an incompressible transverse perturbation of the plasma element.

Entropy wave and Magnetosonic waves The remaining five waves satisfy the following eigenvalue problem:

$$-{\rm i}\omega \begin{pmatrix} p \\ v_y \\ v_z \\ B_y \\ B_z \end{pmatrix} = \begin{pmatrix} 0 & -{\rm i}k_\perp \gamma p_0 & -{\rm i}k_\parallel \gamma p_0 & 0 & 0 \\ -\frac{{\rm i}k_\perp}{\rho_0} & 0 & 0 & \frac{{\rm i}k_\parallel B_{0z}}{\mu_0\rho_0} & -\frac{{\rm i}k_\perp B_{0z}}{\mu_0\rho_0} \\ -\frac{{\rm i}k_\parallel}{\rho_0} & 0 & 0 & 0 & 0 \\ 0 & {\rm i}k_\parallel B_{0z} & 0 & 0 & 0 \\ 0 & -{\rm i}k_\perp B_{0z} & 0 & 0 & 0 \end{pmatrix} \begin{pmatrix} p \\ v_y \\ v_z \\ B_y \\ B_z \end{pmatrix}. \tag{2.46}$$

The eigenvalues are obtained by means of the sweeping-out method, which leads to the dispersion relation

$$\omega[\omega^4 - k^2(v_{\rm A}^2 + v_{\rm s}^2)\omega^2 + k^2 k_\parallel^2 v_{\rm A}^2 v_{\rm s}^2] = 0, \tag{2.47}$$

where $v_{\rm s} = \sqrt{\gamma p_0/\rho_0}$ denotes the phase velocity of the sound wave. Thus, it is found that there are an entropy wave which satisfies

$$\omega = 0, \tag{2.48}$$

and magnetosonic waves which satisfy

$$\omega^2 = \frac{1}{2}\left[k^2(v_{\rm A}^2 + v_{\rm s}^2) \pm \sqrt{k^4(v_{\rm A}^2 + v_{\rm s}^2)^2 - 4k^2 k_\parallel^2 v_{\rm A}^2 v_{\rm s}^2}\right]. \tag{2.49}$$

Here, two of the magnetosonic waves (+ sign) denote fast waves and the other two (− sign) denote slow waves, respectively, and $k^2 = k_\perp^2 + k_\parallel^2$.

In the case of $k_\parallel = 0$ in Eq. (2.47), we obtain the following eigenvalues

$$\omega = 0, \tag{2.50}$$

$$\omega = 0, \tag{2.51}$$

$$\omega = \pm k_\perp \sqrt{v_{\rm A}^2 + v_{\rm s}^2}, \tag{2.52}$$

and the corresponding eigenvectors

$$\rho \neq 0,\ p \neq 0,\ B_z \neq 0, \quad v_x = v_y = v_z = B_x = B_y = 0, \tag{2.53}$$

$$v_z \neq 0, B_y \neq 0, \quad \rho = p = v_x = v_y = B_x = B_z = 0, \tag{2.54}$$

$$\rho \neq 0,\ p \neq 0,\ v_y \neq 0,\ B_z \neq 0, \quad v_x = v_z = B_x = B_y = 0, \tag{2.55}$$

respectively. It is noted that the slow waves are degenerated here to give zero eigenvalues. The fast waves are reduced to a couple of oppositely propagating compressional Alfvén waves.

By putting $k_\perp = 0$ in Eq. (2.47), we can decouple two magnetosonic waves and the eigenvalues become

$$\omega = 0, \tag{2.56}$$

$$\omega = \pm k_\parallel v_\mathrm{s}, \tag{2.57}$$

$$\omega = \pm k_\parallel v_\mathrm{A}, \tag{2.58}$$

where the corresponding eigenvectors are shown as

$$B_z \neq 0, \quad \rho = p = v_x = v_y = v_z = B_x = B_y = 0, \tag{2.59}$$

$$\rho \neq 0,\ p \neq 0,\ v_z \neq 0, \quad v_x = v_y = B_x = B_y = B_z = 0, \tag{2.60}$$

$$v_y \neq 0,\ B_y \neq 0, \quad \rho = p = v_x = v_z = B_x = B_z = 0, \tag{2.61}$$

respectively. In this case, the slow waves reduce to the sound waves which propagate with the same mechanism in neutral fluids. It is noted that the sound waves do not carry any electric field ($E_\parallel = 0$) in the description of single fluid MHD equations.[2] The fast waves reduce to the degenerated shear Alfvén waves whose eigenvalues and eigenvectors are same as Eqs. (2.44) and (2.45), since x and y directions are not distinguishable in this situation.

In general, the magnetosonic wave accompanies compression of the plasma, $\boldsymbol{k} \cdot \boldsymbol{v} \neq 0$. This means that these two branches will be excluded from the system by assuming incompressibility on the perturbed velocity. However, as will be discussed in Sec. 4.3, we should be careful for an additional condition on the original MHD system. Actually, incompressibility is consistent with the adiabatic pressure equation only in the limit $\gamma \to \infty$ in the way that

$$\gamma(\nabla \cdot v) \to -\frac{1}{p}\frac{\mathrm{d}p}{\mathrm{d}t}. \tag{2.62}$$

The limit $\gamma \to \infty$ corresponds to the situation that the sound wave will be excluded from the system with $v_\mathrm{s} \to \infty$. For the mathematical discussions, see Ref. [116] and the references therein. The problem encountered in the determination of the pressure for the incompressible fluid is also discussed in Ref. [93].

[2] On the contrary, in the two fluid theory, electric field plays a role in the propagation of ion sound waves.

2.5 Linearized one dimensional reduced magneto-hydrodynamic equations

In this section, we will consider the linearized one dimensional reduced magnetohydrodynamic (RMHD) equations for a low beta static plasma. The first simplification was done by Strauss [123].

2.5.1 Derivation

Here we will simplify the derivation without discussing the detailed physical situations. It is noted that the MHD equilibria are described as

$$\boldsymbol{j}_0 \times \boldsymbol{B}_0 = \nabla p_0, \tag{2.63}$$

where the plasma current density is taken $\boldsymbol{j}_0 = j_0 \boldsymbol{e}_z$ with $\boldsymbol{e}_z$ denoting the unit vector in the z direction, and the strong magnetic field is applied in the z direction.

Under the above situation, we may assume that the perturbation fields come from two dimensional incompressible motions and are written as

$$\boldsymbol{v}_1 = \nabla\phi \times \boldsymbol{e}_z, \quad \boldsymbol{B}_1 = \nabla\psi \times \boldsymbol{e}_z. \tag{2.64}$$

Here, ϕ and ψ denote the stream function and the flux function, respectively. By assuming $\rho = \rho_0 = \text{const}$, the continuity equation becomes a trivial relation. It is noted that the incompressibility is a valuable relation to assume for the simple description of (magneto)fluids, however, such a simplification sometimes spoils physical consistency. Therefore, we have to be careful for introducing additional constraints. The consistency of the incompressibility assumption is discussed in the Appendix A and Sec. 4.3.

Taking the curl of the equation of motion (2.10) gives the vorticity evolution equation;

$$\rho_0 \partial_t (\nabla \times \boldsymbol{v}_1) = \boldsymbol{B}_0 \cdot \nabla \boldsymbol{j}_1 + \boldsymbol{B}_1 \cdot \nabla \boldsymbol{j}_0 - \boldsymbol{j}_0 \cdot \nabla \boldsymbol{B}_1 - \boldsymbol{j}_1 \cdot \nabla \boldsymbol{B}_0. \tag{2.65}$$

Here, the third and the last terms in the right hand side can be omitted when we take the z component of the vorticity equation. It is because the spatial variation of the z component in equilibrium and perturbed magnetic fields are negligible under the application of strong magnetic field B_{0z}. By substituting Eq. (2.64), we can rewrite Eq. (2.65) in terms of stream function ϕ and flux function ψ as

$$\partial_t \Delta\phi = \frac{1}{\mu_0\rho_0} \boldsymbol{B}_0 \cdot \nabla \Delta\psi + \frac{1}{\rho_0} (\nabla j_0 \times \boldsymbol{e}_z) \cdot \nabla\psi, \tag{2.66}$$

where $\Delta = \partial_x^2 + \partial_y^2$ denotes the two dimensional Laplacian operator in the perpendicular direction of the ambient strong magnetic field (z direction).

Let us now formulate the induction equation. It is noted that the right hand side of the induction equation (2.7) can be manipulated to give

$$\begin{aligned} \nabla \times (\boldsymbol{v}_1 \times \boldsymbol{B}_0) &= \nabla \times [(\nabla\phi \times \boldsymbol{e}_z) \times \boldsymbol{B}_0] \\ &= \nabla \times [(\boldsymbol{B}_0 \cdot \nabla\phi)\boldsymbol{e}_z], \end{aligned} \tag{2.67}$$

where we have assumed that the axial equilibrium magnetic field is homogeneous. Moreover, by using the relation $\nabla\psi \times \boldsymbol{e}_z = \nabla \times (\psi \boldsymbol{e}_z)$, Eq. (2.7) leads to

$$\partial_t[\nabla \times (\psi \boldsymbol{e}_z)] = \nabla \times [(\boldsymbol{B}_0 \cdot \nabla\phi)\boldsymbol{e}_z]. \tag{2.68}$$

If we omit the curl operator on both sides of this equation, we obtain

$$\partial_t \psi = \boldsymbol{B}_0 \cdot \nabla\phi, \tag{2.69}$$

where it is shown in Ref. [123] that the arbitrariness of the gradient field may be neglected due to the ambient strong magnetic field B_{0z}.

The somewhat different formalisms which lead to three fields evolution equations are seen for high beta tokamaks [124] or stellarators [125, 27, 32]. The latter will be used in the analysis in Chap. 3.

2.5.2 Hermiticity of Alfvén operator

Here we discuss the formal Hermiticity of the Alfvén operator embedded in the energy norm. First we introduce the matrix representation of the linearized RMHD equations (2.66) and (2.69). Let B, a, and $\tau_{\rm A} = a\sqrt{\mu_0\rho_0}/B$ be the characteristic magnetic field strength, scale length, and time scale, respectively. Then the physical quantities are normalized as

$$\phi \to \frac{a^2}{\tau_{\rm A}}\phi, \quad \psi \to aB\psi, \quad \boldsymbol{B}_0 \to B\boldsymbol{B}, \quad j_0 \to \frac{B}{a\mu_0} j. \tag{2.70}$$

With a state vector $u = {}^T(\Delta\phi, \psi)$, the evolution equations (2.66) and (2.69) are combined and written in the operator matrix form as

$$\partial_t u = \mathcal{A} u, \tag{2.71}$$

where the operator matrix $\mathcal{A}$ is defined as

$$\mathcal{A} = \begin{pmatrix} 0 & \boldsymbol{B} \cdot \nabla\Delta + \nabla j \times \boldsymbol{e}_z \cdot \nabla \\ \boldsymbol{B} \cdot \nabla\Delta^{-1} & 0 \end{pmatrix}, \tag{2.72}$$

and the superscript T denotes the transpose of the matrix.

Magnetic derivative operator Let ϕ and ϕ^* be two scalar functions defined in the plasma domain Ω satisfying the boundary condition

$$\phi = 0, \quad \phi^* = 0 \quad \text{on } \partial\Omega. \tag{2.73}$$

Then, it is readily shown that the magnetic derivative operator $\boldsymbol{B} \cdot \nabla$ is anti-Hermitian with the simple norm

$$(\phi \,|\, \phi^*) = \int \bar{\phi}\phi^* \,\mathrm{d}V \tag{2.74}$$

according to the equality

$$\begin{aligned}(\bar{\phi}\boldsymbol{B}) \cdot \nabla\phi^* &= \nabla \cdot (\bar{\phi}\phi^*\boldsymbol{B}) - [\nabla \cdot (\bar{\phi}\boldsymbol{B})]\phi^* \\ &= \nabla \cdot (\bar{\phi}\phi^*\boldsymbol{B}) - (\boldsymbol{B} \cdot \nabla\bar{\phi})\phi^*,\end{aligned}$$

which comes from Gauss' law $\nabla \cdot \boldsymbol{B} = 0$. It reads as

$$(\phi \,|\, \boldsymbol{B} \cdot \nabla\phi^*) = -(\boldsymbol{B} \cdot \nabla\phi \,|\, \phi^*). \tag{2.75}$$

Norm of state vector u It is clear that Hermiticity condition is not obtained with the simple norm defined by Eq. (2.74) for the state vector u. We will introduce a 'modified norm' here. Let $u = {}^T(\Delta\phi, \psi)$ and $u^* = {}^T(\Delta\phi^*, \psi^*)$ be two state vectors. By taking the metric as

$$\mathcal{M} = \begin{pmatrix} -\Delta^{-1} & 0 \\ 0 & -\Delta \end{pmatrix}, \tag{2.76}$$

we can define the formal scalar product as

$$\langle u \,|\, u^* \rangle \equiv (\Delta\phi \,|\, -\Delta^{-1} \,|\, \Delta\phi^*) + (\psi \,|\, -\Delta \,|\, \psi^*), \tag{2.77}$$

where $(\ |\ )$ denotes the simple norm defined by Eq. (2.74). Physically, it is shown that this metric gives the bilinear form corresponding to perturbed energy as

$$\langle u \,|\, u \rangle = \int \Delta\bar{\phi}(-\Delta^{-1})\Delta\phi + \bar{\psi}(-\Delta)\psi \,\mathrm{d}V \tag{2.78}$$

$$= \int |\nabla\phi|^2 + |\nabla\psi|^2 \,\mathrm{d}V, \tag{2.79}$$

where we have omitted the factor $1/2$ for simplicity.

Anti-Hermiticity of $\mathcal{A}$ with homogeneous $\boldsymbol{B}$ Firstly, we will assume here that the magnetic field is spatially homogeneous. In this case, the current density j is eliminated and $\mathcal{A}$ becomes

$$\mathcal{A}_\mathrm{h} = \begin{pmatrix} 0 & \boldsymbol{B} \cdot \nabla\Delta \\ \boldsymbol{B} \cdot \nabla\Delta^{-1} & 0 \end{pmatrix}. \tag{2.80}$$

By taking two state vectors u and u^* as before, we can show the anti-Hermiticity in the matrix form after careful calculations;

$$\begin{aligned}
\langle u \,|\, \mathcal{A}_{\rm h} u^* \rangle &\equiv \int (\Delta\bar{\phi}, \bar{\psi})\, \mathcal{M}\mathcal{A}_{\rm h} \begin{pmatrix} \Delta\phi^* \\ \psi^* \end{pmatrix} \mathrm{d}V \\
&= -\int (\Delta\bar{\phi}, \bar{\psi}) \begin{pmatrix} 0 & \Delta^{-1}\boldsymbol{B}\cdot\nabla\Delta \\ \Delta\boldsymbol{B}\cdot\nabla\Delta^{-1} & 0 \end{pmatrix} \begin{pmatrix} \Delta\phi^* \\ \psi^* \end{pmatrix} \mathrm{d}V \\
&= -\int (\Delta\bar{\phi})(\Delta^{-1}\boldsymbol{B}\cdot\nabla\Delta\psi^*) + \bar{\psi}(\Delta\boldsymbol{B}\cdot\nabla\phi^*)\,\mathrm{d}V \\
&= -\int (\boldsymbol{B}\cdot\nabla\Delta^{-1}\Delta\bar{\phi})(-\Delta)(\psi^*) + (\boldsymbol{B}\cdot\nabla\Delta\bar{\psi})(-\Delta^{-1})(\Delta\phi^*)\,\mathrm{d}V \\
&= \int {}^T \left\{ \begin{pmatrix} 0 & -\boldsymbol{B}\cdot\nabla\Delta \\ -\boldsymbol{B}\cdot\nabla\Delta^{-1} & 0 \end{pmatrix} \begin{pmatrix} \Delta\bar{\phi} \\ \bar{\psi} \end{pmatrix} \right\} \\
&\quad \times \begin{pmatrix} -\Delta^{-1} & 0 \\ 0 & -\Delta \end{pmatrix} \begin{pmatrix} \Delta\phi^* \\ \psi^* \end{pmatrix} \mathrm{d}V \\
&= -\langle \mathcal{A}_{\rm h} u \,|\, u^* \rangle,
\end{aligned} \tag{2.81}$$

where we have used the Hermiticity and anti-Hermiticity of the operator Δ and $\boldsymbol{B}\cdot\nabla$ with the simple norm, respectively. Since all eigenvalues of the anti-Hermitian operator are pure imaginary, the time evolution of $\mathcal{A}$ will give the simple oscillatory behavior representing the Alfvén wave. However, it is difficult to check the Hermiticity for the operator matrix form in the case of inhomogeneous magnetic field. The reason is the existence of kink instability.

Hermiticity of unified scalar Alfvén operator Let us consider then the unified scalar Alfvén operator. Combining Eqs. (2.66) and (2.69), we can write the unified equation for the vorticity $\Delta\phi$ as

$$\partial_t^2 \Delta\phi = \boldsymbol{B}\cdot\nabla\Delta\boldsymbol{B}\cdot\nabla\Delta^{-1}(\Delta\phi) + (\nabla j \times \boldsymbol{e}_z)\cdot\nabla\boldsymbol{B}\cdot\nabla\Delta^{-1}(\Delta\phi). \tag{2.82}$$

If we just consider the operator

$$\boldsymbol{B}\cdot\nabla\Delta\boldsymbol{B}\cdot\nabla + (\nabla j \times \boldsymbol{e}_z)\cdot\nabla\boldsymbol{B}\cdot\nabla \tag{2.83}$$

for the stream function ϕ with the simple norm (2.74), it seems Hermitian because the second term yields a multiplication operator for the one dimensional MHD equilibrium. However, since Eq. (2.82) is an evolution equation for the vorticity, we should consider the following generator

$$\mathcal{A}_{\rm u} = \boldsymbol{B}\cdot\nabla\Delta\boldsymbol{B}\cdot\nabla\Delta^{-1} + (\nabla j \times \boldsymbol{e}_z)\cdot\nabla\boldsymbol{B}\cdot\nabla\Delta^{-1}, \tag{2.84}$$

for the vorticity, and we should take the energy norm as discussed in the previous paragraph. We just consider the one dimensional MHD equilibrium and take $\boldsymbol{B}$ in

the yz (θz) plane depending only on x (r) in the Cartesian (cylindrical) coordinates. Then, the operator $(\nabla j \times \boldsymbol{e}_z) \cdot \nabla \boldsymbol{B} \cdot \nabla$ reduces to a multiplication operator with wave numbers in y and z (θ and z) directions. By introducing

$$f(\boldsymbol{x}) = (\nabla j \times \boldsymbol{e}_z) \cdot \nabla \boldsymbol{B} \cdot \nabla. \tag{2.85}$$

we may simplify the expression of the generator as

$$\mathcal{A}_{\mathrm{u}} = \boldsymbol{B} \cdot \nabla \Delta \boldsymbol{B} \cdot \nabla \Delta^{-1} + f(\boldsymbol{x}) \Delta^{-1}. \tag{2.86}$$

With the energy norm by following Eq. (2.77) as

$$\langle \Delta\phi \,|\, \Delta\phi^* \rangle = (\Delta\phi \,|\, -\Delta^{-1} \,|\, \Delta\phi^*), \tag{2.87}$$

where $(\ |\ )$ denoting the simple norm (2.74), the Hermiticity of the operator $\mathcal{A}_{\mathrm{u}}$ is shown as

$$\begin{aligned} \langle \Delta\phi \,|\, \mathcal{A}_{\mathrm{u}} \Delta\phi^* \rangle &= -(\Delta\phi \,|\, \Delta^{-1} \boldsymbol{B} \cdot \nabla \Delta \boldsymbol{B} \cdot \nabla \Delta^{-1} \Delta\phi^*) - (\Delta\phi \,|\, \Delta^{-1} f(\boldsymbol{x}) \Delta^{-1} \Delta\phi^*) \\ &= (\boldsymbol{B} \cdot \nabla \Delta \boldsymbol{B} \cdot \nabla \Delta^{-1} \Delta\phi \,|\, -\Delta^{-1} \,|\, \Delta\phi^*) \\ &\quad + (f(\boldsymbol{x}) \Delta^{-1} \Delta\phi \,|\, -\Delta^{-1} \,|\, \Delta\phi^*) \\ &= \langle \mathcal{A}_{\mathrm{u}} \Delta\phi \,|\, \Delta\phi^* \rangle. \end{aligned} \tag{2.88}$$

Here we have used the Hermiticity and anti-Hermiticity of the operators Δ and $\boldsymbol{B} \cdot \nabla$ with the simple norm, respectively.

2.6 Spectra of Alfvén waves in static equilibria

A complete spectral ordinary differential equation for studying MHD perturbations in a static cylindrical plasma (general screw pinch) is derived by Hain and Lüst [76]. Instead of Hain-Lüst equation, we will treat a simpler equation under the assumption of incompressibility. The spectral properties of the Alfvén wave are focused on in the slab geometry (Sec. 2.6.1) and in the cylindrical geometry (Sec. 2.6.2). We will start from the unified scalar Alfvén equation (2.82) without normalization;

$$\partial_t^2 \Delta\phi = \frac{1}{\mu_0 \rho} \boldsymbol{B} \cdot \nabla \Delta \boldsymbol{B} \cdot \nabla \phi + \frac{1}{\rho} (\nabla j \times \boldsymbol{e}_z) \cdot \nabla \boldsymbol{B} \cdot \nabla \phi, \tag{2.89}$$

where we have omitted the subscript 0 denoting the equilibrium quantities. The assumptions which we have imposed here are the *incompressibility*

$$\nabla \cdot \boldsymbol{v} = 0 \tag{2.90}$$

of the ideal MHD plasma instead of the adiabatic equation of state (2.3), and the *one dimensionality* of the *static* equilibrium. The variation of the equilibrium quantities are taken in the x (r) direction of the Cartesian (cylindrical) coordinate system.

2.6.1 Slab geometry — continuous spectra —

The equilibrium magnetic field is assumed as

$$\boldsymbol{B} = (0, B_y(x), B_z), \tag{2.91}$$

with $B_z = \text{const}$ in the Cartesian coordinates. From the homogeneity of the equilibrium quantities in the y and z directions, the wave numbers in both directions become good quantum numbers and we take $\boldsymbol{k} = (0, k_y, k_z)$. Since the generator is Hermitian as shown in Sec. 2.5.2, we may consider the eigenvalue λ of the generator with replacing ∂_t by $-\mathrm{i}\omega$ ($\lambda = -\omega^2$). Then, Eq. (2.89) gives

$$-\omega^2\Big(\frac{\mathrm{d}^2}{\mathrm{d}x^2} - k_y^2\Big)\phi = -\frac{F}{\mu_0\rho}\Big(\frac{\mathrm{d}^2}{\mathrm{d}x^2} - k_y^2\Big)F\phi + \frac{1}{\mu_0\rho}\frac{\mathrm{d}^2F}{\mathrm{d}x^2}F\phi, \tag{2.92}$$

where we have defined $F(x) = \boldsymbol{k}\cdot\boldsymbol{B}(x)$. After some manipulations, we obtain the following eigenmode equation;

$$\frac{\mathrm{d}}{\mathrm{d}x}\Big[(\omega^2 - \omega_{\mathrm{A}}^2)\frac{\mathrm{d}\phi}{\mathrm{d}x}\Big] - k_y^2(\omega^2 - \omega_{\mathrm{A}}^2)\phi = 0, \tag{2.93}$$

where $\omega_{\mathrm{A}}(x) = F(x)/\sqrt{\mu_0\rho}$.

The singular solution of the spectral equation (2.93) can be obtained as follows. Since Eq. (2.93) is a Sturmian equation, it should not have any singular solution except the Alfvén resonance ($\omega^2 - \omega_{\mathrm{A}}^2 = 0$). Suppose that $\omega^2 - \omega_{\mathrm{A}}^2(x)$ has the zero of order h ($\in \mathbb{N}$) at $x = x_{\mathrm{s}}$, i.e.

$$\omega^2 - \omega_{\mathrm{A}}^2(x) = c(x)(x - x_{\mathrm{s}})^h, \tag{2.94}$$

where $c(x)$ is an analytic function with finite value at $x = x_{\mathrm{s}}$. It is noted that, since the coefficient of the highest order derivative vanishes at $x = x_{\mathrm{s}}$, it constitutes a singular point of the spectral equation (2.93). For investigating the behavior of the solution in the vicinity of the singular point x_{s}, we will take the leading order of the Taylor expansion (2.94) and substitute it into Eq. (2.93), which yields

$$\frac{\mathrm{d}^2\phi}{\mathrm{d}x^2} + \frac{h}{x - x_{\mathrm{s}}}\frac{\mathrm{d}\phi}{\mathrm{d}x} + k_y^2\phi = 0. \tag{2.95}$$

It is clearly seen that the point $x = x_{\mathrm{s}}$ is found to be a regular singular point of the spectral equation (2.93). The behavior of the solution around the singular point is investigated by means of the Frobenius expansion [16]. There is a logarithmic singularity in the solution since two solutions of the indicial equation have an integral difference for any $h \in \mathbb{N}$. Therefore, the solution is written in the vicinity of the regular singular point as

$$\phi(x) = a_1 g_1(x) + a_2[g_1(x)\log|x - x_{\mathrm{s}}| + g_2(x)], \tag{2.96}$$

where $g_1(x)$ and $g_2(x)$ are analytic functions with $g_1(x_\mathrm{s}) \neq 0$. The energy norm (2.77) will be applied to the solution (2.96), which now reads as

$$\langle \phi \,|\, \phi \rangle = (\phi \,|\, -\Delta \,|\, \phi). \tag{2.97}$$

Thus, it is found that Eq. (2.96) actually gives a non square integrable solution corresponding to the continuous spectrum.

Furthermore, the fact that Eq. (2.96) is the only solution for the spectral equation (2.93) is shown as follows. Let $\underline{\omega_\mathrm{A}^2}$ ($\overline{\omega_\mathrm{A}^2}$) be the lower (upper) bound value of the Alfvén wave frequency

$$\underline{\omega_\mathrm{A}^2} = \inf_{x\in\Omega} \omega_\mathrm{A}^2 \quad (\overline{\omega_\mathrm{A}^2} = \sup_{x\in\Omega} \omega_\mathrm{A}^2), \tag{2.98}$$

if it exists in the plasma domain Ω. Here we divide the Alfvén singular factor as

$$\omega^2 - \omega_\mathrm{A}^2 = (\omega^2 - \underline{\omega_\mathrm{A}^2}) + (\underline{\omega_\mathrm{A}^2} - \omega_\mathrm{A}^2), \tag{2.99}$$

and multiply $\bar{\phi}$ denoting the complex conjugate of the stream function ϕ. Then, the integrated form of Eq. (2.93) gives

$$(\omega^2 - \underline{\omega_\mathrm{A}^2}) \int_\Omega \left(\left| \frac{\mathrm{d}\phi}{\mathrm{d}x} \right|^2 + k_y^2 |\phi|^2 \right) \mathrm{d}x = - \int_\Omega (\underline{\omega_\mathrm{A}^2} - \omega_\mathrm{A}^2) \left(\left| \frac{\mathrm{d}\phi}{\mathrm{d}x} \right|^2 + k_y^2 |\phi|^2 \right) \mathrm{d}x. \tag{2.100}$$

Since we have taken the lower bound of ω_A^2 by $\underline{\omega_\mathrm{A}^2}$, we see that $(\underline{\omega_\mathrm{A}^2} - \omega_\mathrm{A}^2) \leq 0$ at any position. Moreover, the large round bracket of the right hand side integrand denotes the local kinetic energy; i.e. $|\nabla\phi|^2 \geq 0$. Thus, it is shown that

$$- \int_\Omega (\underline{\omega_\mathrm{A}^2} - \omega_\mathrm{A}^2) \left(\left| \frac{\mathrm{d}\phi}{\mathrm{d}x} \right|^2 + k_y^2 |\phi|^2 \right) \mathrm{d}x \geq 0. \tag{2.101}$$

The right hand side of Eq. (2.100) is shown to be positive and the integral of the left hand side is also positive, therefore

$$\omega^2 \geq \underline{\omega_\mathrm{A}^2} \tag{2.102}$$

must hold. It is concluded that the Alfvén eigenmode equation (2.93) has no eigenvalue lower than the lower bound of the Alfvén continuous spectrum. If we trace the same discussion on the upper bound $\overline{\omega_\mathrm{A}^2}$ of the Alfvén continuum, we can also prove that the Alfvén equation (2.93) does not have any eigenvalue upper than the upper bound of the continuum. Since it is quite natural to assume that $\omega_\mathrm{A}(x)$ is a smooth function of x, we may conclude that the slab Alfvén equation has only Alfvén continuous spectrum. The spectra of Eq. (2.93) is shown as

$$\sigma_\mathrm{c} = \{\omega^2 \,|\, \min_{x\in\Omega} \omega_\mathrm{A}^2 \leq \omega^2 \leq \max_{x\in\Omega} \omega_\mathrm{A}^2\}. \tag{2.103}$$

It is noted here that a meticulous care should be taken for the norm of the system. For example, in determining the square integrability of the solution (2.96), the energy norm (2.97) plays an essential role. If we take a simple norm (|) here, then we find that the solution (2.96) does not give non square integrability since the square of the logarithmic function is integrable around the singular point $x = x_{\rm s}$. Furthermore, if we write the equation for the artificially introduced variable $\phi^\dagger = (\omega^2 - \omega_{\rm A}^2)\phi$ as

$$\frac{\mathrm{d}}{\mathrm{d}x}\Big[(\omega^2 - \omega_{\rm A}^2)\frac{\mathrm{d}}{\mathrm{d}x}\Big(\frac{\phi^\dagger}{\omega^2 - \omega_{\rm A}^2}\Big)\Big] - k_y^2\phi^\dagger = 0, \tag{2.104}$$

in order to eliminate the singularity from the equation, and take the simple norm (|) again, we find that even the Alfvén equation can be rewritten in apparently non-Hermitian form. In this case, we have to take the norm as

$$\langle \phi^\dagger \,|\, \phi^\dagger \rangle = -\int \frac{\bar{\phi}^\dagger}{\omega^2 - \omega_{\rm A}^2}\,\Delta\Big(\frac{\phi^\dagger}{\omega^2 - \omega_{\rm A}^2}\Big)\,\mathrm{d}x, \tag{2.105}$$

which recovers the original Hermiticity of the system and the non square integrability of the solution.

It is also noted that the shear Alfvén continuum is not the only continuum in the MHD system. Their existence is first conjectured by Grad [74]. Firstly, he conjectured four branches of such continuum, however, it is clarified later by Appert *et al.* that the MHD system contains just two [36, 69]; one is the above shear Alfvén wave continuum, and the other is related to the sound wave.

2.6.2 Cylindrical geometry

Here the equilibrium magnetic field is assumed as

$$\boldsymbol{B} = (0, B_\theta(r), B_z), \tag{2.106}$$

with $B_z = \text{const}$ in the cylindrical coordinates. Then, we may take the wave number vector $\boldsymbol{k} = (0, m/r, k_z)$ due to the homogeneity of the equilibrium fields in the θ and z direction. In the same way as in the slab geometry, we replace ∂_t by $-\mathrm{i}\omega$. Then, Eq. (2.89) becomes

$$-\omega^2\Big[\frac{1}{r}\frac{\mathrm{d}}{\mathrm{d}r}\Big(r\frac{\mathrm{d}}{\mathrm{d}r}\Big) - \frac{m^2}{r^2}\Big]\phi = -F\Big[\frac{1}{r}\frac{\mathrm{d}}{\mathrm{d}r}\Big(r\frac{\mathrm{d}}{\mathrm{d}r}\Big) - \frac{m^2}{r^2}\Big]F\phi + \frac{m}{r}\frac{\mathrm{d}j}{\mathrm{d}r}F\phi, \tag{2.107}$$

where $F(r) = \boldsymbol{k}\cdot\boldsymbol{B}(r)$. Since the relation between the current density and $F(r)$ differs from the slab geometry due to the curvature effect, we will obtain the following spectral equation which is different from that in the slab geometry [Eq. (2.93)]

$$\frac{1}{r}\frac{\mathrm{d}}{\mathrm{d}r}\Big[r(\omega^2 - \omega_{\rm A}^2)\frac{\mathrm{d}\phi}{\mathrm{d}r}\Big] - \frac{m^2}{r^2}(\omega^2 - \omega_{\rm A}^2)\phi + \frac{2}{r}\frac{\mathrm{d}F}{\mathrm{d}r}F\phi = 0, \tag{2.108}$$

where, $\omega_{\rm A}(r) = F(r)/\sqrt{\mu_0\rho}$.

Singular solution may be also obtained from the singularity of the equation;

$$\omega^2 = \omega_{\rm A}^2(r) \quad (\exists r \in \Omega). \tag{2.109}$$

It is noted that, however, this singularity is no longer regular due to the existence of the last term of Eq. (2.108). Therefore, we do not have general explicit representation of the singular solution. Moreover, the last term in Eq. (2.108) admits the point spectra which is the essential difference from the case in the slab geometry. Namely, even if ω^2 is less than the lower bound of the Alfvén wave frequency $\underline{\omega_{\rm A}^2} = \inf \omega_{\rm A}^2$,

$$\begin{aligned}
&(\omega^2 - \underline{\omega_{\rm A}^2}) \int_\Omega r \left(\left| \frac{{\rm d}\phi}{{\rm d}r} \right|^2 + \frac{m^2}{r^2} |\phi|^2 \right) {\rm d}r \\
&\quad = - \int_\Omega r(\underline{\omega_{\rm A}^2} - \omega_{\rm A}^2) \left(\left| \frac{{\rm d}\phi}{{\rm d}r} \right|^2 + \frac{m^2}{r^2} |\phi|^2 \right) {\rm d}r + \int_\Omega 2F \frac{{\rm d}F}{{\rm d}r} |\phi|^2 \, {\rm d}r,
\end{aligned} \tag{2.110}$$

can be satisfied for an appropriate F satisfying

$$\int_\Omega 2F \frac{{\rm d}F}{{\rm d}r} |\phi|^2 \, {\rm d}r = - \int_\Omega r(\omega^2 - \omega_{\rm A}^2) \left(\left| \frac{{\rm d}\phi}{{\rm d}r} \right| + \frac{m^2}{r^2} |\phi|^2 \right) {\rm d}r \geq 0 \tag{2.111}$$

for a certain nontrivial eigenfunction ϕ.

Due to Sturm's oscillation theorem [16], if the solution for $\omega^2 = 0$ satisfying the boundary condition only on $r = 0$ have any node in the domain Ω, we will have unstable eigenvalue $\omega^2 < 0$ which also satisfies the boundary condition on the plasma edge. Furthermore, the number of these point spectra are infinite, which has a property to accumulate on the edge of the continuum $\omega^2 = \underline{\omega_{\rm A}^2}$. This property can be used in order to judge the stability of the resonant mode which has the edge of the continuum at $\underline{\omega_{\rm A}^2} = 0$. When the smallest eigenvalue is positive and the mode has no resonant surface inside the plasma, the eigenfunction shows a global stable oscillation, which is called the global Alfvén eigenmode [35].

2.7 Non-Hermiticity in shear flow systems

We will consider the shear flow introduced non-Hermiticity in this section. For simplicity, we will assume that the plasma is not magnetized and consider the electrostatic response. If we neglect the charge separation of the plasma, the plasma behaves in the same way as the neutral fluids. The equilibrium velocity field is assumed as

$$\boldsymbol{v}_0 = (0, v_{0y}(x), 0), \tag{2.112}$$

in the Cartesian coordinates. Then, the vorticity equation (2.66) for two dimensional incompressible motion of the plasma will be rewritten in the form of Rayleigh equation as

$$(\partial_t + v_{0y}\partial_y)\Delta\phi - v_{0y}''\partial_y\phi = 0. \tag{2.113}$$

Here, the prime denotes the derivative with respect to x and $\Delta = \partial_x^2 + \partial_y^2$. Assuming two dimensional perturbation, the wave number in the y direction becomes a good quantum number. Equation (2.113) will be written in the form of the Schrödinger type as

$$\mathrm{i}\partial_t\Delta\phi = k_y v_{0y}\Delta\phi - k_y v_{0y}''\phi. \tag{2.114}$$

We can play with Eq. (2.114) on the definition of the norm. If we regard Eq. (2.114) as a vorticity evolution equation, the generator is written as

$$\mathcal{L} = k_y v_{0y} - k_y v_{0y}''\Delta^{-1}. \tag{2.115}$$

Firstly, let us see how the simple norm for the vorticity field works. Suppose that the norm is defined by the enstrophy bilinear form;

$$\langle\langle \Psi \,|\, \Psi \rangle\rangle = (\Delta\phi \,|\, \Delta\phi) = \int |\Delta\phi|^2 \,\mathrm{d}V, \tag{2.116}$$

where we have defined $\Psi = -\Delta\phi$. Then, the first operator in Eq. (2.115) trivially gives Hermiticity as

$$\begin{aligned}\langle\langle \Psi \,|\, k_y v_{0y}\Psi^* \rangle\rangle &= \int k_y v_{0y}\bar{\Psi}\Psi^* \,\mathrm{d}V \\ &= \langle\langle k_y v_{0y}\Psi \,|\, \Psi^* \rangle\rangle.\end{aligned} \tag{2.117}$$

The second operator gives non-Hermiticity with the enstrophy norm;

$$\begin{aligned}\langle\langle \Psi \,|\, k_y v_{0y}''\Delta^{-1}\Psi^* \rangle\rangle &= \langle\langle \Delta^{-1} k_y v_{0y}''\Psi \,|\, \Psi^* \rangle\rangle \\ &\neq \langle\langle k_y v_{0y}''\Delta^{-1}\Psi \,|\, \Psi^* \rangle\rangle.\end{aligned} \tag{2.118}$$

However, if we define the energy norm as

$$\begin{aligned}\langle \Delta\phi \,|\, \Delta\phi \rangle &= -\int (\Delta\bar{\phi})\,\Delta^{-1}(\Delta\phi)\,\mathrm{d}V \\ &= \int |\nabla\phi|^2 \,\mathrm{d}V,\end{aligned} \tag{2.119}$$

then, the second operator in Eq. (2.115) gives Hermiticity as

$$\begin{aligned}\langle \Psi \,|\, k_y v_{0y}''\Delta^{-1}\Psi^* \rangle &= -\int \bar{\Psi}\,\Delta^{-1}(k_y v_{0y}''\Delta^{-1}\Psi^*)\,\mathrm{d}V \\ &= -\int (k_y v_{0y}''\Delta^{-1}\bar{\Psi})\,\Delta^{-1}\Psi^* \,\mathrm{d}V \\ &= \langle k_y v_{0y}''\Delta^{-1}\Psi \,|\, \Psi^* \rangle,\end{aligned} \tag{2.120}$$

whereas the first operator gives non-Hermiticity;

$$\begin{aligned}\langle \Psi \,|\, k_y v_{0y} \Psi^* \rangle &= -\int \bar{\Psi}\, \Delta^{-1}(k_y v_{0y} \Psi^*)\, \mathrm{d}V \\ &= -\int (k_y v_{0y} \Delta^{-1} \bar{\Psi})\, \Delta\Delta^{-1} \Psi^*\, \mathrm{d}V \\ &= -\int (\Delta k_y v_{0y} \Delta^{-1} \bar{\Psi})\, \Delta^{-1} \Psi^*\, \mathrm{d}V \\ &= \langle \Delta k_y v_{0y} \Delta^{-1} \Psi \,|\, \Psi^* \rangle. \end{aligned} \tag{2.121}$$

Let us then regard Eq. (2.114) as an evolution equation for the stream function ϕ;

$$\mathrm{i}\partial_t \phi = k_y \Delta^{-1} v_{0y} \Delta\phi - k_y \Delta^{-1} v_{0y}'' \phi. \tag{2.122}$$

Then, we can readily show that the first operator is non-Hermitian with the energy norm

$$\begin{aligned}\langle \phi \,|\, \phi \rangle &= -\int \bar{\phi}\, \Delta\phi\, \mathrm{d}V \\ &= \int |\nabla\phi|^2\, \mathrm{d}V, \end{aligned} \tag{2.123}$$

however, it is Hermitian with the enstrophy norm

$$\begin{aligned}\langle\!\langle \phi \,|\, \phi \rangle\!\rangle &= \int \bar{\phi}\, \Delta^2 \phi\, \mathrm{d}V \\ &= \int |\Delta\phi|^2\, \mathrm{d}V. \end{aligned} \tag{2.124}$$

On the other hand, the second operator is Hermitian with the energy norm and non-Hermitian with the enstrophy norm. It is, therefore, concluded that the Hermiticity of the operator does not change by the form of the evolution equation if we take the common norm.

It has been shown that neither energy norm nor enstrophy norm gives Hermiticity of the combined operator for the vorticity evolution equation (2.114). However, when $v_{0y}'' \neq 0$ in the domain, we can make them Hermitian by taking the norm

$$\langle\!\langle\!\langle \phi \,|\, \phi \rangle\!\rangle\!\rangle = \int \frac{1}{|v_{0y}''|} \bar{\phi}\, \phi\, \mathrm{d}V. \tag{2.125}$$

It is straightforwardly shown that the combined operator is Hermitian with the norm (2.125) as

$$\begin{aligned}\langle\!\langle\!\langle \Psi \,|\, k_y (v_{0y} - v_{0y}'' \Delta^{-1}) \Psi^* \rangle\!\rangle\!\rangle &= \int \frac{k_y v_{0y}}{v_{0y}''} \bar{\Psi} \Psi^* - \bar{\Psi}\, k_y \Delta^{-1} \Psi^*\, \mathrm{d}V \\ &= \int \frac{k_y}{v_{0y''}} (v_{0y} - v_{0y}'' \Delta^{-1}) \bar{\Psi}\, \Psi^*\, \mathrm{d}V \\ &= \langle\!\langle\!\langle k_y (v_{0y} - v_{0y}'' \Delta^{-1}) \Psi \,|\, \Psi^* \rangle\!\rangle\!\rangle, \end{aligned} \tag{2.126}$$

where we have assumed that $v''_{0y} > 0$ for simplicity. In this case, the spectra of the generator $k_y(v_{0y} - v''_{0y}\Delta^{-1})$ are real, which yields stability of the system. This fact shows that the shear flow is stable when the system does not contain any inflection point (Rayleigh's inflection point theorem [111, 7]).

Chapter 3

Non-resonant type pressure driven instabilities in stellarators

3.1 Introduction

Although Mercier criterion is useful for investigating the pressure driven instabilities in tokamaks [119] and stellarators [118], it does not predict the limiting conditions in some cases within the ideal MHD model [107, 108]. For deriving the Mercier criterion it is assumed that the unstable mode is radially localized near the mode resonant surface. There is a tendency that the radial mode structure becomes narrow in the vicinity of the mode resonant surface with the increase of mode number. Even the interchange mode with $m = 1/n = 1$ also has a property that the radial mode structure becomes highly localized near the marginal regime [126], where m (n) is a poloidal (toroidal) mode number. This result explains why the Mercier limit correlates with the beta limit due to the interchange instabilities with the low mode numbers [104, 67]. However, this situation changes substantially, when the pressure gradient becomes locally flat at the mode resonant surface [144]. Details of pressure profile effect on the interchange modes will be shown in this paper with use of a cylindrical plasma model for a low shear stellarator with a magnetic hill.

In order to destabilize the interchange mode, the resonant surface is not always necessary. It is reasonable that in a low shear region with a steep pressure gradient, non-resonant modes approximately satisfying the resonant condition are destabilized. First unstable non-resonant resistive modes were shown for a Heliotron-E plasma with a highly peaked pressure profile [86]. Recently ideal non-resonant modes were shown unstable in the central region of Heliotron-E [48], which seems consistent with the $m = 2/n = 1$ mode triggering the sawtooth [156]. It is noted that non-resonant modes usually have global mode structures, which requires numerical

analysis to clarify the property. For studying the details of ideal non-resonant instabilities we use a cylindrical plasma model which saves computational time greatly. Since the non-resonant mode is hard to be excited in a high shear region, our interest is in a low shear stellarator with a magnetic hill.

It is noted that Fu *et al.* [67] studied the relation between the Mercier modes and the low-n modes with a full 3-D stability code for $l = 2$ stellarators. They found that the unstable localized low-n modes are correlated with the Mercier criterion. However, the stability of global-type low-n modes was found to be decorrelated from that of Mercier modes for the case with a fairly large outward magnetic axis shift. It seems that the strong poloidal coupling in the toroidal geometry is essential for this type of unstable mode which may be a tokamak-type ballooning mode. In this paper our interest is in the decorrelation between the low-n pressure driven modes and the Suydam modes in the cylindrical model. Thus both the rotational transform and pressure profiles are important here.

In Sec. 3.2, we derive an eigenmode equation for studying linear interchange modes in stellarators, which is derived from the reduced MHD equations [125]. In Sec. 3.3, we first solve the eigenmode equation analytically in the low shear limit, and discuss about the non-resonant mode. Next we solve the same eigenvalue equation numerically for a finite shear case in Sec. 3.4. Here we show examples to highlight various properties for both the resonant and non-resonant modes. Finally in Sec. 3.5, we summarize the obtained results and give some physical interpretations for the behavior of non-resonant mode.

3.2 Eigenmode equation

For analyzing pressure driven instabilities in stellarators, we use the ideal reduced MHD equations which are derived under the specific ordering for stellarators [125]. Intrinsically, stellarator is a three dimensional configuration which is quite difficult and an open problem as a spectral theory. Here, by averaging in toroidal direction, we can reduce the problem into two dimensions which is the same as axially symmetric systems. This approximation is valid for the modes which have toroidally global structures and when the toroidal mode coupling do not play a major role. The equations are written as

$$\partial_t \psi = \boldsymbol{B} \cdot \nabla \phi, \tag{3.1}$$

$$\rho \frac{\mathrm{d}\Delta\phi}{\mathrm{d}t} = -\boldsymbol{B} \cdot \nabla j_z + \nabla\kappa \times \nabla p \cdot \boldsymbol{e}_z, \tag{3.2}$$

$$\frac{\mathrm{d}p}{\mathrm{d}t} = 0, \tag{3.3}$$

where

$$\boldsymbol{B}\cdot\nabla = B_0\partial_z + \nabla\psi\times\boldsymbol{e}_z\cdot\nabla, \tag{3.4}$$

$$\frac{\mathrm{d}}{\mathrm{d}t} = \partial_t + \nabla\phi\times\boldsymbol{e}_z\cdot\nabla, \tag{3.5}$$

$$\kappa = \frac{2r\cos\theta}{R_0} + \frac{\overline{(\nabla\eta)^2}}{B_0^2}, \tag{3.6}$$

$$j_z = -\Delta A_z, \tag{3.7}$$

$$A_z = \psi + \frac{1}{2B_0}\overline{\nabla\langle\eta\rangle\times\nabla\eta}\cdot\boldsymbol{e}_z. \tag{3.8}$$

Here ψ, ϕ, κ', and η denote the poloidal flux function, the stream function, the averaged curvature of the helical magnetic field, and the magnetic field potential due to helical coils, respectively. Bars denote the averaged equilibrium quantities over a single helical period. The quasi-toroidal coordinates are introduced here whose metrics are written as

$$\mathrm{d}\ell^2 = \mathrm{d}r^2 + r^2\,\mathrm{d}\theta^2 + (R_0 + r\cos\theta)^2\,\mathrm{d}\zeta^2, \tag{3.9}$$

where R_0 denotes the major radius of the torus, r the minor radius, θ and $\zeta = z/R_0$ the poloidal and toroidal angle, respectively. Here the perfectly conducting wall is placed at the plasma boundary, and the boundary conditions are given by $B_r = \partial_\theta\psi = 0$, $v_r = \partial_\theta\phi = 0$, and $p = 0$ at $r = a$.

In the following study, we neglect the toroidal effect in the reduced MHD equations. We also assume that the equilibrium quantities do not depend on the poloidal angle θ. This assumption means that the averaged flux surfaces have circular cross section in the large aspect ratio limit. Then the rotational transform is written as

$$\iota(r) \equiv \frac{R_0}{rB_0}\frac{\mathrm{d}\psi_0}{\mathrm{d}r}, \tag{3.10}$$

where the equilibrium poloidal flux function is given by $\psi_0(r)$. Since the correction due to the diamagnetic current gives higher order contribution in this formulation, the rotational transform includes only the vacuum helical field contribution in this approximation.

For the stability analysis, we use the following normalization for variables,

$$\begin{aligned}
&\psi \to aB_0\psi, && \phi \to \frac{aR_0}{\tau_\mathrm{A}}\phi, && t \to \tau_\mathrm{A}t,\\
&p \to p_0(r=0)p, && r \to ar, && j_z \to \frac{B_0}{\mu_0 a}j_z,\\
&\Delta\phi \to \frac{R_0}{a\tau_\mathrm{A}}\Delta\phi, && A_z \to aB_0A_z,
\end{aligned} \tag{3.11}$$

where $\tau_{\rm A} = R_0\sqrt{\mu_0\rho}/B_0$ denotes the poloidal Alfvén time, a the minor radius of the plasma column, respectively. Then the linearized reduced MHD equations can be written as

$$\gamma(\Delta\phi) = -\frac{n-m\iota}{\gamma}\Delta[(n-m\iota)\,\phi] - \frac{D_{\rm s}}{\gamma}\frac{m^2}{r^2}\phi, \tag{3.12}$$

where $D_{\rm s}$ and the averaged helical curvature κ' are expressed as

$$D_{\rm s} = -\frac{\beta_0}{2\epsilon^2}p'\kappa', \tag{3.13}$$

$$\kappa = \epsilon^2 N\Big(r^2\iota + 2\int r\iota\,{\rm d}r\Big). \tag{3.14}$$

Here $\epsilon \equiv a/R_0$ denotes the inverse aspect ratio, $\beta_0 \equiv 2\mu_0 p_0(r=0)/B_0^2$ the central plasma beta value, and N the toroidal period number of the helical field, respectively. In order to derive Eq. (3.12), all perturbed quantities are assumed to be proportional to $\exp[\gamma t - {\rm i}(m\theta + n\zeta)]$, where m (n) denotes the poloidal (toroidal) mode number. In Eq. (3.13), the prime denotes the derivative with respect to the normalized minor radius r. The perpendicular Laplacian operator in Eq. (3.12) is shown as

$$\Delta = \frac{1}{r}\frac{\rm d}{{\rm d}r}\Big(r\frac{\rm d}{{\rm d}r}\Big) - \frac{m^2}{r^2}. \tag{3.15}$$

Then the ordinary differential equation (3.12) for the stream function ϕ with the mode number (m,n) is written as

$$\begin{aligned}
&\frac{{\rm d}^2\phi}{{\rm d}r^2} + \Big[\frac{1}{r} - \frac{2m\iota'(n-m\iota)}{\gamma^2+(n-m\iota)^2}\Big]\frac{{\rm d}\phi}{{\rm d}r} \\
&- \Big\{\frac{m^2}{r^2} + \frac{1}{\gamma^2+(n-m\iota)^2} \\
&\quad\times\Big[\Big(\frac{m\iota'}{r} + m\iota''\Big)(n-m\iota) - \frac{D_{\rm s}m^2}{r^2}\Big]\Big\}\phi = 0,
\end{aligned} \tag{3.16}$$

which is an eigenmode equation with the eigenvalue γ^2.

For solving Eq. (3.16), the boundary condition at the plasma surface $r = 1$ is $\phi = 0$ under the fixed boundary condition. We also impose the regularity of the solution at $r = 0$. With these boundary conditions, we can set up an eigenvalue problem for the eigenvalue or growth rate γ^2 and the corresponding eigenfunction ϕ.

3.3 Analytic solution of eigenmode equation

3.3.1 Eigenmode properties for shearless case

In this subsection, we assume $\iota' = 0$ for obtaining an analytic solution, then Eq. (3.16) is written as

$$\frac{\mathrm{d}^2\phi}{\mathrm{d}r^2} + \frac{1}{r}\frac{\mathrm{d}\phi}{\mathrm{d}r} + \frac{m^2}{r^2}\Big[\frac{D_\mathrm{s}}{\gamma^2 + (n - m\iota)^2} - 1\Big]\phi = 0. \tag{3.17}$$

For the parabolic pressure profile, $p = p_0(1 - r^2)$, the analytic solution is readily obtained with the transformation $\tilde{r} \equiv \{\widetilde{D}_\mathrm{s} m^2/[\gamma^2 + (n - m\iota)^2]\}^{1/2} r$, where $\widetilde{D}_\mathrm{s} = 4\beta_0 N\iota$. From the solution $u \propto J_m(\tilde{r})$ for the (m, n) mode and the boundary condition $u = 0$ at $r = 1$, the growth rate is written as

$$\gamma^2 = \frac{\widetilde{D}_\mathrm{s} m^2}{Z^2(m, k)} - (n - m\iota)^2, \tag{3.18}$$

where $Z(m, k)$ is the k-th zero point of the m-th order Bessel function of the first kind $J_m(\tilde{r})$.

Although the resonant surface does not exist inside the plasma column, it is seen that the mode satisfying $n \simeq m\iota$ is most unstable and the unstable mode has a global structure without localizing in the radial direction unlike the resonant mode. Further we notice that, when there is no magnetic shear, the radial mode structure, $J_m(Z(m, k)r)$, is not affected by the beta value. We notice from Eq. (3.18) that the more unstable mode has the less node number, and the eigenvalue is discrete with respect to k for the specified (m, n). The generalization of this property will be discussed in the next subsection.

Since the left hand side of Eq. (3.18) is proportional to γ^2 and the right hand side is linear with respect to the plasma beta, the relation (3.18) gives a parabolic line in the (β, γ) plane. Thus a small variation in β_0 from the marginal equilibrium may cause an abrupt increase of growth.

The beta limit for stability is obtained by substituting $\gamma^2 = 0$ into Eq. (3.18), which yields

$$\beta_{0\mathrm{c}} = \frac{Z^2(m, k)(n - m\iota)}{4N\iota m^2}. \tag{3.19}$$

In order to examine the beta limit of the higher harmonic modes with same helicity, we use the transformation of the variables $(m, n) \mapsto l(m, n)$, which yields

$$\beta^l_{0\mathrm{c}} = \frac{Z^2(lm, k)(n - m\iota)}{4N\iota m^2}. \tag{3.20}$$

Since $Z(lm, k) > Z(m, k)$ for $l \geq 2$, the beta limit of the higher harmonic mode, $\beta^l_{0\mathrm{c}}$, is higher than the $l = 1$ case, $\beta_{0\mathrm{c}}$. This is different from the resonant modes with the same helicity, which give the same beta limit given by the Suydam criterion [126].

3.3.2 Radial structure of most unstable mode

In this subsection we show that the more unstable mode has the less node number in radial direction with the specified (m, n). We follow the proof shown by Goedbloed and Sakanaka [72, 10]. By introducing a variable $\xi = \phi/r$, the eigenmode equation (3.16) is written in the Sturmian form as

$$\frac{\mathrm{d}}{\mathrm{d}r}\Big(K\frac{\mathrm{d}\xi}{\mathrm{d}r}\Big) - G\xi = 0, \tag{3.21}$$

where

$$K(\gamma^2; r) = r^3[\gamma^2 + (n - m\iota)^2],$$
$$G(\gamma^2; r) = r\{(m^2 - 1)[\gamma^2 + (n - m\iota)^2] + (3m\iota' r + m\iota'' r^2)(n - m\iota) - D_{\mathrm{s}} m^2\}.$$

Let two solutions corresponding to two neighboring growth rates, $\gamma^2 = \gamma_1^2$ and $\gamma_1^2 + \delta\gamma^2$ be ξ_1 and $\xi_1 + \delta\xi$, respectively, which only satisfy the boundary condition at $r = 0$. When we substitute the first solution ξ_1 corresponding to the parameter γ_1^2 in Eq. (3.21), we obtain

$$\frac{\mathrm{d}}{\mathrm{d}r}\Big(K(\gamma_1^2; r)\frac{\mathrm{d}\xi_1}{\mathrm{d}r}\Big) - G(\gamma_1^2; r)\xi_1 = 0. \tag{3.22}$$

Substituting the second solution into Eq. (3.21) and subtracting Eq. (3.22) leads to

$$\frac{\mathrm{d}}{\mathrm{d}r}\Big(K(\gamma_1^2; r)\frac{\mathrm{d}\delta\xi}{\mathrm{d}r}\Big) - G(\gamma_1^2; r)\delta\xi = -\delta\gamma^2\Big[\frac{\mathrm{d}}{\mathrm{d}r}\Big(\frac{\partial K}{\partial\gamma^2}\Big|_{\gamma_1^2}\frac{\mathrm{d}\xi_1}{\mathrm{d}r}\Big) - \frac{\partial G}{\partial\gamma^2}\Big|_{\gamma_1^2}\xi_1\Big]. \tag{3.23}$$

Assume now that $\xi_1(r_1) = 0$ at $0 < r_1 \leq 1$, which is possible for an unstable case. We make the product of $\delta\xi$ with Eq. (3.22), ξ_1 with Eq. (3.23) and integrate from 0 to r_1. Subtracting both sides leads to

$$K\delta\xi\frac{\mathrm{d}\xi_1}{\mathrm{d}r}\Big|_{r_1} = -\delta\gamma^2\int_0^{r_1}\Big[\frac{\partial K}{\partial\gamma^2}\Big(\frac{\mathrm{d}\xi_1}{\mathrm{d}r}\Big)^2 + \frac{\partial G}{\partial\gamma^2}\xi_1^2\Big]\,\mathrm{d}r, \tag{3.24}$$

after some partial integrations, where we have used the fact that $\delta\xi(0) = 0$, $K(\gamma_1^2; 0) = 0$. Here K, G and their derivatives with respect to γ^2 are all evaluated at $\gamma^2 = \gamma_1^2$. Since $\partial K/\partial\gamma^2 = r^3$ and $\partial G/\partial\gamma^2 = r(m^2 - 1)$, the integrand is positive for $m \geq 1$ at all radial points. Provided that $\delta\gamma^2 > 0$, or $\xi_1 + \delta\xi$ is more unstable than ξ_1, the right hand side of Eq. (3.24) becomes negative. Since K is positive in $(0, 1)$, the radial position of $\xi_1 + \delta\xi = 0$ moves to outer due to the increase of the parameter γ^2. Since K and G are monotonic functions of γ^2 for $m \geq 1$, we can conclude that the radial positions of all zeros move to the outer direction with the increase of the parameter γ^2. If we further impose another boundary condition at $r = 1$, it is confirmed that the eigenvalue is discrete and the more unstable mode has the less node number. In other words, the most unstable mode has no node.

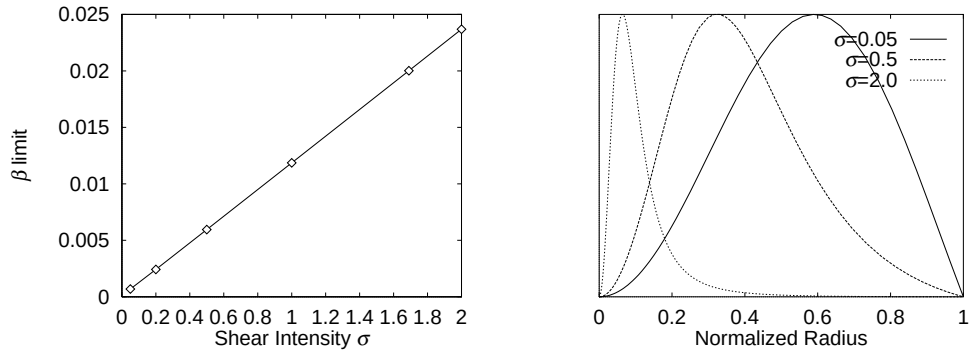

(a) (b)

Figure 3.1: (a) Dependence of the beta limit on the magnetic shear parameter σ for the non-resonant $(2, 1)$ mode. (b) Radial mode structures in cases of $\sigma = 0.05$, 0.5, and 2.0 for the parabolic pressure profile with $\beta_0 = 0.03$.

3.4 Numerical solution of eigenmode equation

3.4.1 Resonant and non-resonant modes for standard pressure profiles

We have solved Eq. (3.16) numerically by the shooting method using the fourth order Runge-Kutta formula. At first we picked up the same eigenvalue problem as shown in section 3.3 in order to validate the numerical code. The obtained growth rates for the $(m, n) = (2, 1)$ mode coincide well with the analytic solution, Eq. (3.18), and the radial mode structures described by the Bessel function $J_2(\tilde{r})$ seems to be unchanged by the variation of β_0.

Next we have investigated the effect of the magnetic shear on the non-resonant modes for the standard parabolic pressure profile. For the assumed rotational transform profile, $\iota = 0.51 + \sigma r^2$, σ is changed from 0.05 to 2.0. The rotational transform profile in the case of $\sigma = 1.69$ is approximately coincides with that in Heliotron-E [48]. When the beta value is fixed, the growth rate of the non-resonant $(2, 1)$ mode is decreased with the increase of the magnetic shear intensity σ. Or the beta limit is increased almost linearly with the increase of σ as shown in Fig. 3.1. The radial mode structure is shifted to the inner region when σ is increased (see Fig. 3.1). This result can be interpreted in the following way. As σ is increased, there are two effects. First, the magnetic shear becomes larger in the outer region compared to the inner region. Second, the outer region is removed further away from the resonance than the inner region. These may account for the mode structure becoming more lo-

calized towards the magnetic axis. Also when β_0 is decreased, since the destabilizing effect due to the plasma pressure gradient becomes weak, the non-resonant mode can be excited only in the inner region. However, since there is no resonant surface, the radial mode structure is not highly localized and still has a global structure. The behavior of the growth rate near the marginal beta value for the non-resonant mode is different from that for the resonant mode as shown in Fig. 3.2. The growth rate of non-resonant mode decreases to zero without the tail at $\beta_0 \simeq \beta_{0c}$, where β_{0c} is the beta limit for the non-resonant $(2,1)$ mode.

Here we study transition from the resonant mode to the non-resonant one. For currentless plasmas in Heliotron-E, MHD equilibria show that the central rotational transform is increased with the increase of beta value. When the vacuum rotational transform at the plasma center is lower than 0.5, the resonant surface for the $(2,1)$ mode exists inside the plasma column. The resonant mode may not be excited due to the low beta value at the initial state. Experimental results show that the $(2,1)$ mode becomes unstable for $\beta_0 \gtrsim 0.7\%$ in the neutral beam heating plasmas, which leads to the occurrence of sawtooth [48]. However, when the ECRH is applied to the central region, the pressure profile becomes more peaked and the $(2,1)$ mode is stabilized. These data could be understood with disappearance of the $\iota = 0.5$ surface according to the increase of the central beta value. Linear stability of the ideal $(2,1)$ mode in the toroidal geometry shows that the resonant mode appears first, then it changes to the non-resonant mode with the increase of β_0. Finally the non-resonant mode becomes stable, when $\iota(0)$ is deviated far from 0.5 [48].

In the cylindrical model we simulate the above situation by changing the central value of the rotational transform artificially. For clarifying the property of the non-resonant mode, we consider a weak shear configuration with the resonant surface for the $(2,1)$ mode at first. Then we exclude the resonant surface of $\iota = 0.5$ by increasing $\iota(0)$. Figure 3.2 shows the numerical results for the pressure profile $p = p_0(1 - r^4)$. White squares correspond to the growth rates for the equilibria with rotational transform profile, $\iota = 0.499 + 0.2r^2$, which has the resonant surface for the $(2,1)$ mode at the normalized radius $r \simeq 0.07$. Black squares correspond to the growth rates for the equilibria with $\iota = 0.501 + 0.2r^2$, which has no resonant surface for the $(2,1)$ mode. The beta limit for the resonant case seems to be 1.14×10^{-3} or less, while for the non-resonant mode it is 5.97×10^{-3}. The difference between these beta limits correlates with the radial mode structure. In the small growth rate regime, when β_0 is decreased, the radial mode structure of the resonant mode becomes more localized. Thus the highly localized mode with an extremely small growth rate is possible as shown in Fig. 3.2. Thus, in the β-γ space the line for the resonant mode case extends to the lower beta region with small growth rates. On the contrary,

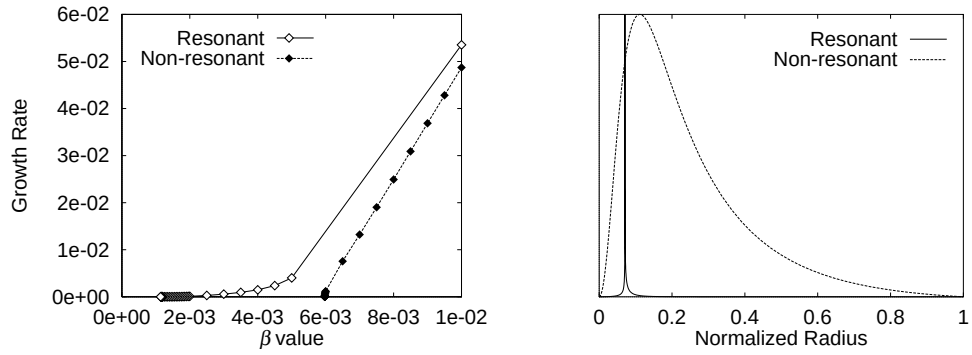

(a) (b)

Figure 3.2: (a) Dependence of the growth rate of $(2,1)$ mode on the central beta value β_0 for $p = p_0(1-r^4)$. Squares denote numerical results. The white ones correspond to the resonant case and the black ones to the non-resonant case. (b) Radial mode structures corresponding to the resonant ($\beta_0 = 1.35 \times 10^{-3}$), and non-resonant case ($\beta_0 = 5.97 \times 10^{-3}$). Here the rotational transform profile is $\iota(r) = 0.499 + 0.2r^2$ for the resonant case and $\iota(r) = 0.501 + 0.2r^2$ for the non-resonant case.

since the non-resonant mode cannot be localized at a particular surface, the growth rate decreases to zero without the tail with the decrease of β_0.

We may apply the Suydam criterion to resonant modes, which can be derived from the indicial equation of Eq. (3.16) at the singular point, or the resonant surface. It is written as

$$\frac{D_{\rm s}}{\iota'^2 r_{\rm s}^2} < \frac{1}{4}, \tag{3.25}$$

for the stability, where $D_{\rm s}$ and ι' are evaluated at the resonant surface, $r = r_{\rm s}$, for the corresponding mode. In the case of Fig. 3.2, the resonant surface of the $(2,1)$ mode is $r_{\rm s} \simeq 0.07$. Here the beta limit obtained from the criterion (3.25) is $\beta_0 \simeq 1.05 \times 10^{-3}$. Generally it is difficult to obtain the beta limit for the resonant mode numerically. One reason is the extension of the growth rate to the low beta side as mentioned above, and the other is the localization of the mode structure in the vicinity of the resonant surface. In Fig. 3.2, however, the difference between the analytic evaluation and the numerical result is less than 10%, and the growth rate at numerically obtained beta limit is 4.49×10^{-11}, which is normalized by poloidal Alfvén time.

It is noted that the global-type mode is shown in Ref. [67] in toroidal stellarators. However, this mode is different from the non-resonant mode shown here, since the poloidal coupling in the toroidal geometry is essential to destabilize the global-type mode.

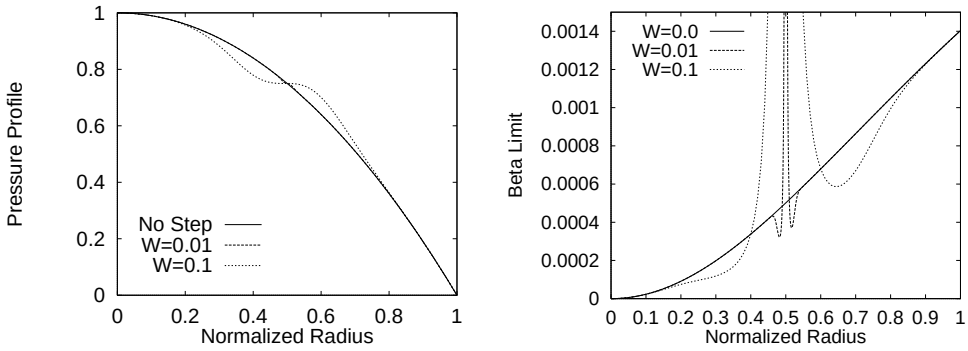

Figure 3.3: Left figure shows the pressure profiles given by Eq. (3.26) for $\lambda = 1$. The effect of pressure flattening is very small for $W = 0.01$. Right figure shows the Suydam critical β corresponding to each W.

3.4.2 Resonant modes for locally flattened pressure profiles at resonant surface

Here we consider equilibria with the resonant surface at $\iota = 0.5$ for the $(2, 1)$ mode in the plasma column, but without the pressure gradient on the resonant surface. In the experimental situation of Heliotron-E there may exist small magnetic islands due to resistive interchange instabilities at the low order resonant surfaces [68, 105], which may be nonlinearly saturated at low fluctuation levels. In such a case the equilibrium may not be violated by the resistive mode, however, the local plasma profile will change and the pressure gradient becomes small near the resonant surface [48, 106]. For this situation the Suydam criterion (3.25) predicts stability at the $\iota = 0.5$ surface.

Here we will show that low m modes can be unstable due to the finite negative pressure gradient at elsewhere other than the resonant surface. For simplicity the pressure profile is assumed as

$$p = 1 - r^2 + \lambda(r - r_{\rm s}) \exp\Big[-\frac{1}{2}\Big(\frac{r - r_{\rm s}}{W}\Big)^2\Big], \tag{3.26}$$

where $r_{\rm s}$ is the position of the mode resonant surface, and the choice $\lambda = 2r_{\rm s}$ makes p' vanish at $r = r_{\rm s}$. The width of the flat region is controlled with the parameter W. Several pressure profiles given by Eq. (3.26) and corresponding critical β_0 values evaluated by Suydam criterion (3.25) are shown in Fig. 3.3. We assume $\iota = 0.45 + 0.2r^2$ and consider the $(2, 1)$ mode again. The resonant surface exists at $r_{\rm s} = 0.5$ where the pressure gradient vanishes. We can see that the pressure flattening region is very narrow in $W = 0.01$ case, which connects with the steepness of the pressure gradient near resonant surface, therefore, the destabilizing effect around resonant surface is considerably large. However, we consider that the high

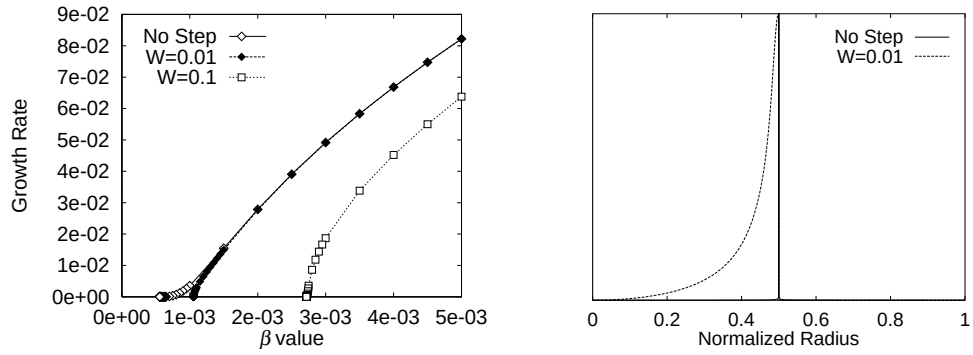

(a) (b)

Figure 3.4: (a) Dependence of the growth rate of $(2,1)$ mode on the central beta value β_0 for $W = 0$, 0.01 and 0.1. (b) Radial mode structures for $W = 0$ ($\beta_0 = 5.62\times10^{-4}$), and $W = 0.01$ ($\beta_0 = 1.05 \times 10^{-3}$). The radial mode structures for $W = 0.1$ are shown in Fig. 3.5.

(m, n) modes which has resonant surface close to $\iota \simeq 0.5$ might be stabilized by non-MHD effect.

For three cases with $W = 0$, 0.01, and 0.1 shown in Fig. 3.3, growth rates of the $(2, 1)$ mode are shown as a function of β_0 in Fig. 3.4(a). Although the highly localized mode structure is observed in the case of $W = 0$, it is not localized even in the case of $W = 0.01$, and the beta limit is increased with a factor of 2. Furthermore, in Fig. 3.4(a) the growth rate decreases to zero without the tail near the beta limit for $W = 0.01$, while the growth rate in the higher beta regime is not affected. The growth rates and the radial mode structures in the case of $W = 0.1$ are shown separately in Fig. 3.5, where both the first growing mode with the maximum growth rate and the second growing mode with the next growth rate are shown. In Figs. 3.4(b) and 3.5(b) we see that the radial mode structures are quite different from the case with $W = 0$. They are restricted in one side of the mode resonant surface, and change sharply at the mode resonant surface in the case of $W \neq 0$. In order to understand the role of the second growing mode, it is interesting to study nonlinear behavior of the $(2, 1)$ mode for an equilibrium with a flat pressure region in the neighborhood of resonant surface. It is considered that, since the average magnetic shear is weak in the inner side of the resonant surface, the first growing mode is restricted to the region $[0, r_s]$ in the case of $W = 0.01$, whereas in the case of $W = 0.1$, it is restricted to the outer region since the average pressure gradient seems larger in the outer side. It is noted that the beta limit of the $W = 0.01$ case, $\beta_{0c} = 1.0 \times 10^{-3}$, is lower than that of the $W = 0.1$ case, $\beta_{0c} = 2.7 \times 10^{-3}$. In both

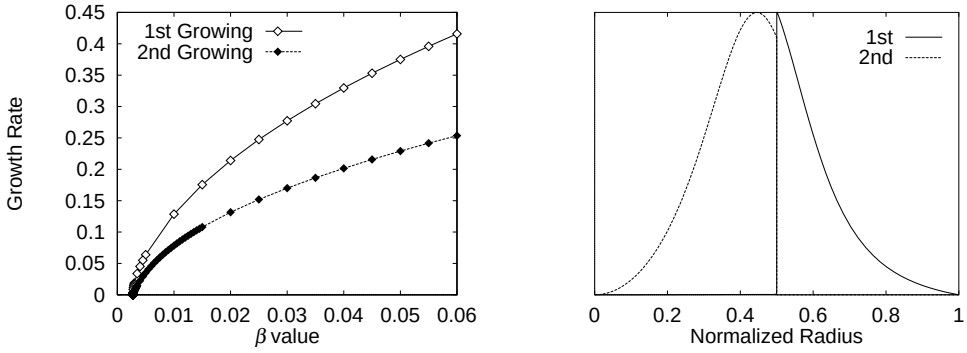

(a) (b)

Figure 3.5: (a) Dependence of the growth rate of $(2,1)$ mode on the central beta value β_0 for $W = 0.1$. (b) Radial mode structure of the first growing mode ($\beta_0 = 2.72 \times 10^{-3}$) and that of the second growing mode ($\beta_0 = 2.76 \times 10^{-3}$). It is noted that the growth rates of the first growing mode are the same as those in Fig. 3.4(a).

cases the second growing mode appears in the opposite region to the first growing mode.

To investigate why the steep mode structure appears at the resonant surface, we expand the coefficients in Eq. (3.16) in the neighborhood of the mode resonant surface $r = r_{\rm s}$. Since the rotational transform is expanded as $\iota(r) \approx \iota(r_{\rm s}) + \iota'(r_{\rm s})(r - r_{\rm s}) + \cdots$, the resonant denominator is expressed as

$$n - m\iota \approx -m\iota'(r_{\rm s})(r - r_{\rm s}) + \cdots. \tag{3.27}$$

Since the pressure becomes flat at the mode resonant surface, $p'(r_{\rm s})$ becomes zero, but $p'(r)$ is still negative in both sides of the mode resonant surface. Therefore p'' is also zero at $r = r_{\rm s}$, thus p' is expanded in the neighborhood of the mode resonant surface as

$$p' \approx \frac{p'''(r_{\rm s})}{2}(r - r_{\rm s})^2 + \cdots, \tag{3.28}$$

where $p'''(r_{\rm s}) < 0$. Substituting the leading terms of Eqs. (3.27) and (3.28) into Eq. (3.16) yields

$$\begin{aligned} &\frac{{\rm d}^2\phi}{{\rm d}r^2} + \Big[\frac{1}{r} + \frac{2m^2\iota'^2(r - r_{\rm s})}{\gamma^2 + m^2\iota'^2(r - r_{\rm s})^2}\Big]\frac{{\rm d}\phi}{{\rm d}r} \\ &- \Big[\frac{m^2}{r^2} - \frac{m\iota'(r - r_{\rm s})}{\gamma^2 + m^2\iota'^2(r - r_{\rm s})^2}\Big(\frac{m\iota'}{r} + m\iota''\Big) \\ &\quad + \frac{m^2\beta_0 N p'''(4r_{\rm s}\iota + r_{\rm s}^2\iota')}{4r_{\rm s}^2[\gamma^2 + m^2\iota'^2(r - r_{\rm s})^2]}(r - r_{\rm s})^2\Big]\phi = 0. \end{aligned} \tag{3.29}$$

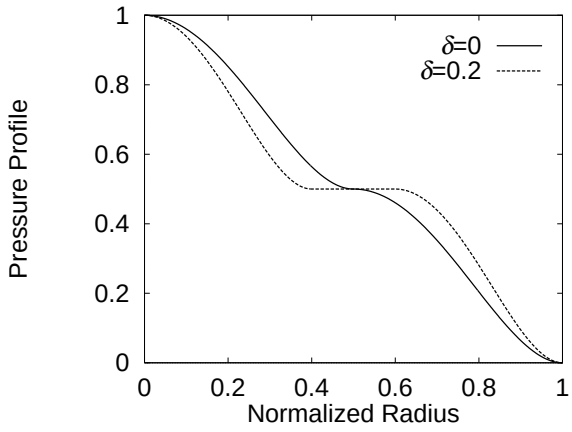

Figure 3.6: Pressure profiles with the locally flat regions around the mode resonant surface. The solid line corresponds to Eq. (3.30) and the broken line to Eq. (3.31).

As seen here, the effect of the pressure near the resonant surface appears in the higher order with respect to $(r - r_{\rm s})$. Thus the pressure is negligible and does not affect the steep mode structure.

In order to confirm this situation, we have calculated the radial mode structure of nearly marginal mode for the following pressure profiles numerically. One is

$$p = \begin{cases} \dfrac{1}{2}(1-4r^2)^2 + 0.5 & (r < 0.5), \\ \dfrac{1}{2}[1-4(r-0.5)^2]^2 & (r > 0.5), \end{cases} \tag{3.30}$$

and the other is

$$p = \begin{cases} \dfrac{1}{2}\Big(1 - \dfrac{25}{4}r^2\Big)^2 + 0.5 & (r < 0.4), \\ 0.5 & (0.4 < r < 0.6), \\ \dfrac{1}{2}\Big[1 - \dfrac{25}{4}(r-0.5)^2\Big]^2 & (r > 0.6). \end{cases} \tag{3.31}$$

The latter pressure profile contains a completely flat region whose width is noted as δ in $[0.4, 0.6]$ in order to eliminate the effect of the pressure gradient. Those profiles are shown in Fig. 3.6. By assuming the same rotational transform profile as the previous case in Figs. 3.4 and 3.5, the obtained mode structures are shown in Fig. 3.7. The reason why the mode structure of the first growing mode is restricted in the inner region is that, since the average pressure gradient is equal in both sides of $r = 0.5$, the interchange mode is considered to be excited in the weaker shear region. It is interesting that the mode structure with the sharp decrease at $r = r_{\rm s}$ is observed even though the pressure is completely flat in a region with a finite width

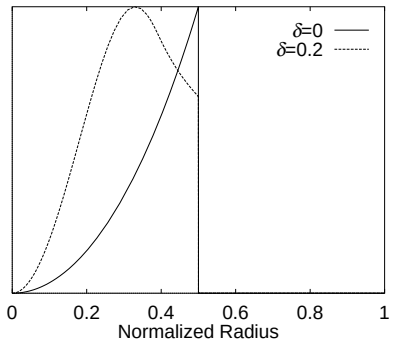

(a)

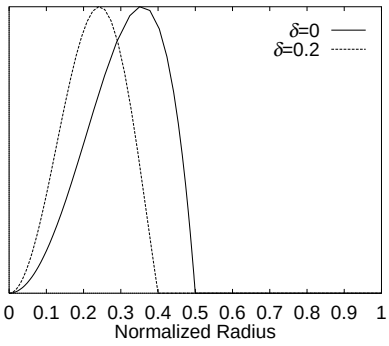

(b)

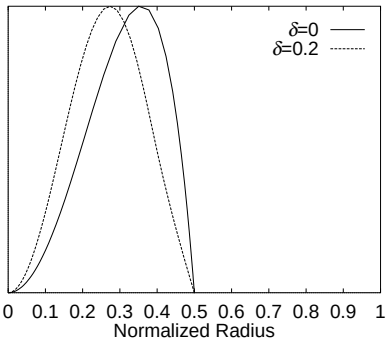

(c)

Figure 3.7: (a) Radial mode structures of $(2, 1)$ mode for the pressure profile corresponding to Eq. (3.30) ($\delta = 0$ curves) and to Eq. (3.31) ($\delta = 0.2$ curves). Both lines show the radial mode structure of each first growing mode. Here all perturbed functions are shown; (a) $\tilde{\phi}$, (b) $\tilde{p}$, (c) $\tilde{\psi}$.

around the mode resonant surface. This assures our conjecture that the locally steep profile of the mode structure such as in Figs. 3.5 and 3.7 is caused only by the profile of the magnetic shear, not by the pressure profile any more. We note that a *non-resonant feature* is seen in the radial mode structure for the second growing mode in Fig. 3.5(b) and the first growing mode for the second pressure profile (3.31) in Fig. 3.7(b), i.e. the peak is shifted from the resonant surface. This clearly shows that the unstable mode is driven by the negative pressure gradient at elsewhere other than the resonant surface.

The appearance of the sharp decrease to zero at the resonant surface in the radial mode structure or $u(r)$ is considered as follows. Consider a resonant layer satisfying $|r - r_{\rm s}| = |x| \sim \epsilon$. Since our interest is in the small growth rate limit, $\gamma \sim \epsilon$ is also assumed. Under these assumptions, if we assume $p' \simeq 0$ in the resonant layer, the

second term in Eq. (3.21) becomes negligible and

$$\frac{\mathrm{d}}{\mathrm{d}r}\Big(K(\gamma^2;r)\frac{\mathrm{d}\xi}{\mathrm{d}r}\Big) = 0 \tag{3.32}$$

decide the behavior of eigenfunction $\xi(r)$ in the resonant layer. It is noted that Eq. (3.32) is exactly same as that given by Rosenbluth, Dagazian and Rutherford for the $m = 1$ internal kink mode in the cylindrical tokamak [113]. They gave the solution

$$\xi = \frac{1}{2}\xi_a\Big[1 - \frac{2}{\pi}\arctan\Big(\Big|\frac{m\iota'}{\gamma}\Big|x\Big)\Big], \tag{3.33}$$

for the boundary conditions $\xi \to \xi_a$ as $x \to -\infty$ and $\xi \to 0$ as $x \to \infty$. Since $m\iota'/\gamma \sim O(\epsilon^{-1})$, the eigenfunction ξ has the largest gradient at $r = r_\mathrm{s}$ and has a step function structure near the resonant surface. Further, since $u \simeq r_\mathrm{s}\xi$ in the neighborhood of the resonant layer, this type of solution may explain the behavior of the sharp decrease to zero of the eigenfunction with the largest growth rate near the resonant surface $r = r_\mathrm{s}$ for $\gamma \to 0$.

3.4.3 Behavior of non-resonant type mode

We will show that the non-resonant type mode is also excited even if pressure profiles do not have exact zero gradient at the resonant surface. For small and nonzero values of p' at $r = r_\mathrm{s}$, we discuss about transition from the resonant mode to the non-resonant type one. We assume $p = p_0(1 - r^2)^\alpha$, where α is changed from 4 to 14 (see Fig. 3.8). The profile of the rotational transform is fixed as $\iota = 0.4 + 0.2r^2$, where the resonant surface for the $(2, 1)$ mode exists at $r_\mathrm{s} = \sqrt{2}/2$. Figure 3.8 shows that the mode structure gradually changes from the resonant one to the non-resonant type one. Particularly the $\alpha = 14$ case shows that the peak of the radial mode structure exists at the position different from the resonant surface, which is considered as the non-resonant feature. It does have a step function structure instead of a peak at the mode resonant surface for the nearly marginal beta value. In other words, the driving force to the instability comes from the largest pressure gradient region different from the resonant surface. From the sharp decrease of ϕ to zero at the resonant surface in the $\alpha = 14$ case, it is considered that the pressure has almost no effect on the mode structure at the resonant surface, since p' and p'' are negligibly small. In the $\alpha = 10$ case, the mode structure has the maximum value at the resonant surface; however, there exists another broad peak in the inner side of the resonant surface. Also the growth rate vanishes without the tail near the beta limit (see Fig. 3.8(b)). In the $\alpha = 8$ case, the situation is more ambiguous. The mode structure has a maximum value at the resonant surface and has no other peak. However, the dependence of γ on β near the beta limit is different from the standard

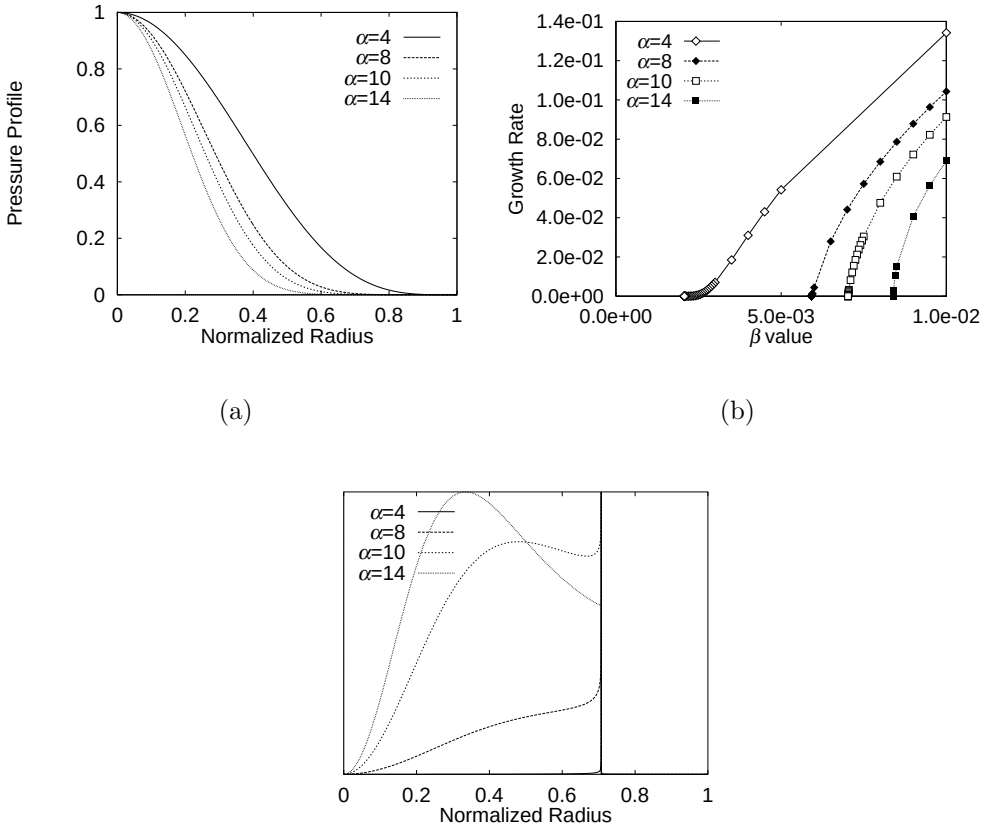

Figure 3.8: (a) Pressure profiles given by $p = p_0(1 - r^2)^\alpha$ for $\alpha = 4$, 8, 10, and 14. (b) Dependence of the growth rate on the central beta value β_0 for different α. (c) Radial mode structures near the beta limit for different α. The height of the mode structure is normalized with its own maximum value.

resonant mode. Thus the case with $\alpha = 8$ or 10 seems to have a mixed property between the resonant and non-resonant type mode. For the $\alpha = 4$ case, the clear feature of the resonant mode is seen, i.e. the small growth rate regime is extended to the low beta side in the β-γ space, and the nearly marginal mode structure is highly localized at the resonant surface. For comparison, the beta limit given by the Suydam criterion is calculated for each equilibrium in Fig. 3.8. Table 3.1 shows both the beta limit obtained from Suydam criterion (3.25) at the resonant surface of the $(2, 1)$ mode, $\beta_{\rm S}$, and the one shown in Fig. 3.8(b), $\beta_{\rm n}$. From Table 3.1, in cases of $\alpha \geq 8$, the non-resonant type $(2, 1)$ modes are unstable even when the central beta value is smaller than the Suydam limit. The beta limit in case of $\alpha = 4$ almost coincides with the Suydam limit since the radial mode structure is highly localized around the resonant surface.

α	$\beta_{\rm S}$	$\beta_{\rm n}$	p'
4	1.91×10^{-3}	2.07×10^{-3}	-0.707
8	1.53×10^{-2}	5.92×10^{-3}	-8.84×10^{-2}
10	4.90×10^{-2}	7.02×10^{-3}	-2.76×10^{-2}
14	0.560	8.39×10^{-3}	-2.41×10^{-3}

Table 3.1: Comparison between the marginal beta values from Suydam criterion, $\beta_{\rm S}$, and the ones shown in Fig. 3.8(b), $\beta_{\rm n}$. The equilibrium pressure gradient at the resonant surface is also shown. The pressure is normalized by the central value and the radial variable by the minor radius of the plasma column.

Finally, we considered a reversed shear profile, which will be realized in the high beta equilibrium of toroidal stellarator. Here we assume a cylindrical plasma with $\iota' < 0$ in the central region and $\iota' > 0$ in the outer region. We also assume the following profile of the rotational transform,

$$\iota = \iota(0) + \sigma r^2 - \lambda \exp\Big[-\frac{1}{2}\Big(\frac{r - r_{\rm c}}{W}\Big)^2\Big], \tag{3.34}$$

where σ is the previously defined shear parameter, $r_{\rm c}$ is the parameter for the minimum point of $\iota(r)$, and W denotes the characteristic width of non-monotonic region of $\iota(r)$. Here $\sigma = 0.2$, $r_{\rm c} = 0.5$, $W = 0.15$, and $\lambda = 0.2$ are chosen as an example. The pressure profile is again assumed to be parabolic, $p = p_0(1-r^2)$. We have calculated two cases which are parameterized as follows. One is the double resonant case, $\iota(0) = 0.6$, in which the radial positions of two resonant surfaces for the $(2, 1)$ mode are at 0.35 and 0.59, where the beta limits predicted from the Suydam criterion (3.25) are 6.61×10^{-3} and 8.25×10^{-3}, respectively. The other is the non-resonant case, $\iota(0) = 0.66$, in which the rotational transform has its minimum value 0.508 at $r = 0.478$. The both profiles of the rotational transform and the nearly marginal mode structures are shown in Fig. 3.9.

In the double resonant case the radial mode structure is localized dominantly at the inner resonant surface. The reason is that, since the beta limit from the Suydam criterion is lower at the inner resonant surface than that at the outer one, the pressure driven mode is more unstable at the inner resonant surface. In the non-resonant case the radial mode structure is restricted near the minimum point of the rotational transform and the beta limit is much lower than that in the double resonant case. It can be interpreted that, since the pressure driven mode is excited near the minimum point of ι in the non-resonant case, which is fairly close to $\iota = 0.5$, the stabilizing magnetic shear is very weak there. On the other hand, the resonant mode is localized at the resonant surface where the magnetic shear is relatively strong in the double resonant case, thus the beta limit becomes higher than that in

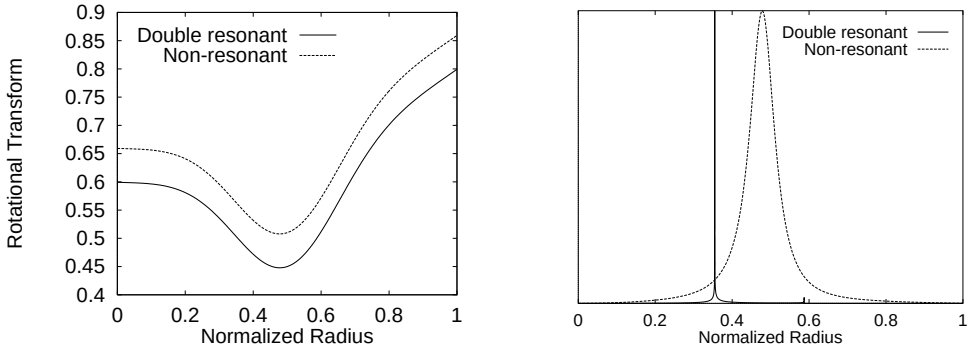

(a) (b)

Figure 3.9: (a) Profiles of the rotational transform for $\iota(0) = 0.6$, $\sigma = 0.2$, $r_c = 0.5$, $W = 0.15$, $\lambda = 0.2$ (double resonance) and $\iota(0) = 0.66$, $\sigma = 0.2$, $r_c = 0.5$, $W = 0.15$, $\lambda = 0.2$ (no resonance). (b) Radial mode structure of the $(2, 1)$ mode near the beta limit; $\beta_0 = 7.79 \times 10^{-3}$ for double resonant case, or $\beta_0 = 4.87 \times 10^{-4}$ for non-resonant case.

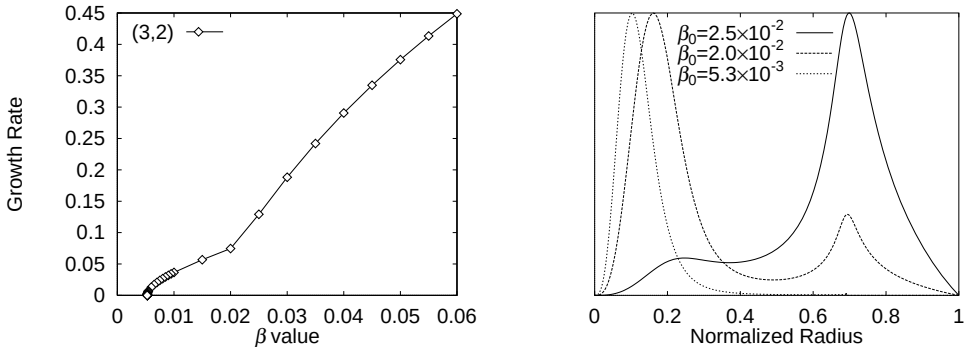

(a) (b)

Figure 3.10: (a) Growth rate as a function of β_0. (b) Radial mode structures for $\beta_0 = 2.5 \times 10^{-2}$, 2.0×10^{-2}, 5.3×10^{-3}. The beta limit is estimated as 5.27×10^{-3}, which is lower than the Suydam limit at the resonant surface of the $(3, 2)$ mode.

the non-resonant case.

We have also calculated the $(3, 2)$ mode in the non-resonant case with the rotational transform shown by dashed line in Fig. 3.9(a). This mode has one resonant surface at $r_s = 0.691$, where the beta limit from the Suydam criterion is $\beta_S = 8.28 \times 10^{-3}$. The numerical results are shown in Fig. 3.10. Figure 3.10(a) shows a transition in the growth rate depending on β_0, which occurs at $\beta_0 \sim 0.02$.

This transition is understood from the mode structures shown in Fig. 3.10(b). The maximum point of the unstable mode structure is placed at the resonant surface for $\beta_0 \gtrsim 0.025$. However, it moves to the inner weak shear region for the non-resonant type mode with $\beta_0 \lesssim 0.02$. This type of mode structure has a small peak at r_s near the beta limit, however, it does not decrease to zero at the resonant surface as shown previously, since the pressure gradient is not small there.

3.5 Summary

We have clarified the properties of the non-resonant pressure driven instabilities and the relation to the resonant instabilities in the cylindrical plasma model. The behavior of the non-resonant type mode depends strongly on the profile of both the pressure and rotational transform. For some cases the instability has a mixed character between the resonant and non-resonant modes. Also the transition from the resonant mode to the non-resonant type one occurs, when the pressure gradient is increased in the central region or the pressure profile becomes peaked.

At first we have solved the eigenmode equation analytically with respect to the perturbed stream function for an equilibrium with a constant rotational transform and a parabolic pressure profile. It is noted that the non-resonant mode has a global structure, and the dependency of γ on β is parabolic [see Eq. (3.18)]. In this case it can be shown that, the mode with fewest node number has the larger growth rate, and the higher harmonic mode with the same helicity has the higher beta limit.

With the numerical calculations, it is shown that the growth rate of the non-resonant mode decreases to zero without the tail near the beta limit, while the resonant mode has a fairly wide small growth rate regime expressed as $\gamma \propto e^{-1/\sqrt{\beta_0-\beta_S}}$ [126], where β_S denotes the central beta value given by the Suydam criterion. A physical interpretation is as follows. Although the resonant mode becomes localized at the resonant surface with the decrease of the beta value, the non-resonant mode does not have such a surface in the plasma column. Therefore the free energy necessary to excite the non-resonant modes is always finite, since the parallel wave number along the magnetic field line is also finite. Thus the growth rate decreases to zero without the tail near the beta limit. In the resonant case, since the higher harmonic modes have larger poloidal and toroidal wave numbers than the fundamental one, they can be more localized in the radial direction. Thus the growth rates at the same beta value are larger than the fundamental mode. However, all modes can be highly localized at the resonant surface as the central beta value decreases, the beta limit does not depend on the mode numbers and agrees with the Suydam limit. On the contrary, in the non-resonant case, since the parallel wave number

of higher harmonic mode becomes larger than the fundamental mode, the higher harmonics need more energy for excitation in the low beta regime. Thus the beta limit of the non-resonant mode with a higher harmonic mode number is larger than the fundamental mode.

When the pressure profile becomes locally flattened with the width of W around the resonant surface, the resonant mode shows the non-resonant feature. The beta limit in this case is increased with the small flattening region. The marginal mode structure is quite different from the case with $W = 0$, i.e. it is restricted to the one side of the resonant surface and the growth rate decreases to zero without the tail when β_0 approaches to the marginal value. It is noted that this non-resonant feature also appears in case of the nonzero but small pressure gradient at the resonant surface.

In Heliotron-E, when the beta value is increased, the central rotational transform is increased and the profile becomes non-monotonic. We have studied this situation by changing the rotational transform artificially. Even if there is no resonant surface for the $(2, 1)$ mode, when the minimum of the rotational transform, $\iota_{\min}$, is close to 0.5, the non-resonant $(2, 1)$ mode becomes unstable, which is independent of the Suydam criterion. When $\iota_{\min}$ is less than 0.5, the double resonant mode becomes unstable. Also, the non-resonant type $(3, 2)$ mode is unstable below the Suydam limit at the $\iota = 2/3$ surface. In this case the radial mode structure is observed in the central region when $\iota(0)$ is sufficiently close to $2/3$.

In later publications, the analytically approximated solution is obtained for cylindrical model equilibrium with the assumption that the mode structure has a step like structure around the resonant surface [46, 47]. It is shown that the beta limit of the non-resonant mode becomes mostly an order of magnitude higher than that obtained from Suydam criterion for the smooth pressure profile. Moreover, the toroidal effect on the non-resonant mode is also analyzed for the typical LHD configuration by means of the numerical computation [85, 87, 88]. The radial step like structure is also found in the toroidal case for the eigenmode with the toroidal mode number $n = 1$, however, it is not the case that the eigenmode with the least node number is the most unstable one.

Chapter 4

Phase mixing damping of surface Alfvén wave in a slab plasma

4.1 Introduction

The first careful treatment of plasma wave in an inhomogeneous plasma was presented by Barston [39]. He applied the normal mode analysis to the electrostatic plasma waves in the inhomogeneous cold plasma for a plane-pinch. He considered two density profiles; one was everywhere continuous and nowhere constant, and the other was piecewise continuous and differentiable. It was shown that there exists no dispersion relation and the spectrum of frequency is continuous with real values in the former case. In the latter case discrete modes appear with the same number as that of discontinuities in the density profile. Sedláček [117] had studied the same problem using the Laplace transformation in time and showed that the normal mode approach is equivalent to the Laplace transformation approach. It was concluded that even in the continuous profile case, there exists a dispersion relation which Barston did not appreciate, and both continuous and discrete spectrum of frequency appear. The dispersion relation is interpreted in the same way as in the case of Landau damping in hot plasmas, and the discrete spectrum is considered as the 'virtual' eigenmode of the system.

Uberoi [141] has pointed out that there exists an interesting similarity of the forms between the equation governing Alfvén waves in the presence of an inhomogeneous magnetic field and that governing electrostatic plasma oscillations in a cold inhomogeneous plasma. By following Barston's analysis, the incompressible Alfvén wave can be treated in the same way as the electrostatic plasma oscillation in the cold inhomogeneous plasma. Tataronis and Grossmann [75, 129] also followed Sedláček to study the incompressible shear Alfvén wave in the magnetized slab

plasma. While Tataronis and Grossmann assumed the incompressibility of plasma, Chen and Hasegawa [54] showed that the Alfvén wave damps in the inhomogeneous plasma without assuming incompressibility, and they proposed to use the Alfvén wave for heating the magnetically confined plasma [55].

Although these theories have mainly been developed for the surface waves at the plasma-vacuum interface, they will be applicable to an inhomogeneous plasma with a sharp density gradient formed by the injection of hydrogen ice pellet. Since the pellet is considered to be ablated in a narrow region, the density has a locally peaked profile. In the Heliotron-E experiment, magnetic fluctuations are often observed with the magnetic probe located near the wall of vacuum chamber [155], which are considered to be induced by the pellet injection. The frequency $\omega_{\rm r}$ and damping rate $\omega_{\rm i}$ are evaluated from experimental data as $\omega_{\rm r} \sim 2.3 \times 10^6$ [$\rm s^{-1}$] and $\omega_{\rm i} \sim 6.9 \times 10^4$ [$\rm s^{-1}$]. If we assume that this magnetic fluctuation is induced by Alfvén waves and that this damping is caused by plasma resistivity, the damping rate will be estimated as 10-10^2 [$\rm s^{-1}$]. Thus we need another mechanism to enhance the damping. The Alfvén resonance occurred in strongly inhomogeneous plasmas is such a candidate. It is noted that a detailed experimental investigation of Alfvén continuum damping is also reported in Ref. [51].

In Sec. 4.2, we show the wave equation for the shear Alfvén wave and discuss its general property. We derive the dispersion relation and analytic solution for the slab plasma with steep density gradient regions at the plasma surface in Sec. 4.4. In Sec. 4.6, we show the numerical solution of the dispersion relation. Our interest is in the dependence of damping rate on the scale length of density gradient. We present an interpretation that the pellet induced magnetic fluctuation disappears with a fairly large damping rate, when the singularity exists in the Alfvén wave equation at the surface of slab plasma.

4.2 Alfvén wave equation

Since we are interested in magnetic fluctuations in high density and high temperature plasmas, we use the ideal magnetohydrodynamic (MHD) equations for describing the wave phenomena. We consider a slab configuration with straight magnetic field lines for simplicity. It is a rough approximation for an annular high density plasma produced by the pellet injection into a toroidal plasma [155]. The equilibrium magnetic field is assumed in the z direction, and to vary only in the x direction; i.e.,

$$\boldsymbol{B}_0 = (0, 0, B_0(x)), \tag{4.1}$$

in the Cartesian coordinate. (In the toroidal plasma, x, y, and z correspond to radial, poloidal, and toroidal directions, respectively.) In addition, we assume that the equilibrium mass density ρ_0 and plasma pressure p_0 also vary only in the x direction.

The linearized ideal MHD equation is written as

$$\begin{aligned}\rho_0 \partial_t^2 \boldsymbol{\xi} = &-\nabla(\gamma p_0 \nabla \cdot \boldsymbol{\xi} + \boldsymbol{\xi} \cdot \nabla p_0) \\ &+ \frac{1}{\mu_0}(\nabla \times \boldsymbol{B}_0) \times [\nabla \times (\boldsymbol{\xi} \times \boldsymbol{B}_0)] \\ &+ \frac{1}{\mu_0}[\nabla \times (\nabla \times (\boldsymbol{\xi} \times \boldsymbol{B}_0))] \times \boldsymbol{B}_0, \end{aligned} \tag{4.2}$$

where $\boldsymbol{\xi}$, γ, and μ_0 denote the plasma displacement, the specific heat ratio, and permeability, respectively. We use the Fourier transformation in y and z, and the Laplace transformation in t,

$$\tilde{\boldsymbol{\xi}}(x, k_\perp, k_\parallel, \omega) = \int_0^\infty \mathrm{d}t \int_{-\infty}^\infty \mathrm{d}y \int_{-\infty}^\infty \mathrm{d}z\, \boldsymbol{\xi}(x, y, z, t)\, \mathrm{e}^{\mathrm{i}(\omega t - k_\perp y - k_\parallel z)}, \tag{4.3}$$

for $\boldsymbol{\xi}(x, y, z, t)$. By applying the Fourier-Laplace transformation to Eq. (4.2), the MHD wave equation is given as [54]

$$\frac{\mathrm{d}}{\mathrm{d}x}\Big[\frac{\epsilon\alpha B^2}{\epsilon - \alpha k_\perp^2 B^2}\frac{\mathrm{d}\tilde{\xi}_x}{\mathrm{d}x}\Big] + \epsilon\tilde{\xi}_x = S^*(x, k_\perp, k_\parallel, \omega), \tag{4.4}$$

where

$$\alpha(x) = 1 + \beta + \frac{\beta^2 k_\parallel^2 B^2}{\omega^2\mu_0\rho - \beta k_\parallel^2 B^2}, \tag{4.5}$$

$$\beta(x) = \frac{\gamma\mu_0 p}{B^2}, \tag{4.6}$$

$$\epsilon(x) = \omega^2\mu_0\rho - k_\parallel^2 B^2. \tag{4.7}$$

Here, the subscript zero which denotes equilibrium quantity is omitted, and $\tilde{\xi}_x$, and $S^*(x, \omega)$ denote the Fourier-Laplace transform of the x component of the plasma displacement vector, and the source term coming from initial conditions for the Laplace transform, respectively, and $k_\parallel$ denotes the wavenumber parallel to equilibrium magnetic field (z direction), $k_\perp$ the wavenumber in the y direction. The other components of the displacement vector $\tilde{\xi}_y$ and $\tilde{\xi}_z$ are expressed in terms of $\tilde{\xi}_x$ as,

$$\tilde{\xi}_y = -\frac{\mathrm{i}\alpha k_\perp B^2}{\epsilon - \alpha k_\perp^2 B^2}\partial_x\tilde{\xi}, \tag{4.8}$$

$$\tilde{\xi}_z = \frac{-\mathrm{i}\gamma\mu_0 p k_\parallel}{\omega^2\mu_0\rho - \beta k_\parallel^2 B^2}\frac{\epsilon}{\epsilon - \alpha k_\perp^2 B^2}\partial_x\tilde{\xi}. \tag{4.9}$$

The boundary conditions for Eq. (4.2) are given as $\tilde{\xi}_x \to 0$ in $x \to \pm\infty$, which correspond to the requirement that the normal component of the perturbed magnetic field vanishes at infinity. Notice that this MHD wave equation has a regular singularity at $\epsilon(x_0) = 0$ where the wave locally satisfies the dispersion relation of the homogeneous shear Alfvén wave. It is also noted that Eq. (4.4) is the slab simplified version of the Hain-Lust equation for the general screw pinch without magnetic shear.

To compare the above model with toroidal experiments, we assume that $|k_\perp|$, corresponding to poloidal wave number, is much larger than $|k_\parallel|$, corresponding to toroidal wave number, and $\beta \lesssim 1$. Since we consider the lower frequency wave than the ion cyclotron frequency, these conditions are equivalent to $|\alpha B^2 k_\perp^2| \gg |\epsilon|$, and therefore setting $S = -k_\perp^2 S^*$ leads to

$$\frac{\mathrm{d}}{\mathrm{d}x}\left[\epsilon(x, k_\parallel, \omega)\frac{\mathrm{d}\tilde{\xi}_x}{\mathrm{d}x}\right] - k_\perp^2 \epsilon(x, k_\parallel, \omega)\tilde{\xi}_x = S(x, k_\perp, k_\parallel, \omega). \tag{4.10}$$

It is noted that this equation also has a regular singularity at $\epsilon(x = x_0) = 0$.

Comparing Eq. (4.10) with the incompressible plasma model [129], we notice that the solution of Eq. (4.10) also describes an incompressible Alfvén wave. Though Eq. (4.4) contains both shear and compressional Alfvén wave, Eq. (4.10) only contains the shear Alfvén wave after $|k_\perp| \gg |k_\parallel|$ and $\beta \lesssim 1$ are assumed. This means that in large-aspect-ratio and low-β device, the shear Alfvén wave is prior to the compressional one.

4.3 Incompressible limit of spectral equation

In this section, we will discuss the consistency of the incompressibility condition by taking incompressible limit of the spectral ordinary differential equation (4.4).

Let us first show the relations among perturbed fields under the incompressible assumption. In the incompressible case [30, 110, 141], the slab Alfvén equation is written as

$$\left[\partial_t^2 - \frac{1}{\mu_0\rho_0}(\boldsymbol{B}_0 \cdot \nabla)^2\right]\boldsymbol{\xi}^{\mathrm{ic}} = -\frac{1}{\rho_0}\nabla\left(p_1^{\mathrm{ic}} + \frac{\boldsymbol{B}_0 \cdot \boldsymbol{B}_1^{\mathrm{ic}}}{\mu_0}\right), \tag{4.11}$$

with the incompressibility condition

$$\nabla \cdot \boldsymbol{\xi}^{\mathrm{ic}} = 0, \tag{4.12}$$

where the superscript ic denotes the perturbed fields under incompressible assumption. Here we will consider the same equilibrium magnetic field with the compressible

case (4.1). Hence, some tedious algebra gives the relation between y and z component of the displacement vector, perturbed pressure p_1^{ic}, and x component of the displacement vector in the Fourier transformed form as

$$\tilde{\xi}_y^{\mathrm{ic}} = \frac{\mathrm{i}k_\perp}{k_\perp^2 + k_\parallel^2}\partial_x \tilde{\xi}_x^{\mathrm{ic}} \tag{4.13}$$

$$\tilde{\xi}_z^{\mathrm{ic}} = \frac{\mathrm{i}k_\parallel}{k_\perp^2 + k_\parallel^2}\partial_x \tilde{\xi}_x^{\mathrm{ic}} \tag{4.14}$$

$$\tilde{p}_1^{\mathrm{ic}} = \frac{\omega^2\rho_0}{k_\perp^2 + k_\parallel^2}\partial_x \tilde{\xi}_x^{\mathrm{ic}} - \tilde{\xi}_x^{\mathrm{ic}}\frac{\mathrm{d}p_0}{\mathrm{d}x}, \tag{4.15}$$

where we have used the equilibrium relation

$$\frac{\mathrm{d}}{\mathrm{d}x}\Big(p_0 + \frac{B_0^2}{2\mu_0}\Big) = 0. \tag{4.16}$$

In order to take the incompressible limit of the physical quantities from the expression obtained under compressible condition, we can invoke the limit of $\gamma \to \infty$ as discussed in Appendix A. It is readily shown that the limit $\gamma \to \infty$ on the expressions (4.8) and (4.9) in the compressible case converges to the values (4.13) and (4.14) evaluated under incompressible condition, respectively. However, the expression of the pressure is not so trivial. Actually, simple substitution of Eqs. (4.13) and (4.14) into the adiabatic relation

$$\tilde{p}_1 = -\tilde{\boldsymbol{\xi}} \cdot \nabla p_0 - \gamma p_0 (\nabla \cdot \tilde{\boldsymbol{\xi}}) \tag{4.17}$$

will not give the same expression with Eq. (4.15). Since $\nabla \cdot \tilde{\boldsymbol{\xi}}$ approaches to zero in the limit $\gamma \to \infty$, we have to include the higher order contributions in the second term of Eq. (4.17). Substituting the expressions (4.8) and (4.9) into Eq. (4.17), the perturbed pressure under compressible condition will be represented in terms of the x component of the displacement vector as

$$\begin{aligned}\tilde{p}_1 &= -\tilde{\xi}_x\frac{\mathrm{d}p_0}{\mathrm{d}x} - \gamma p_0 \partial_x \tilde{\xi}_x \Big[1 + \frac{\alpha k_\perp^2 B^2}{\epsilon - \alpha k_\perp^2 B^2} + \frac{\gamma\mu_0 p k_\parallel^2}{\omega^2\mu_0\rho - \beta k_\parallel^2 B^2}\frac{\epsilon}{\epsilon - \alpha k_\perp^2 B^2}\Big] \\ &= -\tilde{\xi}_x\frac{\mathrm{d}p_0}{\mathrm{d}x} - \frac{\gamma p_0 \epsilon\omega^2\mu_0\rho_0}{(\epsilon - \alpha k_\perp^2 B^2)(\omega^2\mu_0\rho_0 - \beta k_\parallel^2 B^2)}\partial_x\tilde{\xi}_x.\end{aligned} \tag{4.18}$$

By taking the limit $\gamma \to \infty$ directly on Eq. (4.18), it gives

$$\tilde{p}_1 \to -\tilde{\xi}_x\frac{\mathrm{d}p_0}{\mathrm{d}x} + \frac{\omega^2\rho_0}{k_\perp^2 + k_\parallel^2}\partial_x\tilde{\xi}_x, \tag{4.19}$$

which exactly coincides with the relation (4.15) obtained with incompressible assumption.

Thus, it is conclude here that the incompressible result can be obtained by taking the limit $\gamma \to \infty$ on the relations from compressible system of equations, and this limit keeps exact consistency with the adiabatic equation of state.

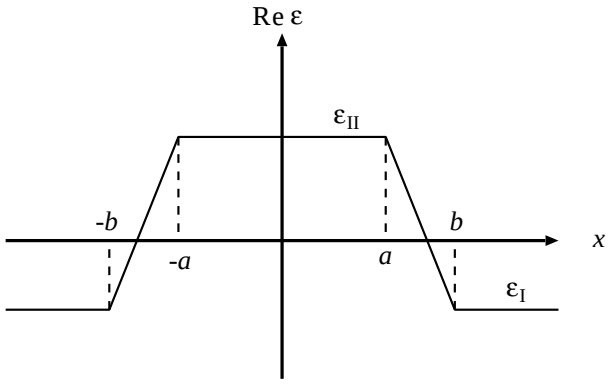

Figure 4.1: Profile of $\epsilon(x, k_\parallel, \omega) = \omega^2\mu_0\rho(x) - k_\parallel^2 B^2(x)$, where $\epsilon_{\rm I}$ and $\epsilon_{\rm II}$ are only functions of $k_\parallel$ and ω. The positions $x = \pm b$ correspond to the surfaces of high density plasma.

4.4 Derivation of dispersion relation

Since the wave equation (4.10) is inhomogeneous, we can solve this equation by using a Green function. When the inverse Laplace transformation is carried out for $\tilde{\boldsymbol{\xi}}$, the contribution from poles of the Green function becomes dominant for $t \to \infty$. For the magnetized plasma with sharp gradients near the surface regions, we assume a profile of ϵ which consists of three spatially constant regions and two linear ones described as

$$\epsilon(x, k_\parallel, \omega) = \begin{cases} \epsilon_{\rm I} & (x < -b) \\ \delta x + \eta & (-b < x < -a) \\ \epsilon_{\rm II} & (-a < x < a) \\ -\delta x + \eta & (a < x < b) \\ \epsilon_{\rm I} & (b < x) \end{cases} , \tag{4.20}$$

where $\epsilon_{\rm I} = \omega^2\mu_0\rho_{\rm I} - k_\parallel^2 B_{\rm I}^2$, $\epsilon_{\rm II} = \omega^2\mu_0\rho_{\rm II} - k_\parallel^2 B_{\rm II}^2$, $\rho_{\rm I,II}$ and $B_{\rm I,II}$ are the constant values, and $\delta(k_\parallel, \omega) = (\epsilon_{\rm II} - \epsilon_{\rm I})/(b - a)$, $\eta(k_\parallel, \omega) = (b\epsilon_{\rm II} - a\epsilon_{\rm I})/(b - a)$. The schematic form which is symmetric with respect to x is illustrated in Fig. 4.1. This model may be applicable to an annular high density plasma produced by an injected ice pellet. The region $(-b, b)$ describes the high density one and the regions $(-\infty, -b)$ and (b, ∞) correspond to the background density ones. The following analysis to obtain the dispersion relation of shear Alfvén wave is parallel to that of Sedláček [117].

There exist non-collective oscillations due to the branch-point singularities of the Green function, which damp proportional to inverse power of time. Since the frequencies of these oscillations, however, depend on position, their behavior may not be seen from the outer magnetic probe [129]. Since the Green function also has simple poles in (a, b) and $(-b, -a)$, their contribution becomes dominant for $t \to \infty$.

Since Eq. (4.10) is an inhomogeneous differential equation of Sturm-Liouville type, the solution can be expressed in terms of the Green function, which can be written as

$$G(x,s;k_\perp,k_\parallel,\omega)=\begin{cases} J^{-1}[\tilde{\xi}_{(1)}(x,k_\perp,k_\parallel,\omega)\,\tilde{\xi}_{(2)}(s,k_\perp,k_\parallel,\omega)] & (x<s) \\ J^{-1}[\tilde{\xi}_{(1)}(s,k_\perp,k_\parallel,\omega)\,\tilde{\xi}_{(2)}(x,k_\perp,k_\parallel,\omega)] & (s<x) \end{cases}. \tag{4.21}$$

Here $\tilde{\xi}_{(1)}$ and $\tilde{\xi}_{(2)}$ are homogeneous solutions of the differential equation (4.10) with satisfying the boundary condition at $x=-\infty$ and $x=\infty$, respectively, J is the conjunct of $\tilde{\xi}_{(1)}$ and $\tilde{\xi}_{(2)}$,

$$\begin{aligned} J(k_\perp,k_\parallel,\omega) &= \epsilon(x)\left[\tilde{\xi}_{(1)}\frac{\mathrm{d}\tilde{\xi}_{(2)}}{\mathrm{d}x}-\frac{\mathrm{d}\tilde{\xi}_{(1)}}{\mathrm{d}x}\tilde{\xi}_{(2)}\right] \\ &= \frac{1}{2}k_\perp\epsilon_{\mathrm{II}}z_1z_4\mathrm{e}^{2k_\perp a}D(k_\perp,k_\parallel,\omega), \end{aligned} \tag{4.22}$$

which can be proved independent of x and s. Here we have introduced the dispersion function

$$\begin{aligned} D(k_\perp,k_\parallel,\omega) &= ([I_0(z_2)+I_1(z_2)][K_0(z_1)+K_1(z_1)]-[I_0(z_1)-I_1(z_1)][K_0(z_2)-K_1(z_2)]) \\ &\quad\times([I_0(z_3)-I_1(z_3)][K_0(z_4)-K_1(z_4)]-[I_0(z_4)+I_1(z_4)][K_0(z_3)+K_1(z_3)]) \\ &\quad+\mathrm{e}^{-4k_\perp a}([I_0(z_2)-I_1(z_2)][K_0(z_1)+K_1(z_1)]-[I_0(z_1)-I_1(z_1)][K_0(z_2)+K_1(z_2)]) \\ &\quad\times([I_0(z_4)+I_1(z_4)][K_0(z_3)-K_1(z_3)]-[I_0(z_3)+I_1(z_3)][K_0(z_4)-K_1(z_4)]), \end{aligned} \tag{4.23}$$

and z_i (i = 1-4) which depend on $k_\perp$, $k_\parallel$, and ω denote the quantity associated with the scale length of the density gradient,

$$z_1=-z_4=\frac{\epsilon_{\mathrm{I}}}{\epsilon_{\mathrm{II}}-\epsilon_{\mathrm{I}}}k_\perp(b-a), \tag{4.24}$$

$$z_2=-z_3=\frac{\epsilon_{\mathrm{II}}}{\epsilon_{\mathrm{II}}-\epsilon_{\mathrm{I}}}k_\perp(b-a), \tag{4.25}$$

and I_n and K_n denote the n-th order modified Bessel function of the first and the second kind, respectively.

With the Green function (4.21), the solution for Eq. (4.10) is described as

$$\tilde{\xi}_x(x,k_\perp,k_\parallel,\omega)=\int_{-\infty}^{\infty}G(x,s;k_\perp,k_\parallel,\omega)S(s,k_\perp,k_\parallel,\omega)\,\mathrm{d}s. \tag{4.26}$$

Then the plasma displacement in the real space is expressed by carrying out the inverse Fourier-Laplace transformation of Eq. (4.26),

$$\boldsymbol{\xi}(x,y,z,t)=\frac{1}{(2\pi)^3}\int_{\mathcal{C}}\mathrm{d}\omega\int_{-\infty}^{\infty}\mathrm{d}k_\perp\int_{-\infty}^{\infty}\mathrm{d}k_\parallel\,\tilde{\boldsymbol{\xi}}(x,k_\perp,k_\parallel,\omega)\,\mathrm{e}^{\mathrm{i}(k_\perp y+k_\parallel z-\omega t)}, \tag{4.27}$$

where $\mathcal{C}$ denotes the integration path in the complex ω plane. When there exist poles of the Green function, their contribution becomes dominant in the limit $t \to \infty$. Therefore $J = 0$ gives a dispersion relation:

$$D(k_\perp, k_\parallel, \omega) = 0. \tag{4.28}$$

Although the discussion of this paper is mainly concerned with density gradient, dispersion relation (4.28) is applicable to the case with inhomogeneous magnetic field.

4.5 Analytic solutions of dispersion relation

If we assume that the density gradients are steep, $|k_\perp(b-a)| \ll 1$, to obtain the analytic solution, the dispersion relation (4.28) has two branches shown as

$$\coth(k_\perp a) + \frac{z_2}{z_1} + z_2 \log \frac{z_2}{z_1} = 0, \tag{4.29}$$

$$\tanh(k_\perp a) + \frac{z_2}{z_1} + z_2 \log \frac{z_2}{z_1} = 0. \tag{4.30}$$

We need to consider Riemannian sheets for the logarithmic function with complex argument. Since there exist no solution on $n = 0$ Riemannian sheet, we carry out the analytic continuation into the other sheets and then calculate the weakest damping solution (or $|\omega_\mathrm{r}| \gg |\omega_\mathrm{i}|$ in $\omega = \omega_\mathrm{r} + \mathrm{i}\omega_\mathrm{i}$). Two solutions exist on the $n = 1$ sheet, which are expressed as

$$\begin{cases} \omega_{\mathrm{r}1} = k_\parallel \sqrt{\dfrac{B_\mathrm{I}^2 + \theta B_\mathrm{II}^2}{\mu_0(\rho_\mathrm{I} + \theta\rho_\mathrm{II})}}, \\ \dfrac{\omega_{\mathrm{i}1}}{\omega_{\mathrm{r}1}} = -\dfrac{1}{4}\pi\theta k_\perp (b-a)(1 - \mathrm{e}^{-2k_\perp a}) \\ \qquad\qquad \times \dfrac{\mu_0\rho_\mathrm{I}\rho_\mathrm{II}(V_\mathrm{AI}^2 - V_\mathrm{AII}^2)}{(\rho_\mathrm{I} + \theta\rho_\mathrm{II})(B_\mathrm{I}^2 + \theta B_\mathrm{II}^2)}, \end{cases} \tag{4.31}$$

$$\begin{cases} \omega_{\mathrm{r}2} = k_\parallel \sqrt{\dfrac{\theta B_\mathrm{I}^2 + B_\mathrm{II}^2}{\mu_0(\theta\rho_\mathrm{I} + \rho_\mathrm{II})}}, \\ \dfrac{\omega_{\mathrm{i}2}}{\omega_{\mathrm{r}2}} = -\dfrac{1}{4}\pi k_\perp (b-a)(1 - \mathrm{e}^{-2k_\perp a}) \\ \qquad\qquad \times \dfrac{\mu_0\rho_\mathrm{I}\rho_\mathrm{II}(V_\mathrm{AI}^2 - V_\mathrm{AII}^2)}{(\theta\rho_\mathrm{I} + \rho_\mathrm{II})(\theta B_\mathrm{I}^2 + B_\mathrm{II}^2)}, \end{cases} \tag{4.32}$$

respectively, which describe the surface Alfvén waves. Here $\theta = \tanh(k_\perp a)$ is the parameter associated with the width of central constant density region, and V_A denotes the Alfvén velocity. Subscripts I and II denote the central and outer constant

regions in Fig. 4.1, respectively. It can be easily shown that the solutions on the other Riemannian sheets damp faster than those on the $n = 1$ sheet by replacing π in $\omega_{\rm i1}$ and $\omega_{\rm i2}$ with $(2n-1)\pi$.

Both real frequencies $\omega_{\rm r1}$ and $\omega_{\rm r2}$ are proportional to $k_\parallel$, which is the same as the frequency of shear Alfvén wave in homogeneous plasmas, however, they include the parameter θ dependent on $k_\perp$. The damping rates are proportional to the scale length of the density gradient, $b-a$, and $|\omega_{\rm i1}|$ and $|\omega_{\rm i2}|$ are nearly equal to each other. Therefore, in the sharp boundary limit ($b-a \to 0$), these modes show undamped oscillations. When the distance of two density gradient regions, $2a$, goes to infinity with keeping $(b-a)$ constant, both the frequencies and damping rates of these two branches converge to the same value, which coincides with Chen and Hasegawa [54].

4.6 Numerical solutions of dispersion relation

In order to evaluate accuracy of the analytic solutions in Eqs. (4.31) and (4.32), numerical solutions of Eq. (4.28) are shown for the particular parameters. In the numerical calculations, it is useful to define the following dimensionless variables:

$$\begin{aligned} \hat{b} = \frac{b}{a}, \quad \hat{\rho} = \frac{\rho_{\rm II}}{\rho_{\rm I}}, \quad \hat{k}_\parallel = k_\parallel a, \quad \hat{k}_\perp = k_\perp a, \\ \hat{\omega}^2 = \frac{\omega^2 a^2}{B_{\rm I}^2/\mu_0\rho_{\rm I}}, \quad \hat{\beta} = 1 - \Big(\frac{B_{\rm II}}{B_{\rm I}}\Big)^2. \end{aligned} \tag{4.33}$$

Then the arguments of the modified Bessel functions are expressed in terms of these variables as

$$z_1 = \hat{k}_\perp(\hat{b}-1)\frac{\hat{\omega}^2 - \hat{k}_\parallel^2}{\hat{\omega}^2(\hat{\rho}-1) + \hat{k}_\parallel^2\hat{\beta}}, \tag{4.34}$$

$$z_2 = \hat{k}_\perp(\hat{b}-1)\frac{\hat{\omega}^2\hat{\rho} - \hat{k}_\parallel^2(1-\hat{\beta})}{\hat{\omega}^2(\hat{\rho}-1) + \hat{k}_\parallel^2\hat{\beta}}. \tag{4.35}$$

The numerical solutions of the dispersion relation (4.28) corresponding to ω_1 and ω_2 are shown in Fig. 4.2. Here we have used the following values for dimensionless parameters,

$$\hat{k}_\perp = 1, \quad \hat{k}_\parallel = 0.01, \quad \hat{\beta} = 0, \quad \hat{\rho} = 6, \tag{4.36}$$

and we have taken into account of the $n = 1$ Riemannian sheet. Though the damping rates are proportional to the scale length of the density gradient in the sharp boundary limit, they do not continue to increase monotonically with the scale length. They have extrema at $\hat{b} \simeq 1.9$ for ω_1 and $\hat{b} \simeq 1.4$ for ω_2, and when the scale length of the density gradient becomes larger than this value, they turn out

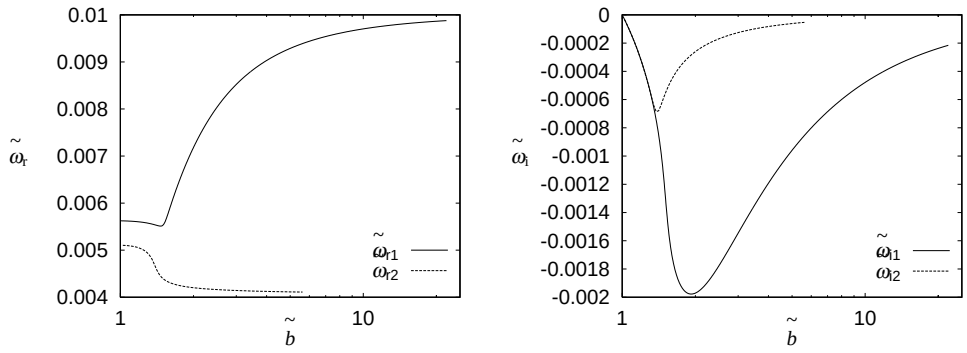

Figure 4.2: Dependence of normalized frequency $\hat{\omega}_{\rm r}$ and damping rate $\hat{\omega}_{\rm i}$ on the scale length of the density gradient. The left figure denotes the frequency and the right one the damping rate. The subscripts 1 and 2 denote the solutions of the exact dispersion relation (4.28) corresponding to Eq. (4.31) and (4.32), respectively.

to decrease with increase of $\hat{b}$. It is considered that $\hat{\omega}_{\rm i}$ finally go to zero in the limit $\hat{b} \to \infty$. Also, $\hat{\omega}_{\rm r1}$ is considered to have a limiting value of 0.01, which is equivalent to the relation $\omega = k_\parallel V_{\rm AI}$. On the other hand, $\hat{\omega}_{\rm r2}$ is considered to have a limiting value of $0.01 \times \sqrt{1/6}$, which is equivalent to the relation $\omega = k_\parallel V_{\rm AII}$. In the region with $\hat{b} \sim 1$, we observe that the analytic solutions (4.31) and (4.32) agree with numerical results. In this region these two branches have almost the same damping rates, however, in the region $\hat{b} \gtrsim 1.5$, the branch ω_2, which has a smaller frequency, has weaker damping rate than ω_1. Since the density profile approaches to a homogeneous one at $\rho = \rho_{\rm I}$ with increase of the scale length of the density gradients, $b - a$, the branch ω_2 remains prior to the other. We also observed that the maximum points of the damping rates go to the right with the increase of the fraction of the density $\hat{\rho}$. They do not move leftward or rightward due to the change of $\hat{\beta}$, although the damping rates themselves increase.

Figure 4.3 shows the deviation of the analytic damping rate from the numerical one. Here the same parameters as in Eq. (4.36) are used. The analytic solution is valid only for the case with the steep density gradient $\hat{b} \lesssim 1.2$. The error of the analytic solution is about 10% at $\hat{b} = 1.2$.

4.7 Summary

It is confirmed that two branches of the surface Alfvén wave exist for the slab plasma, since there are two sharp jump regions of density. However, the frequencies and damping rates of both branches are almost comparable, when the density jump is substantial. It is interpreted that the magnetic fluctuations induced by the pellet

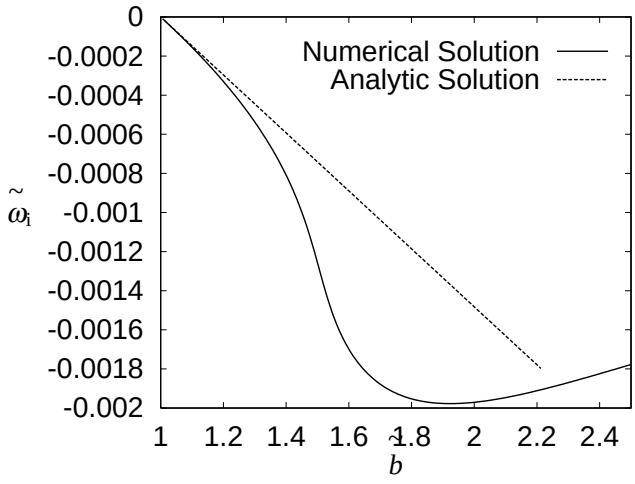

Figure 4.3: Comparison between analytic solution and numerical one of damping rate $\hat{\omega}_{i1}$ in Fig. 4.2. The normalized frequency of the analytic solution $\hat{\omega}_{r1}$ is independent of the scale length of the density gradient.

injection in Heliotron-E are surface Alfvén waves corresponding to Eq. (4.31) or Eq. (4.32). These modes damp with finite scale length of the density gradient. In the limit of sharp boundary, $(b-a) \to 0$, Eqs. (4.31) and (4.32) give undamped oscillations, and so do in the limit of homogeneous plasma, $(b-a) \to \infty$. That is to say, these two modes exist in the sharp boundary limit, while continuous spectrum does not appear.

The initial annular density profile produced by the pellet may have sharp density gradients satisfying $\hat{b} \gtrsim 1$, and the analytic treatment is valid to estimate ω_r and ω_i for comparison with experiments. For example, provided typical plasma parameters for Heliotron-E are assumed as $B_{\rm I} = B_{\rm II} = 1.9$ [T], $n_{\rm I} = 10^{19}$ [m^{-3}], $n_{\rm II} = 6n_{\rm I}$, $a = 10^{-1}$ [m], $b - a = 10^{-2}$ [m], $k_\perp = 10$ [m^{-1}], and $k_\parallel = 2 \times 10^{-2}$ [m^{-1}], we obtain $\omega_{r1} \sim 2 \times 10^6$ [s^{-1}], and $\omega_{i1} \sim 6 \times 10^4$ [s^{-1}], which is comparable to the experimental values expressed in the introduction, and the frequency ω_{r1} is much less than the ion cyclotron frequency $\omega_{ci} \sim 1.8 \times 10^8$. The damping rate is enhanced with the decrease of the density gradient by radial particle transport.

Chapter 5

External kink instabilities in presence of resistive wall

5.1 Introduction

The first research on plasma stability under the existence of surrounding resistive wall was back in the paper by Kruskal *et al.* [94]. They pointed out that, in stellarators which were designed for aiming at stationary operation, the external kink mode will be destabilized due to the penetration of magnetic field in long time discharges, while it would be stabilized in a shorter time scale due to the stabilizing effect of the wall. Later, Pfirsch and Tasso [109] showed that the ideal wall has actually the stabilizing effect on external kink mode of the static plasma due to non-penetration of the magnetic field. In reality, since the surrounding wall has always small but finite resistivity, there appear slow instabilities which grow in a time scale proportional to the resistivity of the wall. The conclusion then is that, the conducting wall should not be considered as a perfect stabilizing tool for the external kink mode of static plasmas.

Goedbloed *et al.* [71] calculated the spectrum of the external kink mode for a z-pinch plasma surrounded with a resistive wall. Here a constant density and magnetic field with surface plasma current are assumed and carries surface current in equilibrium. They investigated the dependence of growth rate of kink mode on the resistivity of the wall. Since the magnetic field has no shear in this system, the Alfvén continuum is shrinked to give two point spectra propagating in the opposite direction in ideal wall case, which turns into the ideal kink mode in case of no wall. With finite resistivity of the wall, there appears a new eigenvalue on the imaginary axis of the complex ω-plane, which is now called a resistive wall mode (RWM). This mode, appearing from the origin, does not exist in the ideal wall case, and quite

resembles the behavior of the tearing mode destabilized by the resistivity of plasma itself. Other two Alfvén eigenmodes show slight damping due to the resistivity of the wall, approach to the imaginary axis, and meet each other on negative side of the imaginary axis when the resistivity is increased. If the resistivity is increased further, one of the eigenvalue on negative side of the imaginary axis moves toward negative infinity on imaginary axis, and the other constructs a pair with the one on positive side of imaginary axis, which behaves as a pair to generate the ideal kink modes.

Haney and Freidberg [80] discussed the stability of three dimensional perturbations of toroidal plasma with arbitrary cross section and current profile by using a variational principle. By introducing the effect of the resistive wall, they have extended the variational principle which is a well defined useful method for the linear stability analysis of static plasmas. It is concluded that the RWM is a purely growing mode with zero frequency, and its critical stability condition is exactly equivalent to the case with the ideal wall at infinity.

In experiments, RWMs were observed in reversed field pinch devices such as OHTE or HBTX which required the conducting wall very close to the plasma for keeping the stability [128, 34]. Since the characteristic time for the magnetic field penetration becomes long for the thick conducting wall, RWM is relatively easily suppressed. However, it becomes shorter than the discharge period when the conducting wall is thin. Thus, some discharges are terminated by the growth of this mode. These results are considered to coincide with theoretical predictions of RWMs for static equilibria.

Recently, the stabilization of RWM was experimentally discovered at DIII-D tokamak in early 90's [135, 121, 122]. According to the experimental results, this mode did not appear for longer discharge period than the time scale of the resistive wall even for the higher β value than the threshold of external kink modes. In DIII-D, plasmas are rotating in the toroidal direction due to the tangential neutral beam injection. Therefore, this plasma rotation was considered as the stabilizing effect on the RWM.

Numerical calculation by Bondeson and Ward was the first theoretical investigation for this topic [44, 147]. With an eigenvalue code including both the resistive wall and the toroidal rigid rotation, they showed that the kink mode belonging to the shear Alfvén branch is stabilized by the sound wave resonance generated by the plasma rotation in the toroidal plasma. Betti and Freidberg has shown the existence of the coupling even in cylindrical geometry, and also concluded that the RWM can be stabilized by the sound wave resonance [41]. Moreover, several other stabilizing mechanisms such as resonance due to Alfvén continuous spectra [153], resonance

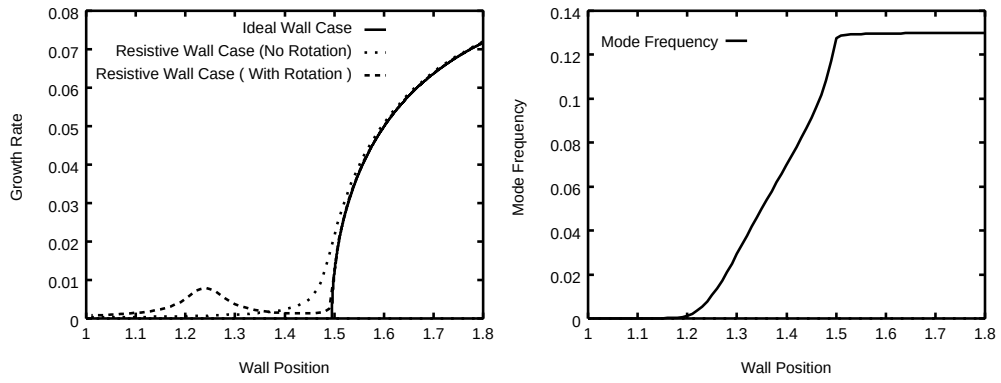

Figure 5.1: Dependence of growth rate or real frequency of the RWM in a cylindrical plasma with rigidly axial flow on the position of resistive wall. Growth rate and frequency are normalized by the poloidal Alfvén time, and the wall position is normalized by plasma radius.

due to cusp continuous spectra [42], resistivity [62] , or viscosity [64], were studied; however, there is no clear correlation to the experimental results. In addition, from the theoretical point of view, mathematical theory is not completed for the effect of continuous spectra or non-Hermiticity of the operator on the stability problem. Instead of solving this difficult problem, many theoretical studies are related to the feedback control of dangerous mode or mode locking phenomena [70, 89, 63, 154].

In this chapter, we will focus on the appearance of non-Hermiticity for the linear instability of the external kink mode under the existence of surrounding resistive walls and rigid plasma flows. As a reference, typical growth rate dependence on the position of the resistive wall relative to the plasma radius is shown in Fig. 5.1 [153]. This figure the obtained for a cylindrical plasma with a rigid axial flow. With the ideal wall placed closer to the plasma column, the ideal external kink mode is stabilized (solid line); however, for the resistive wall, the instability still remains in a time scale of the resistive diffusion of magnetic field in the wall, which is called the resistive wall mode or RWM. The growth rate of the RWM is monotonically increasing and becomes almost equal to that of the ideal external kink mode when the wall position is far from the plasma column if the plasma has no axial flow (dotted line). However, if we introduce the rigid flow (dashed line), the growth rate becomes large once at $c/a \sim 1.2$, where c (a) denote the radius of the resistive wall (plasma column). This small hump is observed in almost all calculations of growth rate of RWM, e.g. Bondeson and Ward [44, 147], Betti and Freidberg [41], Finn [62], and Fitzpatrick and Aydemir [64], and it seems that the wall position corresponding to this small hump determines the closest threshold of the wall position for stabilizing RWM. Nevertheless, no physical or mathematical discussion for the appearance of

the small hump in Fig. 5.1 is found in literatures. From the plot of real frequency for the case of rigidly flowing plasma (right side figure of Fig. 5.1), RWM is locked to the wall in the region $c/a \lesssim 1.2$. It begins to slip with respect to the wall at $c/a \simeq 1.2$, and has the finite frequency for $c/a \gtrsim 1.2$. Therefore, it is conjectured that the non-Hermiticity plays an important role in the behavior of RWM. Also our interest is in the mechanism for the appearance of the hump in the growth rate shown in the left side figure of Fig. 5.1.

We will first show that the Kelvin-Helmholtz instability, which is well known in fluid dynamics as an instability driven by a shear flow, could be described as an interaction of two out-of-phase surface waves in Sec. 5.2. The rest of this chapter is devoted for the detailed study the RWM. We will give the governing equations, then discuss the difficulty in constructing exact mathematical theory in Sec. 5.3. Instead of constructing the complete solutions of the system, we focus on the similarity to the Kelvin-Helmholtz instability, we will introduce a surface current model in Sec. 5.4. With the aid of this simplification, we have given a model with focusing on the non-Hermiticity of RWM. The detailed analysis will be given in Sec. 5.5. We will summarize the obtained results in Sec. 5.6.

5.2 Non-Hermiticity of Kelvin-Helmholtz instability

In this section, we will show that Kelvin-Helmholtz instability, which is one of the most well-known instabilities in fluid dynamics arising from non-Hermiticity of the generator, can be represented in a closed form describing an interaction of two surface waves. We will revise here the piecewise linear shear flow model used in Refs. [134, 73, 7].

For the y directed ambient flow which is sheared in the x direction, the perturbed vorticity of two dimensional incompressible Euler fluid is written in the form of Rayleigh equation:

$$\mathrm{i}\partial_t \Psi = [k v_0(x) + k v_0''(x)\, \mathcal{K}]\, \Psi, \tag{5.1}$$

where the perturbed vorticity $\Psi(x,t)$ and the integral operator $\mathcal{K}$ are expressed as

$$\Psi(x,t) = -\Delta\phi(x,t), \tag{5.2}$$

$$\mathcal{K}\Psi \equiv -\Delta^{-1}\Psi = \frac{1}{2k}\int e^{-k|x-\xi|}\, \Psi(\xi,t)\, \mathrm{d}\xi, \tag{5.3}$$

and ϕ and k denote a stream function and a wave number in the y direction, respectively. Here, $\Delta = \partial_x^2 + \partial_y^2$ denotes the two dimensional Laplacian operator.

Hereafter, we will investigate properties of the operator

$$\mathcal{A} = kv_0(x) + kv_0''(x)\mathcal{K} \tag{5.4}$$

in the infinite domain. It is noted that the non-Hermiticity of this operator is originated from the non-commutativity of two Hermitian operators, the multiplication $v_0''(x)$ and the inverse Laplacian $\mathcal{K}$. Actually, if $v_0''(x)$ does not change its sign over the domain, we can define a norm by introducing a weight function $1/|v_0''(x)|$ and construct a Hermitian operator in such normed domain [38]; however, the Kelvin-Helmholtz unstable system should have an inflection point of $v_0(x)$ [111], and thus, this instability should be considered to be cause by the non-Hermiticity of the operator $kv_0''(x)\mathcal{K}$.

Let us first consider the linear ambient velocity profile

$$v_0(x) = \frac{U}{a}x, \quad (-\infty < x < \infty). \tag{5.5}$$

Since the operator $\mathcal{A}$ is Hermitian due to $v_0''(x) = 0$, it has the continuous spectrum λ ($\in \mathbb{R}$) and the corresponding singular eigenfunction is

$$\varphi = \delta(x - \mu), \tag{5.6}$$

where $\mu = a\lambda/kU$. Here we will pick up the following two eigenfunctions from the continuous spectrum

$$\varphi_1 = \delta(x - a), \quad \varphi_2 = \delta(x + a), \tag{5.7}$$

for later discussions. Taking these eigenfunctions as basis vectors for the linear subspace, the operator will be expressed in terms of these vectors as

$$\mathcal{A} = \begin{pmatrix} kU & 0 \\ 0 & -kU \end{pmatrix}, \tag{5.8}$$

which is a diagonal matrix.

Next, let us consider the equilibrium shear flow in which the velocity profile is assumed to be constant in $x \leq -a$ and $x \geq a$ as illustrated in Fig. 5.2;

$$v_0(x) = \begin{cases} -U & (x \leq -a) \\ Ux/a & (-a < x < a) \\ U & (a \leq x) \end{cases}. \tag{5.9}$$

In this case, $v_0''(x)$ is expressed by the two delta function placed at $x = \pm a$, and the operator is found to be non-Hermitian. Two eigenfunctions in Eq. (5.7) will be modified and yield

$$\tilde{\varphi}_1 = \delta(x - a) + A\delta(x + a), \tag{5.10}$$

$$\tilde{\varphi}_2 = A\delta(x - a) + \delta(x + a), \tag{5.11}$$

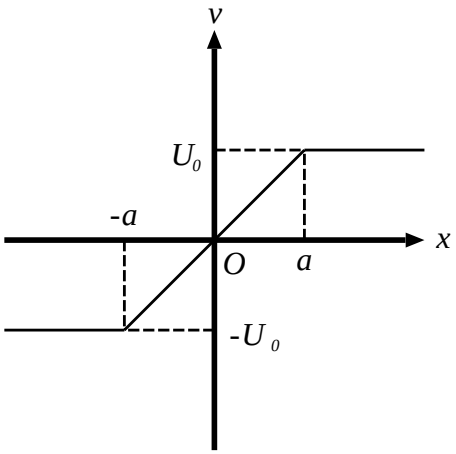

Figure 5.2: A model equilibrium velocity profile unstable against Kelvin-Helmholtz instability.

where A denotes

$$A = (2ka-1)e^{2ka} + \sqrt{(2ka-1)^2 e^{4ka} - 1}. \tag{5.12}$$

When the ambient velocity profile is snapped, two independent surface waves (φ_1 and φ_2) couple each other and they constitute new eigenstates ($\tilde{\varphi}_1$ and $\tilde{\varphi}_2$). The eigenvalues corresponding to them are

$$\tilde{\lambda}_1 = -\frac{U}{2a}\sqrt{(2ka-1)^2 - e^{-4ka}}, \tag{5.13}$$

$$\tilde{\lambda}_2 = \frac{U}{2a}\sqrt{(2ka-1)^2 - e^{-4ka}}, \tag{5.14}$$

respectively. One of them with the eigenvalue $\tilde{\lambda}_1$ corresponding to the eigenfunction $\tilde{\varphi}_1$ turns out to be unstable if the condition

$$(2ka-1)^2 < e^{-4ka} \tag{5.15}$$

is satisfied. Here we have defined $\sqrt{\alpha-\beta} = \mathrm{i}\sqrt{\beta-\alpha}$ for $\alpha < \beta$.

The singular function $\varphi_\mu = \delta(x-\mu)$ $(-a < \mu < a)$, which is the eigenfunction when the ambient velocity profile was completely linear in the whole space, will be modified here as

$$\tilde{\varphi}_\mu = B_-\delta(x-a) + \delta(x-\mu) + B_+\delta(x+a), \tag{5.16}$$

although the eigenvalue does not change, where

$$B_\pm = \frac{[2k(a\pm\mu)-1]e^{-k(a\mp\mu)} + e^{-k(a\pm\mu)}\,e^{-2ka}}{[2k(a-\mu)-1][2k(a+\mu)-1] - e^{-4ka}}. \tag{5.17}$$

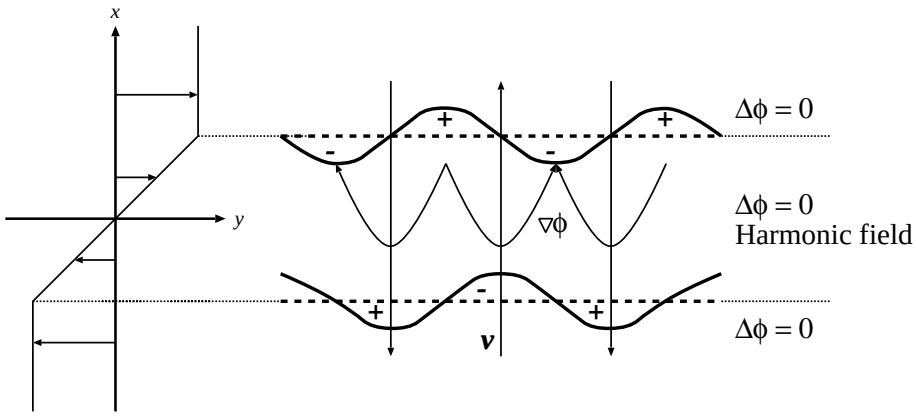

Figure 5.3: Schematic pictures of Kelvin-Helmholtz instability. The piecewise linear line in the left figure denotes the ambient velocity profile. It has the snapping point at $x = \pm a$ and the perturbed vorticity will be excited there which is denoted in the right figure by the wavy line.

If μ satisfies

$$\mu = \pm\sqrt{(2ka-1)^2 - e^{-4ka}}, \tag{5.18}$$

then $\tilde{\varphi}_\mu$ will not be defined by the above expression and the system has a possibility of resonance. However, if we consider the Kelvin-Helmholtz unstable system, the right hand side of Eq. (5.18) becomes purely imaginary from the condition (5.15), and we do not need to care about the resonance. This problem will be discussed more carefully in Chap. 7.

Thus, by taking the eigenfunctions $\tilde{\varphi}_1$, $\tilde{\varphi}_\mu$, and $\tilde{\varphi}_2$ as basis vectors for the linear subspace, the operator will be expressed in terms of these vectors as

$$\mathcal{A} = \frac{U}{2a}\begin{pmatrix} 2ka-1 & -e^{-k(a-\mu)} & -e^{-2ka} \\ 0 & 2k\mu & 0 \\ e^{-2ka} & e^{-k(a+\mu)} & -(2ka-1) \end{pmatrix}, \tag{5.19}$$

under the condition (5.15). Although this matrix may look to have a form of Jordan type with the coincidence of its diagonal elements, when $\pm(2ka-1) = 2k\mu$ is satisfied, it is semi-simple type and can be diagonalized. The important point here is that, the singular eigenfunction does not affect the coupled surface waves, and the instability is independent of the continuous spectrum.

Schematic pictures of the mechanism of Kelvin-Helmholtz instability are illustrated in Fig. 5.3. Physically, two surface waves, which are excited at the place where the ambient velocity profile is snapped, are coupled each other to construct the eigenstate. When the system is Kelvin-Helmholtz unstable, it is noted that the relative amplitude A becomes complex and $|A| = 1$ from Eq. (5.12). Namely they

have the same amplitude with out of phase and are connected by the harmonic field

$$\Delta\phi = 0, \tag{5.20}$$

in the region between two snapped points of $v_0(x)$ $[v_0''(x) = 0]$. Therefore, the gradient field of the stream function points from positive vorticity position to the negative one in the same way as that (electric field) of the electrostatic potential produced by the electric charge. Since the perturbed velocity is orthogonal to the gradient field of the stream function,

$$\boldsymbol{v} = \nabla\phi \times \boldsymbol{e}_z, \tag{5.21}$$

it affects on the other surface to amplify the original disturbance, and vice versa.

Therefore, the mechanism of Kelvin-Helmholtz instability could be understood as a positive feedback between two coupled surface waves, and it could be represented in a closed form of the interaction of such surface waves. Kelvin-Helmholtz instability is shown to be caused by the interaction of two out-of-phase surface waves with the same amplitude which are placed at $x = \pm a$ $[v_0''(x) \neq 0]$.

5.3 Model equations for resistive wall mode

Here we will regard the RWM as a current driven, ideal external kink mode in a low β plasma for simplicity. By neglecting the plasma resistivity, the linearized reduced MHD equations for a static incompressible low β plasma are shown as (see Chap. 2)

$$\partial_t \Delta\phi = \frac{1}{\mu_0\rho_0}\left(\boldsymbol{B}_0 \cdot \nabla\Delta\psi + \boldsymbol{B}_1 \cdot \nabla\Delta\psi_0\right), \tag{5.22}$$

$$\partial_t \psi = \boldsymbol{B}_0 \cdot \nabla\phi. \tag{5.23}$$

Combining them yields

$$\partial_t^2 \psi = \frac{1}{\mu_0\rho_0}(\boldsymbol{B}_0 \cdot \nabla\Delta^{-1}\boldsymbol{B}_0 \cdot \nabla\Delta\psi + \boldsymbol{B}_0 \cdot \nabla\Delta^{-1}\boldsymbol{B}_1 \cdot \nabla\Delta\psi_0), \tag{5.24}$$

where ϕ and ψ denote the stream function and the poloidal flux function, respectively.

On the other hand, by writing the wall permeability and resistivity as μ_w and η_w, the simple diffusion equation,

$$\partial_t \psi = \frac{\eta_\mathrm{w}}{\mu_\mathrm{w}}\Delta\psi, \tag{5.25}$$

holds in the resistive wall. Since the order of time derivative differs between the evolution equation of the plasma and that of the resistive wall, we formally adjust

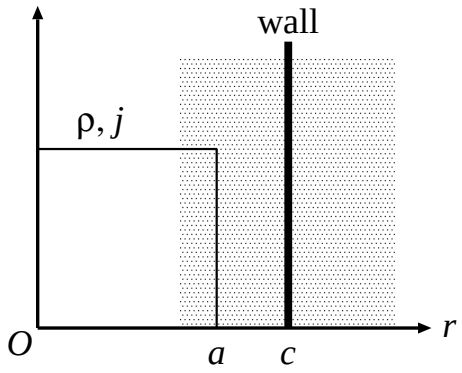

Figure 5.4: The profile of density and current of the cylindrical plasma.

the order of them by taking the time derivative on both side of Eq. (5.25) and combine these equations as

$$\partial_t^2 \psi = \frac{\chi}{\mu_0 \rho_0} \left[\boldsymbol{B}_0 \cdot \nabla \Delta^{-1} \boldsymbol{B}_0 \cdot \nabla \Delta \psi - \mathcal{L}_{\mathrm{K}} \psi \right] + \chi^* (\varepsilon \partial_t \Delta \psi - \partial_t \boldsymbol{v}_0 \cdot \nabla \psi), \qquad (5.26)$$

where we have introduced the driving operator of the kink instability $\mathcal{L}_{\mathrm{K}}\psi = \boldsymbol{B}_0 \cdot \nabla \Delta^{-1} \boldsymbol{B}_1 \cdot \nabla \Delta \psi_0$, χ is the function which has the value 1 in the plasma and 0 in the resistive wall, respectively, and vice versa for χ^*. We have assumed that the plasma is rigidly moving in the axial direction with velocity $\boldsymbol{v}_0$ with respect to the wall, and Eq. (5.26) is written in the rest frame of the plasma. In Eq. (5.26), $\varepsilon = \eta_{\mathrm{w}}/\mu_{\mathrm{w}}$.

In this formal evolution equation, the time derivative is included in the right hand side. It is because the resistive wall has its own time scale which is different from that of the plasma, and it reacts differently depending on the frequency of fluctuations. That is, the magnetic fluctuation cannot deeply penetrate into the wall if the frequency of the fluctuation is high, and the wall behaves as the conductor with less penetrativity, while it behaves as vacuum-like with allowing the magnetic field penetration more easily if the frequency is very low. Therefore, with the above formal evolution equation, it is very difficult to evaluate the mirror current directly by keeping the time derivative. We will study behavior of eigenmodes by assuming the exponential dependence $\psi \propto e^{\gamma t}$ for fluctuations.

5.4 Surface current model

Consider a one dimensional straight cylindrical plasma with radius a surrounded by a concentric conducting wall whose radius and thickness are c ($> a$) and δ ($\ll a$), respectively. Profiles of density and current of the plasma are assumed to be constant as in Fig. 5.4. In this case, wave numbers m and k_z in azimuthal (θ)

and axial (z) directions become good quantum numbers, which reduces Eq. (5.24) and yield

$$\left(1+\frac{\mu_0\rho_0\gamma^2}{F^2}\right)\Delta\psi=\frac{m\mu_0 j_0'(r)}{rF(r)}\psi, \tag{5.27}$$

where $F=mB_{0\theta}/r+k_zB_{0z}$ with the subscript 0 denoting the equilibrium quantity. Prime denotes the derivative with respect to radial coordinate r, and γ denotes the aforementioned time constant (growth rate). Hereafter, we will omit the subscript 1 denoting perturbations for simplicity. Since the safety factor is assumed constant in the whole plasma, the Alfvén velocity does not vary in space. Therefore, Alfvén continuum is shrinked to give point spectra in this system.

Under these assumptions, the system gives just Laplace equation

$$\Delta\psi=0, \tag{5.28}$$

both in plasma ($r<a$) and in vacuum ($r>a$) [62]. A dispersion relation is given by the connection conditions at the plasma edge and the resistive wall which lead to

$$\psi'(a+)-\left(1+\frac{\mu_0\rho_0\gamma^2}{F^2}\right)\psi'(a-)=-\frac{m\mu_0 j_0}{aF}\psi(a), \tag{5.29}$$

$$\left.\frac{\mathrm{d}\psi}{\mathrm{d}r}\right|_{c+}-\left.\frac{\mathrm{d}\psi}{\mathrm{d}r}\right|_{c-}=\frac{\bar{\gamma}\tau_{\mathrm{w}}}{c}\psi(c), \tag{5.30}$$

where $\tau_{\mathrm{w}}=c\delta\mu_{\mathrm{w}}/\eta_{\mathrm{w}}$ and δ denotes the thickness of the wall. Here we have used the solutions of vacuum region ($a<r<c$) and inside the wall region ($c<r<c+\delta$), which are expressed with $r^{\pm m}$ and the Bessel functions, respectively. For the thickness of the wall, $\delta\ll c$ is assumed. It is noted that, since the equations are written in the rest frame of the plasma, the connection condition (5.30) contains the Doppler shifted mode growth rate $\bar{\gamma}\equiv\gamma+\mathrm{i}\Omega$, where $\Omega=\boldsymbol{k}\cdot\boldsymbol{v}_0$ denotes the axial flow velocity of the plasma column normalized by the wave number. The eigenfunction describing the surface current at the plasma edge and at the wall has a physical meaning that the plasma surface current tends to be kink unstable, while the wall surface current tends to suppress it.

Since the inner region (resistive wall) equation is described by the field diffusion equation, the formulation is rather simple here comparing with the resistive instabilities which contains the resistivity of the plasma itself [68, 4, 5, 24]. The time scale of RWM is proportional to the resistive skin time of the wall, while resistive instabilities are described by some fractions of the combination of resistivity and Alfvén time due to the coupling of the plasma motion and resistivity even inside the inner region.

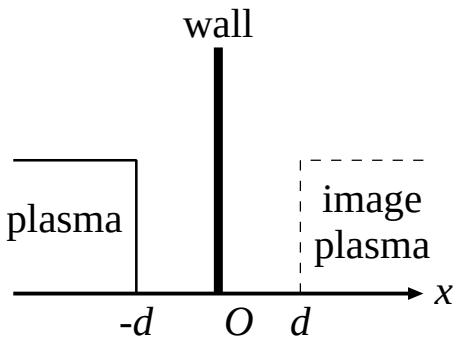

Figure 5.5: A slab model for the calculation of mirror image current.

5.5 Non-Hermiticity of resistive wall mode

In this section, we will discuss the non-Hermiticity on the linear stability problem of RWMs. We have shown in Sec. 5.2 that, as an example for the treatment of non-Hermitian operator, the Kelvin-Helmholtz instability could be described by an interaction of two out-of-phase surface waves with the same amplitude. We will show here that the RWM could also be described as an interaction of two out-of-phase surface waves with the same amplitude in a certain situation.

5.5.1 Calculation of image current in slab geometry

In order to make a comparison between image current and plasma surface current, we will stretch and approximate the shaded region in Fig. 5.4 by a slab geometry as shown in Fig. 5.5. If the radial characteristic length, $1/k_r$, of the unstable mode is much smaller than the radius of the plasma column ($k_r a \gg 1$), we can approximate even the plasma region by a slab geometry with keeping the kink driving term. We will take the origin $x = 0$ at a position of the wall, and assume the plasma to be confined at $x \leq -d$. The connection conditions (5.29) and (5.30) are then written as

$$\psi'(-d+) - \left(1 + \frac{\mu_0 \rho_0 \gamma^2}{F^2}\right) \psi'(-d-) = -\frac{k\mu_0 j_0}{F} \psi(-d), \tag{5.31}$$

$$\left.\frac{\mathrm{d}\psi}{\mathrm{d}x}\right|_{0+} - \left.\frac{\mathrm{d}\psi}{\mathrm{d}x}\right|_{0-} = \frac{\bar{\gamma}\tau_{\mathrm{w}}}{d} \psi(0), \tag{5.32}$$

where $\tau_{\mathrm{w}} = d\delta\mu_{\mathrm{w}}/\eta_{\mathrm{w}}$.

No wall case If the system does not have any conducting wall, the eigenstate is expressed by the surface current flowing on plasma edge;

$$j = \delta(x + d), \tag{5.33}$$

where the corresponding eigenvalue is evaluated as

$$\gamma^2 = \frac{F}{\mu_0 \rho_0}(\mu_0 j_0 - 2F). \tag{5.34}$$

The first term in the expression of the growth rate denotes the destabilizing effect due to the plasma current, and the second one denotes the stabilizing effect due to the Alfvén wave, respectively. Hereafter, we assume for the normalization that the coefficient of the surface current perturbation given by the δ function at the plasma edge to be unity as in Eq. (5.33).

Ideal wall case By assuming the ideal conducting wall at $x = 0$, the boundary condition becomes

$$\tilde{\psi}|_{x=0} = 0, \tag{5.35}$$

which can be represented by assuming the wall current

$$j_{\mathrm{w}} = -e^{-kd}\delta(x). \tag{5.36}$$

The wall current at $x = 0$ can be moved to $x = d$ with keeping the same magnetic field in $x < 0$ as

$$j_{\mathrm{im}}^{(\mathrm{i})} = -\delta(x - d). \tag{5.37}$$

Since the ideal wall does not have its own time constant, it reacts in the same way as for any frequency of magnetic perturbation. Thus, the mirror image current flows in the opposite direction with the same amplitude as the surface current of plasma which is independent of the frequency. Then, corresponding eigenvalues are given by

$$\gamma^2 = \frac{F}{\mu_0 \rho_0}\Big(\mu_0 j_0 - \frac{2F}{1 - e^{-2kd}}\Big). \tag{5.38}$$

Comparing with Eq. (5.34), the effect of conducting wall appears in the second stabilizing term here, which becomes larger than the previous no wall case. Hereafter, we will mainly consider the following parameter regime

$$\frac{2F}{\mu_0} < j_0 < \frac{2F}{\mu_0(1 - e^{-2kd})}, \tag{5.39}$$

where the external kink mode is unstable without the wall [Eq. (5.34)], while for the case with the ideal wall [Eq. (5.38)], it is stable.

Resistive wall case If we put the resistive wall at $x = 0$, the connection condition

$$\left.\frac{\mathrm{d}\tilde{\psi}}{\mathrm{d}x}\right|_{0+} - \left.\frac{\mathrm{d}\tilde{\psi}}{\mathrm{d}x}\right|_{0-} = \frac{\bar{\gamma}\tau_{\mathrm{w}}}{d}\tilde{\psi}(0), \tag{5.40}$$

will be replaced by the following mirror image current;

$$j_{\mathrm{im}}^{(\mathrm{r})} = -\left(1 + \frac{2kd}{\bar{\gamma}\tau_{\mathrm{w}}}\right)^{-1}\delta(x-d), \tag{5.41}$$

instead of Eq. (5.37). Note that the amplitude and phase of the image current now depends on the time constant of the unstable mode.

With the Alfvén time $\tau_{\mathrm{A}}^2 = \mu_0\rho_0/F^2$, the growth rate γ and axial flow frequency Ω are normalized as

$$\hat{\gamma} = \gamma\tau_{\mathrm{A}}, \quad \hat{\Omega} = \Omega\tau_{\mathrm{A}}. \tag{5.42}$$

By further introducing $\epsilon = \tau_{\mathrm{A}}/\tau_{\mathrm{w}}$ as an expanding parameter, the dispersion relation leads to the third order algebraic equation in the form of

$$A\hat{\gamma}^2(\hat{\gamma} + \mathrm{i}\hat{\Omega}) + \epsilon B\hat{\gamma}^2 + C(\hat{\gamma} + \mathrm{i}\hat{\Omega}) + \epsilon D = 0, \tag{5.43}$$

where

$$\begin{aligned} A &= 1 - e^{-2kd}, \\ B &= 2kd, \\ C &= \left[2 - \frac{\mu_0 j_0}{F}(1 - e^{-2kd})\right], \\ D &= 2kd\left(2 - \frac{\mu_0 j_0}{F}\right). \end{aligned}$$

Let us check the sign of them for the following analysis; $A > 0$ and $B > 0$ are always valid. From the condition (5.39), it can be concluded that $D < 0$ holds since the external kink mode is unstable without the wall, and that $C > 0$ holds since it is stabilized by introducing the ideal wall. In summary, the signs of the coefficients in the dispersion relation (5.43) satisfy

$$A > 0, \quad B > 0, \quad C > 0, \quad D < 0, \tag{5.44}$$

in our parameter regime.

5.5.2 Behavior of eigenvalue and eigenvector of resistive wall mode

Let us solve analytically the dispersion relation (5.43) by means of perturbation method under $\epsilon \ll 1$. In the following, we will omit the hat on the eigenvalues for

simplicity. By expanding the eigenvalue as

$$\gamma = \gamma_0 + \epsilon\gamma_1 + \cdots, \tag{5.45}$$

we have three solutions in $O(1)$ as

$$\gamma_0 = \pm \mathrm{i}\sqrt{\frac{C}{A}}, -\mathrm{i}\Omega. \tag{5.46}$$

Taking the next order in $O(\epsilon)$, they are written as

$$\gamma^{(0)} = -\mathrm{i}\Omega - \epsilon\frac{B\Omega^2 - D}{A\Omega^2 - C}, \tag{5.47}$$

$$\gamma^{(\pm)} = \pm\mathrm{i}\sqrt{\frac{C}{A}} \mp \epsilon\frac{BC - AD}{2A\sqrt{C}(\pm\sqrt{C} + \sqrt{A}\Omega)}. \tag{5.48}$$

Due to the signs of the coefficients shown in Eq. (5.44), we see that $B\Omega^2 - D > 0$ and $BC - AD > 0$ hold. Moreover, since $A\Omega^2 - C$ gives

$$\lim_{kd\to 0}(A\Omega^2 - C) = -2, \tag{5.49}$$

$\gamma^{(0)}$ gives the unstable solution for small kd, while other two roots $\gamma^{(\pm)}$ give the damped oscillations. However, it can be seen from Eqs. (5.47) and (5.48) that the denominator of γ_1 has zero while the numerator keeps $B\Omega^2 - D > 0$ from the conditions $B > 0$ and $D < 0$.

It means that the perturbation expansion breaks down in the regime $A\Omega^2 - C \sim O(\epsilon^{-1})$. The position of the wall which gives zero of the denominator will be evaluated by solving $A\Omega^2 - C \sim 0$ for kd as

$$kd \sim -\frac{1}{2}\log\Big[1 - 2\Big(\Omega^2 + \frac{\mu_0 j_0}{F}\Big)^{-1}\Big]. \tag{5.50}$$

After exceeding this value and $A\Omega^2 - C \sim O(1)$ holds again, then $\gamma^{(0)}$ turns out to show damping and $\gamma^{(-)}$ represents unstable RWM which relates to the ideal external kink mode. On the other hand, $\gamma^{(+)}$ shows always damping, and it does not have any break down of the perturbation method.

In order to investigate the detailed behavior of eigenmodes near the wall position expressed in Eq. (5.50), we will show the numerical results of Eq. (5.43) in Figs. 5.6 and 5.7. Analytic solutions $\gamma^{(0)}$ and $\gamma^{(-)}$ are also plotted in them. Numerical calculation is carried out for the parameter $\tau_\mathrm{w}/\tau_\mathrm{A} = 10^4$, $\mu_0 j_0/F = 2.01$, and $\Omega = 0.15$. In this case, the stabilizing parameter regime for the external kink mode with the surrounding ideal wall is evaluated from Eq. (5.39) as

$$kd \lesssim 2.65. \tag{5.51}$$

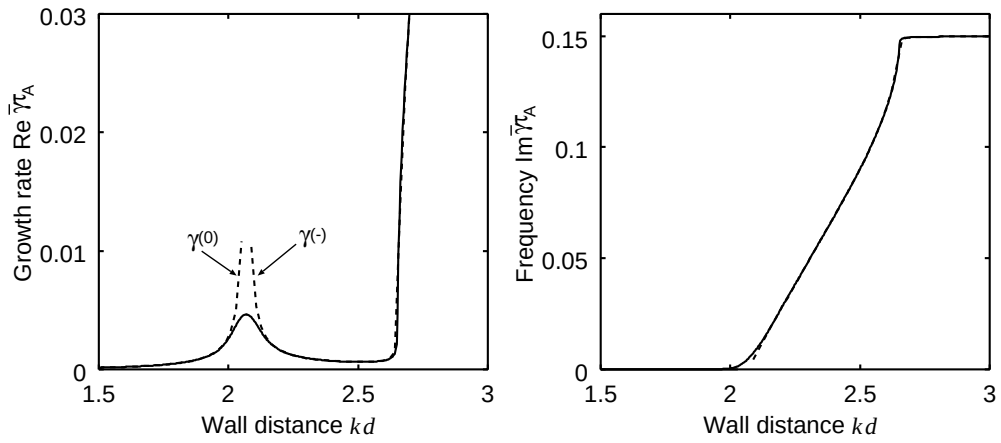

Figure 5.6: Real and imaginary part of the eigenvalue of the dispersion relation (5.43), which corresponds to the unstable RWM.

The large growth rate for the wall position $kd \gtrsim 2.65$ in Fig. 5.6 corresponds to the ideal external kink mode. For the imaginary part of the eigenvalue (frequency), it is seen that the external kink mode moves together with the plasma for $kd \gtrsim 2.65$. The wall position corresponding to the break down of the perturbation expansion is evaluated from Eq. (5.50) as

$$kd \sim 2.07. \tag{5.52}$$

As described in Sec. 5.1, we see in Fig. 5.6 that a small hump of the growth rate in the kink stable region (5.51) of the wall position approximately coincides with the break down point of the perturbation expansion [Eq. (5.52)].

With the numerical solutions, we have evaluated the amplitude and phase of the mirror image current compared to the plasma surface current by using Eq. (5.41) (see Fig. 5.7). It is seen that the amplitude of the image current becomes smaller when they are closer, while the interaction of two surface waves becomes stronger then. Therefore, the RWM in the wall position closer than the value (5.52) is caused by the decrease of the image current which has the effect to stabilize the external kink mode by suppressing the perturbed plasma surface current [10]. However, it is not the case with the wall position $kd \gtrsim 2$.

It is found that the amplitude of the image current is almost unity for the wall position $kd \gtrsim 2$ in Fig. 5.7. Moreover, it is clearly seen from Fig. 5.7 that the phase shift is quite localized at the wall position where the perturbation expansion breaks down, which has not been obtained by the analytic solution $\gamma^{(0)}$. The phase shift is evaluated to be relatively small, i.e. few degrees, which comes from the smallness of the expansion parameter $\epsilon \sim 10^{-4}$. Even for the small but finite phase shift, the interaction of two surface waves in the RWM contains a similar effect to the Kelvin-

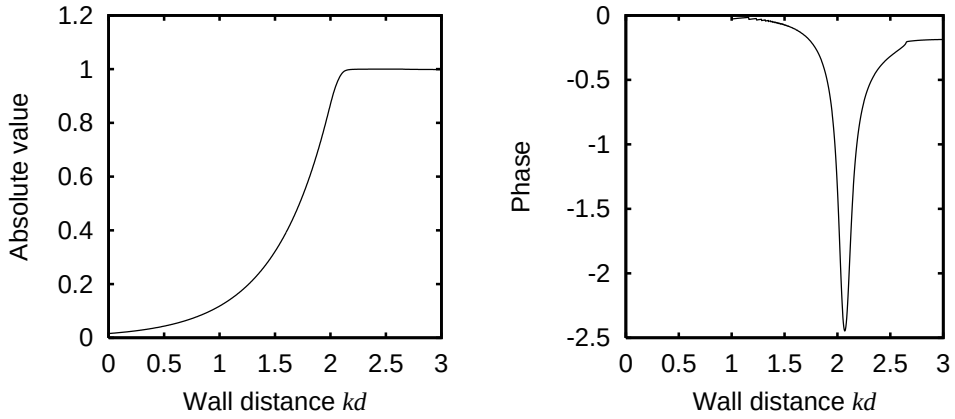

Figure 5.7: Amplitude and phase of the mirror image current relative to plasma surface current obtained with Eq. (5.41). The phase is described in the unit of degree.

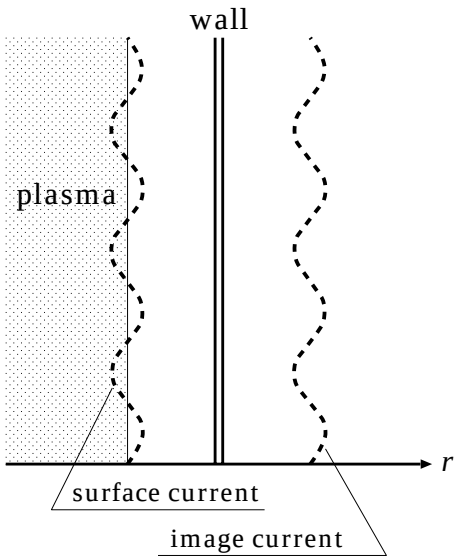

Figure 5.8: Schematic view of the destabilizing mechanism of RWM.

Helmholtz instability, which is another destabilizing mechanism for the RWM as shown in Fig. 5.8.

5.6 Summary

In this chapter, we have analyzed the resistive wall mode (RWM) in the rigidly flowing plasma surrounded by the conducting wall and investigated the situation where non-Hermiticity plays an important role for the destabilization mechanism.

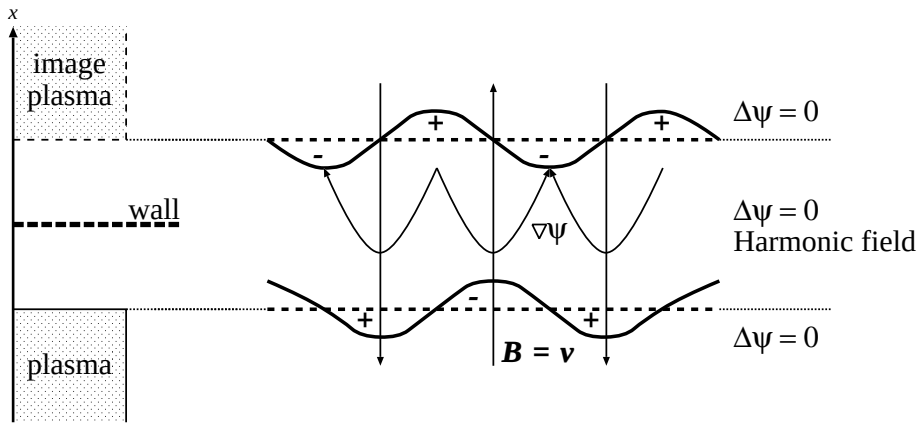

Figure 5.9: Physical mechanism of the destabilizing effect of the RWM. Two surface waves are connected by the harmonic field, which is the same as the Kelvin-Helmholtz instability in neutral fluids.

When the plasma is static with respect to the resistive wall, the amplitude of mirror image current is small due to resistivity, and has the same phase as that of the plasma surface current. When the plasma is rigidly flowing with respect to the resistive wall, the phase shift arises between the plasma surface current and the mirror image current, which brings about the destabilization with a positive feedback mechanism in the same way as Kelvin-Helmholtz instability in neutral fluids. This destabilizing effect creates the small hump of the growth rate depending on the wall position (see Figs. 5.1 and 5.6).

We have derived a third order algebraic dispersion relation of RWM for a simplified slab model, and solved it analytically by means of perturbation expansion as Eqs. (5.47) and (5.48). Analytic solution $\gamma^{(0)}$ does not contain any phase shift, however, we found that the perturbation expansion breaks down due to zero of the denominator at a certain wall position [Eq. (5.50)]. By numerically solving the dispersion relation, the eigenvalue $\bar{\gamma}$ becomes a complex number for the break down condition, which actually gives a substantial phase shift between plasma surface current and mirror image current.

The destabilizing mechanism of RWM can be qualitatively explained as follows. In the situation illustrated in Fig. 5.5, the system has a homogeneous current density j_{0z} in the region $x < -d$ and $d < x$. When we distort the surfaces at $x = \pm d$ as illustrated in Fig. 5.9, positive and negative localized surface current streets are alternatively produced with the wave form. Let us consider the effect of upper surface current on the lower one in the situation shown in Fig. 5.9. Since the region between the two surface current streets are vacuum, the eigenmode of the magnetic

fluctuation satisfies the Laplace equation

$$\Delta\psi = 0, \tag{5.53}$$

in this region. Therefore, harmonic field of the perturbed flux function ψ appears between the two surface current streets. The gradient field $\nabla\psi$ governs the structure of magnetic perturbation as illustrated in Fig. 5.9. Since the magnetic fluctuation is expressed by

$$\boldsymbol{B} = \nabla\psi \times \boldsymbol{e}_z, \tag{5.54}$$

where $\boldsymbol{B}$ is perpendicular to the field $\nabla\psi$ in the xy-plane. For the Alfvén wave branch, since the plasma is frozen in the magnetic field, the direction of the perturbed magnetic field is parallel to the velocity field, whose profile corresponds to the amplification of the accompanying out-of-phase surface current. The lower surface current in Fig. 5.9 will produce the velocity field which amplifies the upper one, and vice versa. Thus, these two surface waves become unstable by amplifying each other.

In previous papers, when the system contains any continuous spectra, it is expected that the RWM is stabilized due to the rigid flow for the outer wall position than that corresponding to the small hump of the growth rate. Therefore, it may be concluded that the resistive wall should be placed at somewhat outer position than that expressed by Eq. (5.50) in order to obtain the stabilizing effect. The expression (5.50) shows that, if the flow velocity is increased, kd becomes small and closer to zero. This means that the wall position which gives the extremum of the growth rate will become closer to the plasma edge; however, the dependence is weak as is expressed from the logarithmic function. Thus, the flow velocity of the plasma does not affect the result significantly.

Chapter 6

Interchange instabilities of slab plasmas with sheared flows

6.1 Introduction

It is widely accepted that a shear flow yields stabilizing effects on various fluctuations through convective deformations of disturbances [97, 99, 136]. However, rigorous treatment of the shear flow effects encounters a serious difficulty arising from the non-Hermiticity of the problem. We may not consider well-defined 'modes' and corresponding 'time constants.' The standard normal mode approach breaks down, and the theory may fail to give correct predictions of evolution even if perturbed fields remain in the linear regime. The discrepancies between the theory and the experiment on the stability limit of neutral fluids are reviewed in Ref. [140, 115]. The aim of this work is to establish a solid foundation for the analysis of shear flow systems. We apply Kelvin's method of shearing modes [139]. This scheme, previously called as 'nonmodal' approach, actually consists in the combination of two methods which have been widely used in solving wave equations; the modal and the characteristics methods.

Many works have been done on instability problems of plasmas with shear flows by means of the simple 'modal' approach. It is implicitly assumed in the application of the modal scheme that the motion can be decomposed into a set of independent 'normal modes' with certain time constants [77, 43]. As is well-known, this method is effective in solving problems involving Hermitian operators. However, when applying it to non-Hermitian systems, we may overlook the secular and transient behaviors. On the other hand, the characteristics method has been used in the context of rapid distortion theory for the fluid turbulence [114] and in the eikonal representation of the ballooning mode stability [79]. If we can treat the non-Hermitian part of the

whole operator as a singular perturbation to the Hermitian operator [66, 68, 151], we may be able to construct a theory in the framework of the perturbation theory for the operator [18]. But unfortunately the convergence of the perturbative series seems to be very ambiguous in case of the shear flows due to the secularity of their time evolutions [33, 84, 152]. Thus, a thorough mathematical treatment of the non-Hermitian operators of shear flow systems has not been accomplished so far. In this chapter, we have analyzed the shear flow effect on interchange instabilities and its non-Hermitian mathematical background with the time asymptotic behavior by means of Kelvin's method.

Recently, Kelvin's method has been applied to a variety of linear shear flow problems [57, 52, 53, 112, 100, 137, 143]. For neutral and magnetized fluids, many new fascinating phenomena were discovered; exchanges of energy between background flows and perturbed fields [53], shear flow induced coupling between sound waves and internal waves and the excitation of beat wave [112], the asymptotic persistence due to the periodic energy transfer for two dimensional shear flows [100], and the emission of magnetosonic waves by the stationary vortex perturbations [137]. These results show that the modes, which are independent for static fluids, are no longer independent and the coupling of these modes induces the energy transfer in the presence of the shear flow. The basic properties of kink-type instabilities in the presence of a background shear flow is also analyzed [143]. It is shown that the shear flow mixing always overcomes the kink driving at sufficiently large time. However, the mathematical significance of this method has not been clarified yet.

In this chapter, we will first revisit Kelvin's method from the viewpoint of the characteristics method in Sec. 6.2. We will review the spectral theory focusing on the general mathematical concept of eigenmode for a better understanding of Kelvin's method. In Sec. 6.3, we will give the equations governing the interchange instabilities. In Sec. 6.4, we will derive the ordinary differential equation (ODE) for the time evolution of the amplitude of the interchange instabilities by applying the analysis of shearing modes. In Sec. 6.5, by drawing an analogy with Newton's equation it will be shown that the solution to the above ODE for the flux function exhibits an asymptotic damped behavior for any strength of instability drive. We will also consider the electrostatic perturbations in Sec. 6.6. Here the solution of the derived ODE for the stream function shows the asymptotic growth or decay of algebraic type depending on the magnitude of instability drive. The difficulty encountered by including the magnetic shear in the present formulation is addressed in Sec. 6.7. We will summarize the obtained results in Sec. 6.8.

6.2 Non-Hermiticity of shear flow systems

Before formulating the interchange instability equations, let us give a rough sketch of the problem and explain the mathematical tool to analyze the non-Hermitian dynamics. As is well known, the force operator governing the linear dynamics of static MHD plasmas is Hermitian [10], and therefore the perturbed fields can be decomposed into a set of orthogonal eigenmodes which show purely exponential (unstable) or purely oscillating (stable) evolutions. A non-triviality stems from the Alfvénic and acoustic continuous spectra; the phase mixing damping occurs. This behavior, however, is totally within the framework of the well-known theory of Hermitian operators due to von Neumann [28].

In the case where ambient the shear flow exists, however, the operator becomes non-Hermitian and the resolution in terms of orthogonal eigenmodes fails. From a dynamical point of view, the system experiences a complex type of non-exponential evolutions. In the following sections, we will show examples of such kind of 'non-Hermitian' dynamics where transient phenomena and secular evolutions play a dominant role. Similar evolutions are found in the case of non-Hermitian operators in finite dimensional vector spaces [61]. It is emphasized that the application of the traditional modal paradigm to non-Hermitian systems, which assumes exponential evolution of the perturbed fields, hinders these rich varieties of transient and algebraic phenomena. In this section, we will discuss Kelvin's method and show its suitability to the analysis of shear flow induced non-Hermitian systems. We will revisit it from the viewpoint of the characteristics method showing that it represents a generalization of the modal approach.

The linearized dynamics of fluid systems in the presence of sheared flow is governed by a general equation of the following type;

$$\partial_t u + \boldsymbol{v} \cdot \nabla u = \mathcal{A} u, \tag{6.1}$$

where $\mathcal{A}$ denotes a Hermitian differential operator (time-independent) defined in a Hilbert space V, $\boldsymbol{v}$ is the stationary mean flow, and u ($\in V$) denotes a perturbed field.

It is the convective derivative, $\boldsymbol{v} \cdot \nabla$, that introduces the non-Hermiticity into problem (6.1) and prevents the possibility of representing the dynamics of the systems in terms of orthogonal and complete set of eigenfunctions. This is a well known difficulty in the stability analysis of neutral fluids, such as Couette or Poiseille flows, where the predictions obtained by means of the modal methods do not match the experiments [140, 115].

In the case of a spatially inhomogeneous stationary flow $\boldsymbol{v}$, Eq. (6.1) becomes

non-Hermitian and a straightforward spectral resolution is not effective. However, Kelvin's method permits to resolve, for some classes of mean flows, the evolution of the system (6.1) into new types of modes by means of which both transient and secular asymptotic behaviors are effectively described. Let us now explain mathematical foundations of this scheme.

As mentioned in Sec. 6.1, Kelvin's method consists in the combined application of two methods which have been extensively used in the analysis of wave equations. Precisely the 'Lagrangian' part of Eq. (6.1), $\partial_t + \boldsymbol{v} \cdot \nabla$, is solved by means of the characteristics method and the 'Hermitian' part $\mathcal{A}$ by means of the standard spectral resolution.

The characteristics method is applied to solve the characteristic ODE associated to the Lagrangian derivative, which is moving along the characteristic curve of the ambient motion, given by

$$\frac{\mathrm{d}\boldsymbol{x}}{\mathrm{d}t} = \boldsymbol{v}, \quad \boldsymbol{x}(0) = \boldsymbol{\xi}. \tag{6.2}$$

By inverting the modes, which are expressed in the Lagrangian coordinates as $\varphi(\boldsymbol{k}, \boldsymbol{\xi})$, they will be represented in the Eulerian coordinates as

$$\tilde{\varphi}(t; \boldsymbol{k}, \boldsymbol{x}) = \varphi(\boldsymbol{k}, \boldsymbol{\xi}(t; \boldsymbol{x})), \tag{6.3}$$

where $\boldsymbol{\xi}(t; \boldsymbol{x})$ denotes the inverse of $\boldsymbol{x}(t; \boldsymbol{\xi})$. The existence of the inverse mapping $\boldsymbol{x}(t) \mapsto \boldsymbol{\xi}$ is guaranteed in the case of incompressible mean flows. Due to Eq. (6.3), $\tilde{\varphi}(t; \boldsymbol{k}, \boldsymbol{x})$ satisfies the characteristic equation

$$\partial_t \tilde{\varphi}(t; \boldsymbol{k}, \boldsymbol{x}) + \boldsymbol{v} \cdot \nabla \tilde{\varphi}(t; \boldsymbol{k}, \boldsymbol{x}) = 0. \tag{6.4}$$

The essential condition for the applicability of Kelvin's method consists in the constraint for the functions $\tilde{\varphi}(t; \boldsymbol{k}, \boldsymbol{x})$ to form the complete set of eigenfunctions of the operator $\mathcal{A}$. If such a set of eigenfunctions exists, we can decompose the perturbed field u by means of

$$u = \int \tilde{u}_k(t)\, \tilde{\varphi}(t; \boldsymbol{k}, \boldsymbol{x})\, \mathrm{d}\boldsymbol{k}. \tag{6.5}$$

We notice that due to Eq. (6.3) the eigenvalues of $\mathcal{A}$ become time dependent. The new eigenvalue problem for $\mathcal{A}$ reads

$$\mathcal{A}\tilde{\varphi}(t; \boldsymbol{k}, \boldsymbol{x}) = \lambda_k(t)\, \tilde{\varphi}(t; \boldsymbol{k}, \boldsymbol{x}). \tag{6.6}$$

Plugging Eq. (6.5) into Eq. (6.1) and exploiting Eqs. (6.4) and (6.6), we have

$$\int [\partial_t \tilde{u}_k(t)]\, \tilde{\varphi}(t; \boldsymbol{k}, \boldsymbol{x})\, \mathrm{d}\boldsymbol{k} = \int \tilde{u}_k(t) \lambda_k(t)\, \tilde{\varphi}(t; \boldsymbol{k}, \boldsymbol{x})\, \mathrm{d}\boldsymbol{k}. \tag{6.7}$$

Due to the orthogonality of the modes $\tilde{\varphi}(t; \boldsymbol{k}, \boldsymbol{x})$, the evolution of $\tilde{u}_k$ is governed by the equation

$$\frac{\mathrm{d}}{\mathrm{d}t}\tilde{u}_k(t) = \lambda_k(t)\, \tilde{u}_k(t). \tag{6.8}$$

If $\tilde{\varphi}(t; \boldsymbol{k}, \boldsymbol{x})$ do not satisfy both conditions given by the characteristic equation (6.4) and the eigenvalue equation (6.6), Eq. (6.7) includes additional terms representing the complicated mode coupling. Thus, the applicability of Kelvin's method is compromised in this case.

Due to the time dependence in the eigenvalues $\lambda_k(t)$, the evolution of $\tilde{u}_k(t)$ will not exhibit a simple exponential dependence as in the Hermitian case. More complicated behaviors appear, which are characteristic of non-Hermitian systems. By analyzing the ODE (6.8), the motion of each mode can be classified, and the time asymptotic behavior can be also shown. The following sections will be devoted to the derivation of ODE (6.8) and the discussion of the behavior of its solution for the case of interchange instabilities in plasmas with shear flow.

6.3 Formulation of interchange instabilities

Interchange instabilities have been analyzed for static (ambient flow $\boldsymbol{v}_0 = 0$) magnetized plasmas by many authors [40, 96, 127, 103, 133]. In the case of static plasmas, the ideal MHD equations can be reduced into a simple partial differential equation of the form [10]

$$\partial_t^2 \boldsymbol{\xi} = \mathcal{F}\boldsymbol{\xi}, \tag{6.9}$$

where $\boldsymbol{\xi}$ is the displacement vector and $\mathcal{F}$ is the force operator which is Hermitian (selfadjoint) when the plasma is surrounded by an ideal conducting wall. In order to analyze the stability of the system, we can apply the spectral method and represent the dynamics in terms of a superposition of harmonic oscillations of normal modes. Another method of analyzing the stability of the static magnetized plasmas is to apply the energy principle [40, 96] which is a variational approach based on the Hermiticity of the force operator $\mathcal{F}$. These methods show that the unstable interchange modes have extremely spatially localized structures near the marginal stability [127, 103] except when $p' \simeq 0$ on the rational surface [133] (see Chap. 3).

It is remarkably difficult to estimate the exact linear stability of the system in the presence of a stationary shear flow, since, as seen in the previous sections, the dynamics become non-Hermitian and both the spectral and the variational methods lose their mathematical foundations. Dispersion relations have been studied in many publications [66, 97, 77, 43], however, as discussed in Sec. 6.1, the evolution of non-Hermitian system cannot be reconstructed from the formal dispersion relation,

because we do not have a spectral theory. Since the proper asymptotic behavior of interchange instabilities are not yet clearly shown in the presence of shear flow, we will first analyze simplified systems focusing on the non-Hermiticity of the system. In this section, we will derive the governing equations for magnetized plasmas with stationary shear flows. Specifically, we will investigate the effect of shear flow on interchange instabilities in plasmas with an ambient homogeneous magnetic field.

In the presence of gravitational force, the ideal incompressible MHD equations are written as

$$\rho \frac{\mathrm{d}\boldsymbol{v}}{\mathrm{d}t} = \boldsymbol{j} \times \boldsymbol{B} - \nabla p + \rho \boldsymbol{g}, \tag{6.10}$$

$$\frac{\mathrm{d}\rho}{\mathrm{d}t} + \rho \nabla \cdot \boldsymbol{v} = 0, \tag{6.11}$$

$$\partial_t \boldsymbol{B} - \nabla \times (\boldsymbol{v} \times \boldsymbol{B}) = \boldsymbol{0}, \tag{6.12}$$

$$\nabla \cdot \boldsymbol{v} = 0, \tag{6.13}$$

where ρ, $\boldsymbol{B}$, and $\boldsymbol{g}$ are the density, magnetic field, and gravitational constant vector, and $\mathrm{d}/\mathrm{d}t = \partial_t + \boldsymbol{v} \cdot \nabla$ denotes the Lagrangian derivative. Here we assume the incompressibility of the velocity field $\boldsymbol{v}$, instead of using the equation of state.

The ambient fields (denoted by the subscript 0) must satisfy

$$\rho_0 \boldsymbol{v}_0 \cdot \nabla \boldsymbol{v}_0 = \boldsymbol{j}_0 \times \boldsymbol{B}_0 - \nabla p_0 + \rho_0 \boldsymbol{g}. \tag{6.14}$$

If we consider a parallel stationary shear flow of the form $\boldsymbol{v}_0 = (0, v_y(x), 0)$, straight homogeneous magnetic field $\boldsymbol{B}_0 = (0, B_y, B_z)$, and gravitational force acting in the positive x direction, the convective derivative gives no contribution to the stationary state and Eq. (6.14) is reduced to

$$\nabla p_0 = \rho_0 \boldsymbol{g}. \tag{6.15}$$

The above equation denotes that the pressure gradient is balanced by the gravitational force in the x direction. This is the same condition which holds for static neutral fluids.

The perturbed magnetic and velocity fields are assumed to be two dimensional in the xy plane, and thus we can introduce the poloidal flux function and stream function;

$$\begin{aligned} \boldsymbol{B}_{1\perp} &= \nabla \psi \times \boldsymbol{e}_z, \\ \boldsymbol{v}_{1\perp} &= \nabla \phi \times \boldsymbol{e}_z, \end{aligned} \tag{6.16}$$

where the subscript 1 denotes the perturbed quantities, $\perp$ expresses the direction perpendicular to the dominant magnetic field directed along the z axis, and $\boldsymbol{e}_z$

denotes the unit vector in the z direction. Using these representations, we can eliminate the pressure from governing equations.

Taking the curl of the equation of motion and projecting it along $\boldsymbol{e}_z$, we obtain

$$\mu_0\rho_0[(\partial_t + v_y\partial_y)\Delta\phi - v_y''\partial_y\phi] = \boldsymbol{B}_0 \cdot \nabla(\Delta\psi) + \mu_0\partial_y\rho_1 g, \tag{6.17}$$

where $\Delta = \partial_x^2 + \partial_y^2$. In deriving Eq. (6.17) we have used the Boussinesq approximation which neglects the spatial variation of the stationary state density in the inertial term of equation of motion, but does not in continuity equation, since it is the driving term for the interchange instability. Physically it is valid provided that the variability in the density is due to variations in the temperature of only moderate amounts [7]. The component of the flow perpendicular to the ambient magnetic field can be considered consistently coming from the $\boldsymbol{E} \times \boldsymbol{B}$ drift, taking into account the ideal Ohm's law. It is noted that, if we neglect the effect of the magnetic field, we recover Rayleigh equation for Kelvin-Helmholtz instability of the incompressible neutral fluid [9].

The density fluctuation can be expressed as

$$(\partial_t + v_y\partial_y)\rho_1 = -\rho_0'\partial_y\phi. \tag{6.18}$$

where the prime denotes the derivative with respect to x. Now ρ_0' is considered as a constant which introduces a destabilizing force. The induction equation is the same as in the ordinary reduced MHD equations [123, 124]. Under the above assumptions on the stationary fields, it reads as

$$(\partial_t + v_y\partial_y)\psi = \boldsymbol{B}_0 \cdot \nabla\phi. \tag{6.19}$$

Equations (6.17)-(6.19) constitute a closed system of equations. It is seen that the static system ($v_y = 0$) governed by these equations is Hermitian. It is the convective derivative ($v_y \neq 0$) that brings the non-Hermiticity into our system. Actually, the system of equations (6.17)-(6.19) can be obtained directly by replacing $g = 2p/\rho R_0$ in the high β reduced MHD equations describing tokamak plasmas [124], where R_0 denotes the major radius of the toroidal device. We will investigate the effect of the shear flow on the interchange instabilities in following sections.

6.4 Derivation of ordinary differential equation for Kelvin's mode

In this section, we derive the ordinary differential equation (ODE) for the amplitude of Kelvin's mode, given in Eq. (6.8), in the case of interchange instabilities of

plasmas. Let us first consider the electromagnetic case where $\boldsymbol{B}_0 \cdot \nabla \neq 0$. From Eqs. (6.18)-(6.19), we have

$$\phi = -\partial_y^{-1}\rho_0'^{-1}(\partial_t + v_y\partial_y)\rho_1 = (\boldsymbol{B}_0 \cdot \nabla)^{-1}(\partial_t + v_y\partial_y)\psi. \tag{6.20}$$

Since we have assumed the mean velocity $v_y = v_y(x)$ and the homogeneous ambient field $\boldsymbol{B}_0 = (0, B_y, B_z)$, the operator $\partial_t + v_y\partial_y$ commutes with both ∂_y^{-1} and $(\boldsymbol{B}_0 \cdot \nabla)^{-1}$. Thus acting on both sides of Eq. (6.20) with the operator $(\partial_t + v_y\partial_y)^{-1}$ gives

$$\rho_1 = -\rho_0'\partial_y(\boldsymbol{B}_0 \cdot \nabla)^{-1}\psi. \tag{6.21}$$

From Eq. (6.19),

$$\Delta\phi = \Delta(\boldsymbol{B}_0 \cdot \nabla)^{-1}(\partial_t + v_y\partial_y)\psi. \tag{6.22}$$

Substituting Eqs. (6.20) and (6.22) into Eq. (6.17), and acting with $\boldsymbol{B}_0 \cdot \nabla$ on both sides, we obtain

$$(\partial_t + v_y\partial_y)\Delta(\partial_t + v_y\partial_y)\psi = \frac{(\boldsymbol{B}_0 \cdot \nabla)^2}{\mu_0\rho_0}\Delta\psi - \frac{\rho_0' g}{\rho_0}\partial_y^2\psi. \tag{6.23}$$

It is noted that the linearity of the ambient velocity profile allows us to eliminate v_y''.

Since the operator on the right hand side is Hermitian, we can decompose the flux function ψ by means of the shearing eigenmodes

$$\psi(\boldsymbol{x}, t) = \int \tilde{\psi}_k(t)\, \tilde{\varphi}(t; \boldsymbol{k}, \boldsymbol{x})\, \mathrm{d}\boldsymbol{k}, \tag{6.24}$$

where each eigenmode can be expressed by the sinusoidal function in our simplified case

$$\begin{aligned} \tilde{\varphi}(t; \boldsymbol{k}, \boldsymbol{x}) &= \exp[\mathrm{i}k_x x + \mathrm{i}k_y(y - v_y t) + \mathrm{i}k_z z] \\ &= \exp[\mathrm{i}\tilde{k}_x(t)x + \mathrm{i}k_y y + \mathrm{i}k_z z]. \end{aligned} \tag{6.25}$$

Here the mean flow is assumed to be $v_y(x) = \sigma x$ and $\tilde{k}_x(t) = k_x - k_y\sigma t$. It is explicitly shown that the wave number in the flow shear direction is linearly increasing with time by the distortion of perturbation due to the sheared mean flow. However, the completeness of the modes $\tilde{\varphi}$ in the Hilbert space will not be lost due to the time dependent wave number $\tilde{k}_x$, therefore, the expansion (6.24) still gives a general solution of the system. Since continuous variation of $\tilde{k}_x(t)$ prevents from imposing the boundary condition in the bounded domain, we will concentrate on the analysis of localized perturbations by considering the infinite domain. Note that $\tilde{\varphi}$ are the eigenfunctions of the right hand side of Eq. (6.23), and also satisfy the characteristic equation (6.4). It should be noted that the presence of the Laplacian operator in

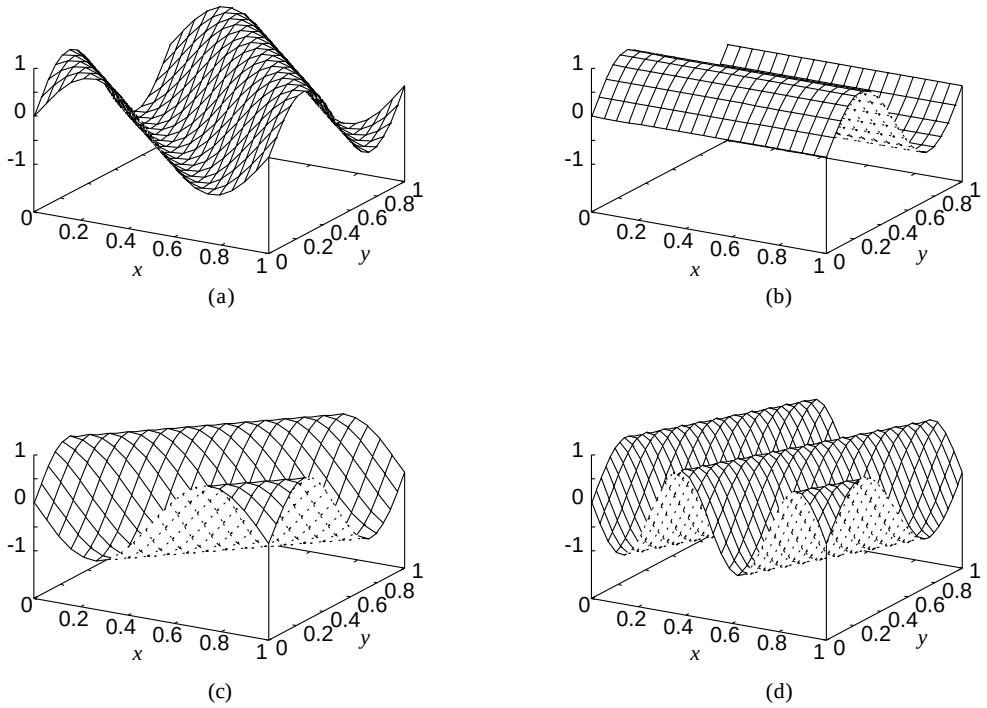

Figure 6.1: Kelvin's mode $\tilde{\varphi}(t; \boldsymbol{k}, \boldsymbol{x})$.

the left hand side of Eq. (6.23) does not hinder the application of Kelvin's method since the modes $\tilde{\varphi}$ are as well eigenfunctions of the Laplacian Δ.

Thus, the time evolution equation for the amplitude $\tilde{\psi}_k$ can be written as

$$\frac{\mathrm{d}}{\mathrm{d}t}\Big[\Big(\tilde{k}_x(t)^2 + k_y^2\Big)\,\frac{\mathrm{d}\tilde{\psi}}{\mathrm{d}t}\Big] = -\frac{F^2}{\mu_0\rho_0}\Big(\tilde{k}_x(t)^2 + k_y^2\Big)\,\tilde{\psi} - k_y^2\frac{\rho_0' g}{\rho_0}\tilde{\psi}, \tag{6.26}$$

where $F = \boldsymbol{k}\cdot\boldsymbol{B}_0 = k_y B_{0y} + k_z B_{0z}$, and we have dropped the subscript k for simplicity. We notice that in the absence of shear flow ($\sigma = 0$) the usual interchange instability equation for static equilibrium can be obtained.

Our procedure can be readily shown to coincide with the traditional formulation of Kelvin's method consisting in the coordinate transform $(t, x, y, z) \mapsto (T, \xi, \eta, \zeta)$ defined by

$$T = t, \quad \xi = x, \quad \eta = y - \sigma t x, \quad \zeta = z, \tag{6.27}$$

and the Fourier transform with respect to the new coordinates

$$\tilde{u}(k_\xi, k_\eta, k_\zeta; T) = \iiint_{-\infty}^{+\infty} u(\xi, \eta, \zeta; T)\, e^{\mathrm{i}(k_\xi\xi + k_\eta\eta + k_\zeta\zeta)}\,\mathrm{d}\xi\,\mathrm{d}\eta\,\mathrm{d}\zeta. \tag{6.28}$$

Normalizing the time t by the poloidal Alfvén time $\tau_A = a\sqrt{\mu_0\rho_0}/F$, we can rewrite Eq. (6.26) in dimensionless form as

$$\frac{\mathrm{d}}{\mathrm{d}t}\Big[\Big(\tilde{k}_x(t)^2 + k_y^2\Big)\,\frac{\mathrm{d}\tilde{\psi}}{\mathrm{d}t}\Big] = -\Big(\tilde{k}_x(t)^2 + k_y^2\Big)\,\tilde{\psi} + k_y^2\frac{\tau_A^2}{\tau_G^2}\tilde{\psi}, \tag{6.29}$$

where the wave vectors are normalized by the characteristic length scale a and $\tau_G^2 = -\rho_0/\rho_0' g$. Further we can rewrite Eq. (6.29) in the form

$$\frac{\mathrm{d}^2\tilde{\psi}}{\mathrm{d}t^2} + \mu(t)\frac{\mathrm{d}\tilde{\psi}}{\mathrm{d}t} + [1 - S(t)]\tilde{\psi} = 0, \tag{6.30}$$

where

$$\mu(t) = -\frac{2\sigma k_y \tilde{k}_x(t)}{\tilde{k}_x(t)^2 + k_y^2},$$
$$S(t) = \frac{k_y^2 G}{\tilde{k}_x(t)^2 + k_y^2},$$

and $G = \tau_A^2/\tau_G^2$. Drawing an analogy with Newton's equation, $\mu(t)$ represents the frictional term and $S(t)$ the interchange drive term. Equation (6.30) is the correspondent of Eq. (6.8). As we have mentioned in Sec. 6.2, the time evolution for the amplitude of each eigenmode is no longer described by a simple exponential function. The behavior of $\tilde{\psi}$ will be discussed in the following sections.

6.5 Asymptotic and transient behavior of Kelvin's mode

In the absence of a density gradient or shear flow, $\mu(t) = S(t) = 0$ in Eq. (6.30) and we have a pure oscillation representing the Alfvén wave. When we include the density gradient, then $S(t)$ becomes nonzero. Then, we obtain an exponentially growing interchange instability for negative ρ_0' which exceeds the threshold value. Since a homogeneous magnetic field is assumed here, we have no stabilizing effect of the magnetic shear. The operator is Hermitian in these two cases, therefore we have the simple exponential evolution with time constants for each mode.

When we include the shear flow, we have $\mu(t) \neq 0$ and we may consider an analogy for the dynamics of a damped oscillator with time dependent frictional coefficient $\mu(t)$. In the following subsections, we will describe both the asymptotic and transient behavior of the amplitude $\tilde{\psi}$.

6.5.1 Transient behavior

In this subsection, we will analyze the transient behavior of each perturbed mode. Since an analytic expression is not available, we discuss the time evolution by qualitatively analyzing the ODE (6.30). In the absence of the instability drive, we have

$$\frac{\mathrm{d}}{\mathrm{d}t}\left[\left(\frac{\mathrm{d}\tilde{\psi}}{\mathrm{d}t}\right)^2 + \tilde{\psi}^2\right] = -\mu(t)\left(\frac{\mathrm{d}\tilde{\psi}}{\mathrm{d}t}\right)^2, \tag{6.31}$$

Case	$\sigma k_x k_y$	$\mu(t=0)$	$\mu(t\to\infty)$
(a)	$-$	$+$	$+$
(b)	$+$	$-$	$+$

Table 6.1: The relation between the sign of quantity $\sigma k_x k_y$ and that of effective frictional coefficient $\mu(t)$.

where

$$\mu(t) = -\frac{2\sigma k_y \tilde{k}_x(t)}{\tilde{k}_x(t)^2 + k_y^2},$$
$$\tilde{k}_x(t) = k_x - \sigma k_y t.$$

Therefore, the frictional coefficient $\mu(t)$ acts as a damping term for $\mu > 0$. It may be considered that this damping is caused by mixing in the same way as Landau damping which is caused by shear flow in the phase space. On the other hand, if $\mu(t) < 0$, the oscillator will be amplified due to shear flow.

Since the sign of the denominator in $\mu(t)$ is always positive, the behavior of the solution will be determined by the sign the numerator

$$\mu(t) \propto -2\sigma k_y \tilde{k}_x(t) = -2\sigma k_x k_y + 2(k_y\sigma)^2 t. \tag{6.32}$$

It can be easily understood from Eq. (6.32) that $\mu(t)$ will certainly be positive for large t regardless of the sign of the wave number or the flow shear. Thus, we may conclude that the shear flow acts to damp the oscillation in a time asymptotic sense. For the negative product $\sigma k_x k_y$ [Table 6.1(a)], the frictional coefficient $\mu(t)$ is always positive, therefore, the mode will be damped from the beginning. On the other hand, for the positive product $\sigma k_x k_y$ [Table 6.1(b)], $\mu(t)$ is negative at first, and goes to positive through zero at the instant $t_* = k_x/\sigma k_y$. Therefore the mode experiences an initial amplification lasting until the time t_*, which is even faster than the case with the interchange drive only.

It is interesting to see the relations between the frictional coefficient and the wave vector. We will take here as $\sigma > 0$ and $k_y > 0$ for simplicity, and the same conclusion may be drawn if we change the corresponding signs appropriately in other cases. As is shown in Fig. 6.1, the eigenfunction is being distorted due to the stretching effect of the shear flow, and the direction of the corresponding wave vector is also shifted. The $|\tilde{k}_x(t)|$ of the mode with negative initial k_x [see Figs. 6.1(c) and 6.2(a)] will be increased monotonically, and its structure becomes finer and finer. Then the mixing is promoted and its amplitude is damped. On the other hand, the $|\tilde{k}_x(t)|$ of the mode with positive initial k_x [see Figs. 6.1(a) and 6.2(b)] will be decreased in $t < t_*$, its

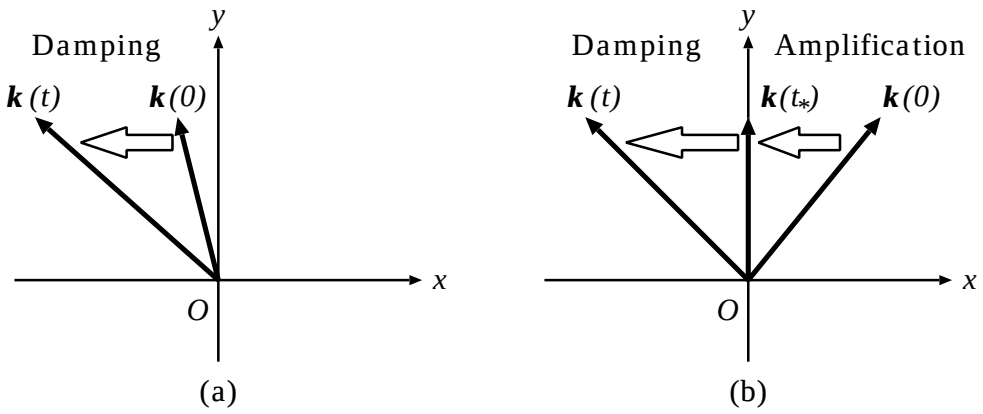

Figure 6.2: Distortion of the wave vector due to shear flow and its effect on the amplitude of magnetic flux.

structure once becomes the most coarse at time $t = t_*$, and becomes finer and finer. Thus the amplitude of the mode is amplified in the period $t < t_*$, and damped after that due to the mixing effect. One example of the numerical solutions of Eq. (6.30) is shown in Fig. 6.3. The result corresponds to the Case (b) of the Table 6.1. It is also seen in this figure that the initial amplification of the perturbation lasts until the turning point $t_* = 50$, then it is followed by the asymptotic decaying phase.

We have observed in the numerical solutions that there is a case where the amplitude is amplified to the value of 10^{30} times larger than the initial one. From a physical point of view, such huge amplifications may break down the linearity of the perturbations and may lead to a nonlinear stage. This case is beyond the scope of the linear theory and no sure conclusion can be drawn from Kelvin's method. Such huge amplifications are experienced by modes with large t_* and G.

6.5.2 Asymptotic behavior

In order to study the time asymptotic behavior, we assume $t \gg k_x/\sigma k_y,\ 1/\sigma$. In this time asymptotic limit we obtain the following ODE

$$\frac{\mathrm{d}^2}{\mathrm{d}t^2}\tilde{\psi} + \frac{2}{t}\frac{\mathrm{d}}{\mathrm{d}t}\tilde{\psi} + \Big(1 - \frac{G/\sigma^2}{t^2}\Big)\tilde{\psi} = 0, \tag{6.33}$$

where $G = \tau_A^2/\tau_G^2$ denotes the magnitude of the instability drive term. In the absence of the instability drive G, the time asymptotic behavior of the solution of Eq. (6.33) is expressed as

$$\tilde{\psi} \sim \frac{1}{t}\sin t, \tag{6.34}$$

which coincides with the result of Koppel [92] who studied a time dependent non-perturbative state. Since Eq. (6.33) corresponds to the spherical Bessel equation,

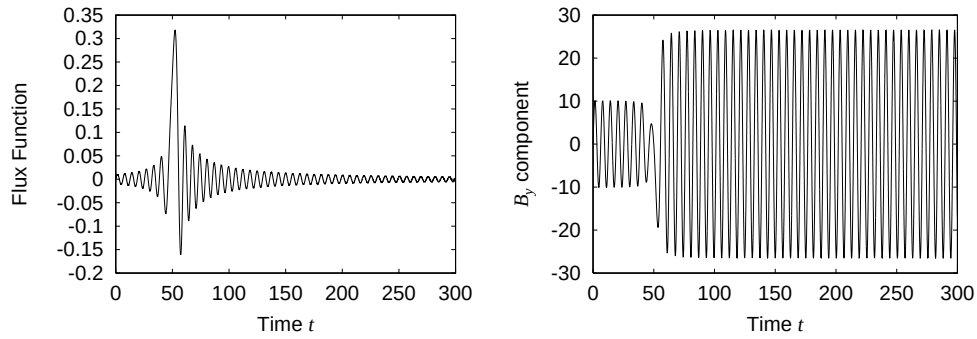

Figure 6.3: Numerical integrations of Eq. (6.30) for the parameters $k_x = 10$, $k_y = 1$, $k_z = 0$, $\sigma = 0.2$, and $G = 1$. Initial perturbations are $\tilde{\psi} = 0$ and $\mathrm{d}\tilde{\psi}/\mathrm{d}t = 1.0$ at $t = 0$.

its general solution for $G \neq 0$ is expressed as

$$\tilde{\psi} = \frac{1}{\sqrt{t}}(C_1 J_\nu(t) + C_2 Y_\nu(t)), \tag{6.35}$$

where J_ν and Y_ν denote the Bessel functions, and $\nu = (G/\sigma^2 + 1/4)^{1/2}$. Therefore the time asymptotic behavior of the mode is expressed generally as

$$\tilde{\psi} \sim \frac{1}{t}\sin\Big(t - \frac{\pi\nu}{2} + \delta\Big), \tag{6.36}$$

where δ denotes a constant phase depending on the initial condition. Therefore, the mode oscillates with amplitude $\tilde{\psi}$ and decays with the inverse power of time. While the x component of the perturbed magnetic field $\tilde{b}_x$ is proportional to ψ, the y component $\tilde{b}_y$ is proportional to $\tilde{k}_x(t)\tilde{\psi}$. Thus $\tilde{b}_y$ tends to the pure oscillatory behavior

$$\tilde{b}_y \sim \sin\Big(t - \frac{\pi\nu}{2} + \delta\Big), \tag{6.37}$$

as $\tilde{k}_x(t)$ increases with proportional to time (see Fig. 6.3). It should be noted that there is no threshold value for the stabilization of the interchange instability, since we obtain the same spherical Bessel equation (6.33) for all modes. All modes asymptotically evolve by following Eq. (6.33) independently of wave numbers $\boldsymbol{k}$.

The final amplitude of each mode depends sensitively on the parameters. As the shear parameter increases, the final amplitude of $\tilde{b}_y$ tends to be larger as is also shown by Chagelishvili *et al.* [52], while the mixing effect on $\tilde{b}_x$ increases. It should be noted that the instability drive G asymptotically has the effect to shift the phase of the oscillations as seen in Eqs. (6.36) and (6.37). However, it does not affect the principal time dependence. The combined effect of the Alfvén wave propagation and shear flow mixing always overcomes the interchange drive. The oscillation of the magnetic flux asymptotically decays with proportionality to the inverse power of time.

6.6 Interchange perturbations perpendicular to ambient magnetic field

When the wave vector is purely perpendicular to the ambient magnetic field, the formulation using the flux function (6.23) fails. As for the condition with $k_\parallel = 0$, we discuss the evolution of the stream function ϕ, where $k_\parallel$ is a parallel wave number to the ambient magnetic field. The governing equations are Eqs. (6.17) and (6.18), since the flux freezing equation can be decoupled due to the fact that $\boldsymbol{B}_0 \cdot \nabla = 0$. Applying $\partial_t + v_y \partial_y$ to both sides of Eq. (6.17) and substituting it into Eq. (6.18), we obtain

$$(\partial_t + v_y \partial_y)^2 \Delta\phi = -\frac{\rho_0' g}{\rho_0} \partial_y^2 \phi, \tag{6.38}$$

for a case of linear shear flow. We represent ϕ in terms of the shearing mode given in Eq. (6.25),

$$\phi(\boldsymbol{x}, t) = \int \tilde{\phi}_k(t)\, \tilde{\varphi}(t; \boldsymbol{k}, \boldsymbol{x})\, \mathrm{d}\boldsymbol{k}. \tag{6.39}$$

By substituting Eq. (6.39) into Eq. (6.38), the following ODE is obtained

$$\frac{\mathrm{d}^2}{\mathrm{d}t^2} \left[\left(\tilde{k}_x(t)^2 + k_y^2 \right) \tilde{\phi} \right] = k_y^2 \gamma_G^2 \tilde{\phi}, \tag{6.40}$$

where $\gamma_G^2 = -\rho_0' g/\rho_0$ $(= \tau_G^{-2})$ denotes the characteristic growth rate of the interchange instability. Here again we have dropped the subscript k for the sake of simplicity. In order to investigate the time asymptotic behavior of each mode, we assume $t \gg k_x/k_y\sigma$ and $t \gg 1/\sigma$. Then Eq. (6.40) becomes

$$\frac{\mathrm{d}^2}{\mathrm{d}t^2}\tilde{\phi} + \frac{4}{t}\frac{\mathrm{d}}{\mathrm{d}t}\tilde{\phi} + \frac{2-\alpha}{t^2}\tilde{\phi} = 0, \tag{6.41}$$

where $\alpha = \gamma_G^2/\sigma^2$ denotes the ratio between the interchange destabilizing effect and flow shear stabilizing one (Richardson number). Note that this ODE is not dependent on the wave numbers $\boldsymbol{k}$. The general solution of Eq. (6.41) is

$$\tilde{\phi} = C_1 t^{m_+} + C_2 t^{m_-}, \tag{6.42}$$

where

$$m_\pm = \frac{-3 \pm \sqrt{1+4\alpha}}{2}. \tag{6.43}$$

The time asymptotic behavior is therefore determined by the larger index m_+. Thus we can state the condition for the boundedness of $\tilde{\phi}$ as

$$\alpha \le 2 \quad \Rightarrow \quad -\frac{1}{2}\frac{\rho_0' g}{\rho_0} \le \sigma^2. \tag{6.44}$$

The condition for the boundedness of $\tilde{\phi}$ is improved compared with the static case $(\rho_0' \ge 0)$ due to the mixing effect of the shear flow. It is noted that this interchange

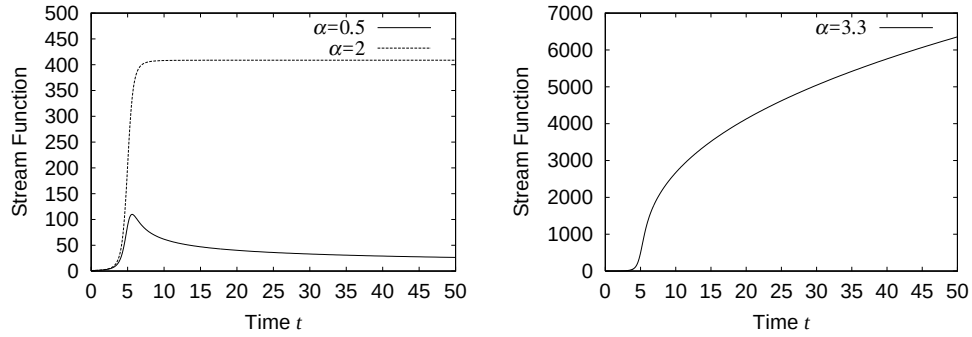

Figure 6.4: Numerical integrations of Eq. (6.40) for different α. The parameters are follows: $k_x = 10$, $k_y = 2$, $\sigma = 1$ and initial perturbations $\tilde{\phi} = 0$ and $\mathrm{d}\tilde{\phi}/\mathrm{d}t = 1.0$ at $t = 0$. The amplitude of the stream function in case of $\alpha = 3.3$ shows the algebraic growth corresponding to $m_+ \simeq 0.35$.

instability can be linearly unstable while the case with $k_\parallel \neq 0$ is completely stabilized. The numerical integrations of the ODE (6.40) are illustrated in Fig. 6.4. The transient behavior is observed until $t_* = 5$, and the asymptotic behavior follows. The asymptotic behavior is algebraic with the power of m_+ as analytically pointed out.

We notice that the 'stability condition' is not well defined here. If we impose the boundedness of $\tilde{v}_y = \mathrm{i}\tilde{k}_x(t)\tilde{\phi} \sim t^{1+m_+}$, the same condition $\rho_0' \geq 0$ as the static case is obtained. However, if we consider the boundedness of other fields which are represented by higher derivatives, e.g. the vortex perturbation, more strict condition will be required. Since the mixing effect of the shear flow distorts the structure of the perturbations into smaller scales, the fields characterized by the higher derivatives will have stronger secularities. Unlike the static case where the evolution of the perturbations can be expressed in the common exponential form, different quantities exhibit different time evolutions in shear flow systems. This could be a pathological problem of defining the 'stability condition' for shear flow systems.

6.7 Effect of magnetic shear on sheared plasma flow

In order to consider the effect of the magnetic shear on sheared plasma flow, let us consider the original linearized MHD equations instead of stream and flux functions, which can be written in the Cartesian coordinates as

$$\rho_0\Big(\partial_t \boldsymbol{v}_1 + \boldsymbol{v}_0 \cdot \nabla \boldsymbol{v}_1 + v_{1x}\partial_x \boldsymbol{v}_0\Big) = \frac{\boldsymbol{B}_0 \cdot \nabla \boldsymbol{b}}{\mu_0} - \nabla\Big(p_0 + \frac{\boldsymbol{B}_0 \cdot \boldsymbol{b}}{\mu_0}\Big), \qquad (6.45)$$

$$\partial_t \boldsymbol{b} + \boldsymbol{v}_0 \cdot \nabla \boldsymbol{b} = \boldsymbol{B}_0 \cdot \nabla \boldsymbol{v}_1 + b_x \partial_x \boldsymbol{v}_0, \tag{6.46}$$

where $\boldsymbol{b}$ denotes the perturbed magnetic field and $\boldsymbol{v}_0 = (0, \sigma x, 0)$. Assuming $\boldsymbol{B}_0 = (0, B_{0y}(x), B_{0z}(x))$, we can transform the coordinate as $(x, y, z) \mapsto (x, \eta, \zeta)$ with ζ along the local ambient magnetic field line and η perpendicular to x and ζ. In this coordinates, we have the stationary flow expressed as $(0, v_{0\eta}(x), v_{0\zeta}(x))$. Here, the spatial dependence of the velocity components is,

$$\begin{aligned} v_{0\eta} &= \frac{1}{B_0} B_{0z} \sigma x, \\ v_{0\zeta} &= \frac{1}{B_0} B_{0y} \sigma x. \end{aligned} \tag{6.47}$$

If the magnetic field is homogeneous, the coordinate transformation is also spatially homogeneous and these velocity components are still linear functions with respect to x. Writing the above MHD equations in the new coordinates yields

$$\rho(\partial_t u + v_{0\eta}\partial_\eta u + v_{0\zeta}\partial_\zeta u) = \frac{B_0 \partial_\zeta b_x}{\mu_0} - \partial_x\Big(p + \frac{B_0 b_\zeta}{\mu_0}\Big), \tag{6.48}$$

$$\rho\Big(\partial_t v + v_{0\eta}\partial_\eta v + v_{0\zeta}\partial_\zeta v + \frac{B_{0z}}{B_0}\sigma u\Big) = \frac{B_0 \partial_\zeta b_\eta}{\mu_0} - \partial_\eta\Big(p + \frac{B_0 b_\zeta}{\mu_0}\Big), \tag{6.49}$$

$$\rho\Big(\partial_t w + v_{0\eta}\partial_\eta w + + v_{0\zeta}\partial_\zeta w + \frac{B_{0y}}{B_0}\sigma u\Big) = \frac{B_0 \partial_\zeta b_\zeta}{\mu_0} - \partial_\zeta\Big(p + \frac{B_0 b_\zeta}{\mu_0}\Big), \tag{6.50}$$

$$\partial_t b_x + v_{0\eta}\partial_\eta b_x + v_{0\zeta}\partial_\zeta b_x = B_0 \partial_\zeta u, \tag{6.51}$$

$$\partial_t b_\eta + v_{0\eta}\partial_\eta b_\eta + v_{0\zeta}\partial_\zeta b_\eta = B_0 \partial_\zeta v + \frac{B_{0z}}{B_0}\sigma b_x, \tag{6.52}$$

$$\partial_t b_\zeta + v_{0\eta}\partial_\eta b_\zeta + v_{0\zeta}\partial_\zeta b_\zeta = B_0 \partial_\zeta w + \frac{B_{0y}}{B_0}\sigma b_x, \tag{6.53}$$

where u, v, and w denote the x, η, and ζ components of the perturbed velocity, respectively. Here the evolution of the amplitude $\tilde{b}_x$ is governed by the same equation as Eq. (6.30) for $\tilde{\psi}$.

If we include the magnetic shear, the inhomogeneity is also introduced in the above coordinate transformation. As is seen from Eqs. (6.47), it brings about a nonlinear spatial dependence of the background shear flow profile even if it is assumed to be linear in original Cartesian coordinates. Thus, it is considered that introduction of the magnetic shear seems equivalent to the study of the shear flow different from the linear dependence on x.

6.8 Summary

Kelvin's method of shearing modes is interpreted as a combination of both modal and characteristic methods for the analysis of a non-Hermitian system. The shear

flow distorts each Fourier mode, resulting in change of the wave number, which represents the stretching effect of the shear flow (see Fig. 6.1). It is noted that the solution obtained by this method gives the general solution of the system due to the completeness of the sinusoidal function in the Hilbert space.

By means of this method, we have first analyzed the incompressible electromagnetic perturbations in the presence of an interchange drive and obtained the ordinary differential equation (6.30) for the amplitude of the modes $\tilde{\psi}_k$. All modes show an asymptotic decay proportional to the inverse power of time (non-exponential) without any threshold value. This means that the interchange instabilities are always damped away at sufficiently large time due to the combined effect of the Alfvén wave propagation and distortion of modes by means of the background shear flow; i.e. the phase mixing effect. However, the transient behavior is not common for all modes, which depends on the initial wave numbers. Some of them show transient amplifications which are even faster than the interchange mode in the static case. These amplifications are so conspicuous that they may lead to the break down of the linearity of the perturbations.

It should be noted that, since our treatment considers the case of parallel linear shear flow, Kelvin-Helmholtz instabilities, which originate from the second order spatial derivative of the background shear flow [7, 9], are beyond the scope of the present theory. From a mathematical point of view, we stress that the Kelvin-Helmholtz instability is a problem involving purely non-Hermitian operators in the sense that the operator $\mathcal{A}$ of Eq. (6.1) itself becomes non-Hermitian. Thus, the method developed in Sec. 6.2 cannot be applied. This is a well known instability in fluid mechanics whose rigorous mathematical treatment includes highly non-trivial difficulties. We will try to construct a spectral theory on this problem in Chap. 7.

We note that the ODE which gives the evolution of the amplitudes of the interchange modes (6.30) and that of kink-type modes (Eq. (32) in Ref. [143]) are mathematically equivalent. Of course these two modes may have spatially different structures at least for static equilibria. However, these modes have no difference in time evolution by means of our treatment. Thus, we can say that these terms have the same effect in the sense that they enlarge the spectrum to unstable eigenvalues. The equivalence stems from the assumption of a spatially homogeneous magnetic field. However, as discussed in Sec. 6.7, the inhomogeneity of the magnetic field hinders the applicability of Kelvin's method.

We have also investigated the time evolution for purely perpendicular perturbations ($\boldsymbol{k} \cdot \boldsymbol{B}_0 = 0$), which do not excite the Alfvén wave, since they do not bend the magnetic field line during their growth. The flow shear has been shown to have a stabilizing effect also on purely perpendicular disturbances; however, the phase mixing

effect alone cannot completely stabilize the interchange instabilities. The condition for the boundedness of the mode amplitudes $\tilde{\phi}_k$ can be expressed in Eq. (6.44) by means of a ratio of instability drive to shear parameter of the mean flow. We have shown that the time evolution of these unstable modes is again of algebraic type. Notice that the conditions for the boundedness of different quantities do not coincide. The discrepancies originate from the fact that, in shear flow systems, different fields experience algebraic evolutions characterized by different powers of time, while the time evolutions for any fields are expressed in a common exponential form for static systems.

Chapter 7

Spectral theory for surface wave model of Rayleigh equation

7.1 Introduction

A variety of complex phenomena occur in non-Hermitian dynamical systems. Non-orthogonality of eigenfunctions (modes) is the deterministic characteristic of such systems, which brings about interactions among different modes. This aspect resembles the mode couplings in nonlinear systems, and hence, the diversity of transient behavior in non-Hermitian systems is rather rich [143, 131, 84].

Let us consider an autonomous evolution equation of the Schrödinger type

$$\begin{cases} \mathrm{i}\partial_t u = \mathcal{H}u \\ u(0) = u_0 \end{cases}, \tag{7.1}$$

where $\mathcal{H}$ is a certain linear operator. When we can generate an exponential function (propagator) $e^{-\mathrm{i}t\mathcal{H}}$, we can write the solution of Eq. (7.1) as

$$u(t) = e^{-\mathrm{i}t\mathcal{H}}u_0.$$

When $u \in \mathbb{C}$ and $\mathcal{H} \in \mathbb{C}$, then $e^{-\mathrm{i}t\mathcal{H}}$ is nothing but the exponential function of elementary mathematics. For vectors $u \in \mathbb{C}^N$ and a linear map $\mathcal{H} : \mathbb{C}^N \to \mathbb{C}^N$, we can define $e^{-\mathrm{i}t\mathcal{H}}$ by the standard power series

$$e^{-\mathrm{i}t\mathcal{H}} = \sum_{n=1}^{\infty} \frac{(-\mathrm{i}t\mathcal{H})^n}{n!}, \tag{7.2}$$

or the Cauchy integral (inverse Laplace transform)

$$e^{-\mathrm{i}t\mathcal{H}} = \frac{1}{2\pi\mathrm{i}} \oint e^{-\mathrm{i}t\lambda}(\lambda\mathcal{I} - \mathcal{H})^{-1}\, \mathrm{d}\lambda, \tag{7.3}$$

where $\mathcal{I}$ denotes the identity operator. For u in a Hilbert space V, $\mathcal{H}$ is an operator in V. For some different classes of operators, we have theories to generate $e^{-\mathrm{i}t\mathcal{H}}$ [28]. A most general theory of generating an exponential function of the type $e^{t\mathcal{A}}$ for positive t (so-called semigroup theory) may be the one due to Hille and Yosida. Although this theory warrants the solvability of initial value problems for a wide class of generators, understanding of the behavior of the solution is not simple. Indeed, the exponential functions of matrices or operators are not necessarily 'exponential' in the conventional sense.

The von Neumann theory for Hermitian (selfadjoint) operators provides a deep insight into the structure of $e^{-\mathrm{i}t\mathcal{H}}$, which invokes the spectral resolution of the generator $\mathcal{H}$ in terms of a complete set of orthogonal modes. The basic idea is that the $e^{-\mathrm{i}t\mathcal{H}}$ may be represented as a sum of independent harmonic oscillators, each of which is an eigenfunction of $\mathcal{H}$ and the corresponding eigenvalue (real number) gives the frequency of the oscillation. Unlike the case of finite dimensional vector space, however, the conventional eigenfunctions may not be complete to span the Hilbert space. The most essential generalization needed to study the infinite dimensional space was the introduction of continuous spectra that correspond to singular eigenfunctions. The spectral resolution of $\mathcal{H}$ is, in general, given by an integral over the spectra (an example will be given in Sec. 7.3). The contribution to the $e^{-\mathrm{i}t\mathcal{H}}$ from the continuous spectra brings about the 'phase mixing' of oscillations with continuous frequencies, resulting in various types of damping. Hence, the reality of the spectra of an Hermitian operator does not necessarily imply a simple sum of harmonic oscillations.

For a linear map in a finite dimensional vector space, the spectral resolution yields the Jordan canonical form, and the explicit representation of $e^{-\mathrm{i}t\mathcal{H}}$ can be constructed using the canonical form. In a Hilbert space, however, such a general theory of spectral resolution is limited to either compact operators or Hermitian ones [11, 6]. This chapter is an attempt to obtain a spectral resolution of a non-Hermitian operator that is not included in the above mentioned categories. The operator is related to an important physics problem (e.g. Kelvin-Helmholtz instability in neutral fluids [83, 138, 7]).

Before formulating the equation, we highlight the essential characteristic of non-Hermitian operator by revisiting the spectral resolution in a finite dimensional vector space. When $\mathcal{H}$ is not a normal map, we can transform it into the Jordan canonical form. By a regular map P, we can transform

$$P^{-1}\mathcal{H}P = \mathcal{J}_1 \dot{+} \mathcal{J}_2 \dot{+} \cdots \dot{+} \mathcal{J}_\nu,$$

where $\dot{+}$ denotes the direct sum of linear maps, and each $\mathcal{J}_j$ is the Jordan block corresponding to the eigenvalue λ_j of $\mathcal{H}$ [$(\lambda_j\mathcal{I} - \mathcal{J}_j)$ is a nilpotent of order N_j, i.e.,

$(\lambda_j I - \mathcal{J}_j)^{N_j} = 0]$, which is represented by the Jordan matrix of order N_j:

$$\mathcal{J}_j = \begin{pmatrix} \lambda_j & 1 & 0 & 0 \\ 0 & \ddots & \ddots & 0 \\ & \ddots & \ddots & 1 \\ 0 & & 0 & \lambda_j \end{pmatrix}. \tag{7.4}$$

When $\mathcal{H}$ is a normal map, all N_j are unity. Then, $\mathcal{H}$ can be diagonalized, and all modes (eigenvectors) are decoupled. A Jordan block of order ≥ 2 represents 'unremovable' interactions among modes. It is remarkable that the canonical representation (7.4) shows such interactions in the form of one-by-one couplings.

Writing

$$e^{-\mathrm{i}t\mathcal{H}} = e^{-\mathrm{i}t\lambda_j} e^{\mathrm{i}t(\lambda_j\mathcal{I}-\mathcal{H})} = e^{-\mathrm{i}t\lambda_j}\left[\mathcal{I} + \mathrm{i}t(\lambda_j\mathcal{I}-\mathcal{H}) - \frac{t^2(\lambda_j\mathcal{I}-\mathcal{H})^2}{2} + \cdots\right],$$

we find that the $e^{-\mathrm{i}t\mathcal{H}}$ acting on the (generalized) eigenspace belonging to λ_j includes factors

$$e^{-\mathrm{i}t\lambda_j},\ te^{-\mathrm{i}t\lambda_j},\ \cdots,\ t^{N_j-1}e^{-\mathrm{i}t\lambda_j}.$$

Therefore, even if every eigenvalue λ_j is real, the $e^{-\mathrm{i}t\mathcal{H}}$ can describe an 'instability' (growth of oscillation amplitude). The algebraic growth of amplitudes (the factors t^p) is called 'secularity.'

On the stability analysis of a fluid, we mainly have two methods which are widely used in literatures. One is based on variational problem [65, 78, 142], and the other is based on the spectral method [37, 98]. Actually, necessary and sufficient condition of Rayleigh equation to have complex eigenvalues is shown in Ref. [37] by means of Nyquist criterion, however, the completeness of the solution is still left open. We will focus on the completeness of the spectral solution and investigate the possibility of the secular behavior. We will introduce a generalized Rayleigh equation in Sec. 7.2, and discuss the properties of two consisting operators in Sec. 7.3. By introducing surface wave model [134, 73, 7], we can describe the system rather simply. Firstly, we will formally investigate the possibility of resonance among modes in Secs. 7.4 and 7.5. Spectral resolution of the generator is given in Sec. 7.6, which will be compared with the Laplace transform method in Sec. 7.7. In Sec. 7.8, we will summarize the obtained results.

7.2 Generalized Rayleigh equation

The vortex dynamics equation in $\mathbb{R}^2$ [the coordinates are denoted by (x, y)] reads as a Liouville equation

$$\partial_t \Psi + \{H, \Psi\} = 0, \tag{7.5}$$

where Ψ is the vorticity, H is the Hamiltonian (stream function) of an incompressible flow $\boldsymbol{v} = (\partial_y H, -\partial_x H)^t$ that transports the vortices, and

$$\{a, b\} = (\partial_y a)(\partial_x b) - (\partial_x a)(\partial_y b) = -\nabla a \times \nabla b \cdot \nabla z$$

is the Poisson bracket.

When the Hamiltonian H depends on Ψ, the evolution equation (7.5) is nonlinear. The dynamics of Ψ can couple with other fields when they are included in H. The simplest example of nonlinear vortex dynamics is the Euler fluid (incompressible ideal flow), where

$$-\Delta H = \Psi, \tag{7.6}$$

or, denoting the Green operator of the Laplacian $-\Delta$ by $\mathcal{K}$

$$H = \mathcal{K}\Psi. \tag{7.7}$$

Physical examples of relevant phenomena are rather rich; the Rossby waves of perturbations in geological jet streams, the diocotron waves in non-neutral plasmas, and the drift waves in magnetized plasmas.

Let us linearize Eq. (7.5) with decomposing Ψ and H into their ambient (denoted by subscript 0) and fluctuation (denoted by subscript 1) parts:

$$\begin{aligned} \Psi &= \Psi_0 + \Psi_1, \\ H &= H_0 + H_1 = \mathcal{K}\Psi_0 + \mathcal{K}\Psi_1. \end{aligned}$$

By neglecting the second-order terms, Eq. (7.5) leads to

$$\partial_t \Psi_1 + \{H_0, \Psi_1\} + \{\Delta H_0, \mathcal{K}\Psi_1\} = 0. \tag{7.8}$$

Hereafter we will omit the subscript 1 denoting the perturbed field for simplicity.

In this chapter, we consider one-dimensional problem with

$$H_0 = H_0(x).$$

Since the ambient Hamiltonian H_0 is independent of y, the wavenumber in y becomes a good quantum number and we can replace ∂_y by $\mathrm{i}k$. We write

$$v(x) = -\partial_x H_0(x),$$

to obtain the standard Rayleigh equation

$$\mathrm{i}\partial_t \Psi = kv(x)\Psi + kv''(x)\mathcal{K}\Psi. \tag{7.9}$$

The Green operator $\mathcal{K}$ is represented by a convolution integral

$$(\mathcal{K}f)(x) = \int_{-\infty}^{+\infty} \frac{e^{-k|x-\xi|}}{2k} f(\xi)\,\mathrm{d}\xi. \tag{7.10}$$

In the following, we denote the Green function by $K(x,\xi)$;

$$K(x,\xi) = \frac{e^{-k|x-\xi|}}{2k}. \tag{7.11}$$

Here we will define a generalized Rayleigh equation as

$$\mathrm{i}\partial_t \Psi = \mathcal{L}\Psi \tag{7.12}$$

$$\mathcal{L} = kv(x) + kw(x)\mathcal{K}, \tag{7.13}$$

where $v(x)$ and $w(x)$ can be independent arbitrary functions. It corresponds to the generalization of the Rayleigh equation (7.9). The case when $w(x) = v''(x)$ recovers the physically relevant equation (7.9) where $v(x)$ denotes the steady flow velocity in the y direction.

7.3 Formal spectra of generalized Rayleigh equation

The generator of the vortex dynamics equation (7.12) consists of two terms, each of which describes different mechanism of the vortex motion. The first term on the right-hand side of Eq. (7.12) [originating from $\{H_0, \Psi\}$ in Eq. (7.8)] represents the transport of the vorticity by the ambient flow $v(x)$. An inhomogeneous (sheared) flow distorts vortices, and hence, no stationary structure can persist in a shear flow [$v(x) \neq$ const]. Such a dynamics is described by a continuous spectrum. On the other hand, the second term [originating from $\{\Delta H_0, \mathcal{K}\Psi\}$ in Eq. (7.8)] describes the interaction between the perturbation and the ambient field. When the ambient vorticity $\Psi_0 = -\Delta H_0$ has a spatial gradient, a flow induced by a perturbation yields a local change of the vorticity. This term, hence, can create perturbed vortices from the ambient field.

Firstly, let us assume $w(x) = 0$ in Eq. (7.13) and consider

$$\mathrm{i}\partial_t \Psi = kv(x)\Psi \tag{7.14}$$

with a 'continuous' real function $v(x)$, which reads as a Schrödinger equation with a Hamiltonian $kv(x)$.

The formal eigenvalue and the corresponding eigenfunction of the generator of Eq. (7.14), with setting

$$kv(x)\Psi = \lambda\Psi$$

[i.e., $\Psi(t) = e^{-\mathrm{i}\lambda t}\Psi$], is given by

$$\lambda = kv(\mu), \quad \Psi = \delta(x-\mu), \tag{7.15}$$

where μ is an arbitrary real number and δ denotes the delta-measure. For convenience, we write

$$(\delta(x-\mu), f(x)) = \int_{-\infty}^{+\infty} \delta(x-\mu) f(x)\,\mathrm{d}x = f(\mu).$$

A formal spectral resolution of the generator is written as

$$\begin{aligned} kv(x)f(x) &= \int_{-\infty}^{+\infty} kv(\mu)(\delta(x-\mu), f)\,\delta(x-\mu)\,\mathrm{d}\mu \\ &= \int_{-\infty}^{+\infty} kv(\mu) f(\mu)\delta(x-\mu)\,\mathrm{d}\mu. \end{aligned} \tag{7.16}$$

Rigorous mathematical representation of this 'continuous spectrum' is given by the spectral resolution of the coordinate operator:

$$xf(x) = \int_{-\infty}^{+\infty} \mu\,\mathrm{d}E(\mu) f(x), \tag{7.17}$$

where $\{E(\mu);\ \mu \in \mathbb{R}\}$ is a family of projectors defined by

$$E(\mu)f(x) = \begin{cases} f(x) & \text{for } x \le \mu \\ 0 & \text{for } x > \mu \end{cases}. \tag{7.18}$$

The projector $E(\mu)$ gives a resolution of the identity:

$$\mathcal{I} = \int_{-\infty}^{+\infty} \mathrm{d}E(\mu). \tag{7.19}$$

Using this representation of the coordinate operator, we can write

$$kv(x)f(x) = \int_{-\infty}^{+\infty} kv(\mu)\,\mathrm{d}E(\mu) f(x), \tag{7.20}$$

which represents the spectral resolution of the generator $kv(x)$ in terms of its generalized eigenfunctions [this corresponds to the continuous version of Eq. (B.28)]. The solution of Eq. (7.14) with initial condition $\Psi(x,0)$ is given by

$$\Psi(x,t) = \int_{-\infty}^{+\infty} e^{-\mathrm{i}tkv(\mu)}\,\mathrm{d}E(\mu)\Psi(x,0) = e^{-\mathrm{i}tkv(x)}\Psi(x,0). \tag{7.21}$$

Next, let us assume

$$v(x) = 0, \tag{7.22}$$

$$w(x) = -\frac{U}{a}[\delta(x-a) - \delta(x+a)], \tag{7.23}$$

then the operator can be written as

$$\mathcal{L}_1 = -\frac{U}{2a}[\delta(x-a) - \delta(x+a)] \int_{-\infty}^{\infty} e^{-k|x-\xi|} \ \cdot \ \mathrm{d}\xi \tag{7.24}$$

There are two solutions which match with the exponential time evolution. Assuming $\varphi \propto e^{-\mathrm{i}\lambda t}$ and substituting it in the place of Ψ, then we obtain the eigenvalue problem

$$\lambda\varphi(x) = -\frac{U}{2a}[\delta(x-a) - \delta(x+a)] \int_{-\infty}^{\infty} e^{-k|x-\xi|}\varphi(\xi)\,\mathrm{d}\xi. \tag{7.25}$$

The eigenvalues and the corresponding eigenfunctions are

$$\lambda = \pm\frac{U}{2a}\sqrt{1-e^{-4ka}}, \quad \varphi(x) = \delta(x-a) - \left(1 \pm \sqrt{1-e^{-4ka}}\right) e^{2ka}\,\delta(x+a). \tag{7.26}$$

Therefore we can write the operator $\mathcal{L}$ in the form of the matrix by taking the basis vector as $\delta(x-a)$ and $\delta(x+a)$,

$$\mathcal{L}_1 = \frac{U}{2a}\begin{pmatrix} -1 & -e^{-2ka} \\ e^{-2ka} & 1 \end{pmatrix}. \tag{7.27}$$

These oscillation denote the coupled diocotron modes which are excited on both surfaces $x = \pm a$. Note that these modes are stable for positive k in the case of no continuous spectra. Since the governing equation is same as the case of diocotron instabilities in non-neutral plasmas [60, 91], these oscillations are called 'diocotron oscillation.'

If we take $v(x)$ to be consistent with $w(x)$ of Eq. (7.23) as

$$v(x) = \begin{cases} -U & (x \le -a) \\ Ux/a & (-a < x < a) \\ U & (a \le x) \end{cases}, \tag{7.28}$$

and again focusing on the subspace spanned by two surface waves, then the operator $\mathcal{L}_2$ is expressed in the matrix form as

$$\mathcal{L}_2 = \begin{pmatrix} kU & 0 \\ 0 & -kU \end{pmatrix} + \mathcal{L}_1. \tag{7.29}$$

This 2×2 matrix $\mathcal{L}_2$ can be readily diagonalized in terms of the non-unitary transform and thus it turns out to be a semi-simple type supposed that $k \neq 1/2a$. Its two eigenvalues denote the famous Kelvin-Helmholtz instability [7], whose dispersion relation is written as

$$\lambda^2 = \frac{U^2}{4a^2}\left[(1-2ka)^2 - e^{-4ka}\right]. \tag{7.30}$$

If λ degenerates to zero, we may have secularity, and moreover, the other part of the matrix may include Jordan block. These details will be discussed later.

7.4 Resonance between point and continuous spectra

We have studied the spectra of the operators separately in the previous section. However, we have to be careful about the resonance (frequency overlapping) between modes. Namely the eigenvalues Eqs. (7.15) and (7.26) may overlap. In this section, we will formally show the effect coming from such resonance or frequency overlapping.

Let us first consider the following consistent case where the operator is expressed as

$$\mathcal{L}_3 = kv(x) - \frac{U}{2a}\delta(x-a)\int_{-\infty}^{\infty} e^{-k|x-\xi|} \ \cdot \ \mathrm{d}\xi, \tag{7.31}$$

$$v(x) = \begin{cases} Ux/a & (x < a) \\ U & (a \le x) \end{cases} . \tag{7.32}$$

By taking the component proportional to $\delta(x-a)$ separately, we divide the vorticity as

$$\Psi(x,t) = \alpha(t)\delta(x-a) \ + \ \tilde{\Psi}(x,t) \tag{7.33}$$

where $\tilde{\Psi}$ does not include any singularity on $x = a$. Then, we can divide the time evolution equation as

$$\mathrm{i}\frac{\mathrm{d}}{\mathrm{d}t}\alpha(t) = \frac{U}{2a}(2ka-1)\alpha(t) - \frac{U}{2a}\int_{-\infty}^{\infty} e^{-k|a-\xi|}\tilde{\Psi}(\xi,t)\,\mathrm{d}\xi, \tag{7.34}$$

$$\mathrm{i}\partial_t\tilde{\Psi}(x,t) = kv(x)\tilde{\Psi}(x,t). \tag{7.35}$$

The second equation can be readily integrated for each x, which gives

$$\tilde{\Psi}(x,t) = e^{-\mathrm{i}tkv(x)}\tilde{\Psi}(x,0). \tag{7.36}$$

Plugging it into Eq. (7.34), we have

$$\mathrm{i}\frac{\mathrm{d}}{\mathrm{d}t}\alpha(t) = \frac{U}{2a}(2ka-1)\alpha(t) - \frac{U}{2a}\int_{-\infty}^{\infty} e^{-k|a-\xi|}e^{-\mathrm{i}tkv(\xi)}\tilde{\Psi}(\xi,0)\,\mathrm{d}\xi, \tag{7.37}$$

where the last integration denotes the phase mixing of each singular eigenfunction. It can be integrated to give

$$\alpha(t) = e^{-\mathrm{i}\omega_1 t}\alpha(0) + \frac{U}{2a}\int e^{-k|a-\xi|}\frac{e^{-\mathrm{i}\omega_1 t} - e^{-\mathrm{i}tkv(\xi)}}{kv(\xi)-\omega_1}\tilde{\Psi}(\xi,0)\,\mathrm{d}\xi, \tag{7.38}$$

where $\omega_1 = (2ka-1)U/2a$ represents the Doppler shifted diocotron frequency.

By assuming $\varphi \propto e^{-\mathrm{i}\lambda t}$, we will obtain the following eigenvalue problem.

$$\lambda\varphi(x) = kv(x)\varphi(x) - \frac{U}{2a}\delta(x-a)\int_{-\infty}^{\infty} e^{-k|x-\xi|}\varphi(\xi)\,\mathrm{d}\xi. \tag{7.39}$$

For this eigenvalue problem, we have the following sets of eigenvalues and the corresponding eigenfunctions:

1. For $\lambda_0 = kU$; the corresponding eigenfunctions are arbitrary continuous functions $\varphi_0(x)$ which satisfy

$$\int_a^\infty e^{k(a-\xi)}\varphi_0(\xi)\,\mathrm{d}\xi = 0, \quad \wedge \quad \varphi_0(x) = 0 \ (x < a). \tag{7.40}$$

2. For $\lambda_1 = kU - U/2a$; the corresponding eigenfunction is

$$\varphi_1(x) = \delta(x-a). \tag{7.41}$$

3. For $\lambda_\mu = kU\mu/a$ $(\mu < a \ \wedge \ \mu \neq a - 1/2k)$; the corresponding eigenfunctions are

$$\varphi_\mu(x) = \delta(x-\mu) + \frac{e^{-k(a-\mu)}}{2k(a-\mu)-1}\delta(x-a). \tag{7.42}$$

However, these eigenvalues are not complete and we have another eigenfunction in a wider sense. That is $\varphi_2(x) = \delta(x-\mu_0)$ where $\mu_0 = a - 1/2k$. We can easily see that

$$(\lambda_1 - \mathcal{L}_3)\varphi_2(x) = \frac{U}{2a}e^{-k(a-\mu_0)}\varphi_1(x), \tag{7.43}$$

where $\lambda_1 = kU - U/2a$. Of course $(\lambda_1 - \mathcal{L}_3)^2\varphi_2(x) = 0$ also holds. These relations are quite similar to the eigenfunction in a wider sense for the finite dimensional matrix operator. Thus we may be able to write the operator $\mathcal{L}_3$ in the following matrix form including the case $\mu = \mu_0$:

$$\mathcal{L}_3 = \begin{pmatrix} kU - \dfrac{U}{2a} & -\dfrac{U}{2a}e^{-k(a-\mu)} \\ 0 & kU\dfrac{\mu}{a} \end{pmatrix}, \tag{7.44}$$

where a Jordan block is obtained when $kU - U/2a = kU\mu/a$ $(\mu = \mu_0)$.

Let us evaluate the time evolution of the perturbation when we have taken this $\varphi_2(x)$ as an initial condition. As we can see from Eq. (7.43), we will have $\varphi_1(x)$ component by applying the generator $\mathcal{L}_3$ on the initial condition $\varphi_2(x)$. Here we may be able to consider the evolution to be closed in the functional space spanned by $\varphi_1(x)$ and $\varphi_2(x)$. Thus it may be natural to assume Ψ as

$$\Psi(x,t) = \sum_{i=1}^{2} \alpha_i(t)\,\varphi_i(x). \tag{7.45}$$

Substituting this expression into the original equation (7.12), we obtain

$$\begin{aligned} \mathrm{i}\partial_t(\alpha_1\varphi_1+\alpha_2\varphi_2) &= \mathcal{L}_3(\alpha_1\varphi_1+\alpha_2\varphi_2) \\ &= \lambda_1\alpha_1\varphi_1+\alpha_2\mathcal{L}_3\varphi_2 \\ &= \Big(\lambda_1\alpha_1-\frac{U}{2a\sqrt{e}}\alpha_2\Big)\varphi_1+\lambda_1\varphi_2 \end{aligned} \tag{7.46}$$

When we decompose Eq. (7.46) into φ_1 and φ_2 by considering them to be independent, we obtain two coupled time evolution equations;

$$\frac{\mathrm{d}\alpha_1}{\mathrm{d}t} = -\mathrm{i}\lambda_1\alpha_1+\mathrm{i}\frac{U}{2a\sqrt{e}}\alpha_2, \tag{7.47}$$

$$\frac{\mathrm{d}\alpha_2}{\mathrm{d}t} = -\mathrm{i}\lambda_1\alpha_2. \tag{7.48}$$

The latter one can be readily integrated to give

$$\alpha_2(t) = \alpha_2(0)e^{-\mathrm{i}\lambda_1 t}. \tag{7.49}$$

The former equation can also be readily solved with the variable constant method.

$$\alpha_1(t) = \Big[\mathrm{i}\frac{U}{2a\sqrt{e}}\alpha_2(0)t+\alpha_1(0)\Big]e^{-\mathrm{i}\lambda_1 t}. \tag{7.50}$$

Here we see that for $\alpha_2(0)\neq 0$, we may have a secularity due to the resonance of the diocotron mode with one of the singular eigenfunction in the continuous spectrum. It is noted that even if all eigenvalues are real, we may have instability due to its secular evolution. However, by introducing a proper Hilbert space, we may show that this apparent secularity is virtual. Physically, it is considered that the algebraic growth of the surface wave does not occur when the resonance is the form that the wave energy flows *from inner singular function to surface wave.*

7.5 Kelvin-Helmholtz system

Let us consider the case with two singular breaks which may lead to the well known Kelvin-Helmholtz instabilities. The generator is written as

$$\mathcal{L}_4 = kv(x)-\frac{U}{2a}[\delta(x-a)-\delta(x+a)]\int_{-\infty}^{\infty}e^{-k|x-\xi|}\ \cdot\ \mathrm{d}\xi, \tag{7.51}$$

where the velocity field is defined as

$$v(x) = \begin{cases} -U & (x\leq -a) \\ Ux/a & (-a<x<a) \\ U & (a\leq x) \end{cases}. \tag{7.52}$$

If we put the basis vectors as $\varphi_1(x) = \delta(x-a)$, $\varphi_\mu(x) = \delta(x-\mu)$, and $\varphi_3(x) = \delta(x+a)$, then we can obtain the following matrix representation for the operator $\mathcal{L}_4$;

$$\mathcal{L}_4 = \frac{U}{2a}\begin{pmatrix} 2ka-1 & -e^{-k(a-\mu)} & -e^{-2ka} \\ 0 & 2k\mu & 0 \\ e^{-2ka} & e^{-k(a+\mu)} & -(2ka-1) \end{pmatrix} \tag{7.53}$$

Note here that $\mu = \pm\mu_0$ does not create a Jordan block any more since the frequencies of diocotron oscillations are shifted due to their coupling.[1]

If we expand the perturbed vortex field as

$$\Psi(x,t) = \sum_{i=1}^{3} \alpha_i(t)\,\varphi_i(x), \tag{7.54}$$

and substitute it into the Rayleigh equation, we obtain

$$\mathrm{i}\frac{\mathrm{d}\alpha_1}{\mathrm{d}t} = \frac{U}{2a}\left[(2ka-1)\alpha_1 - e^{-k(a-\mu)}\alpha_2 - e^{-2ka}\alpha_3\right], \tag{7.55}$$

$$\mathrm{i}\frac{\mathrm{d}\alpha_2}{\mathrm{d}t} = kU\frac{\mu}{a}\alpha_2, \tag{7.56}$$

$$\mathrm{i}\frac{\mathrm{d}\alpha_3}{\mathrm{d}t} = \frac{U}{2a}\left[e^{-2ka}\alpha_1 + e^{-k(a+\mu)}\alpha_2 - (2ka-1)\alpha_3\right]. \tag{7.57}$$

The coupling between two diocotron oscillations is eliminated by diagonalizing the matrix of 2×2 part of the outermost. The eigenvalues are found to be

$$\lambda_1^\dagger = \frac{U}{2a}e^{-2ka}\sinh\psi, \tag{7.58}$$

$$\lambda_3^\dagger = -\frac{U}{2a}e^{-2ka}\sinh\psi, \tag{7.59}$$

and the corresponding eigenfunctions are

$$\varphi_1^\dagger(x) = \delta(x-a) + e^{-\psi}\delta(x+a), \tag{7.60}$$

$$\varphi_3^\dagger(x) = e^{-\psi}\delta(x-a) + \delta(x+a), \tag{7.61}$$

[1]It may be easily understood by considering a simple example

$$\mathcal{A} = \begin{pmatrix} 3 & 2 & 1 \\ 0 & 3 & 0 \\ -1 & -2 & -3 \end{pmatrix}.$$

This matrix can be readily diagonalized and the eigenvalues become

$$\lambda = 3,\ \pm 2\sqrt{2},$$

which are no longer degenerated, and the corresponding eigenfunctions are

$$\varphi = \left(1, \frac{1}{10}, -\frac{1}{5}\right),\ (1, 0, -3 \pm 2\sqrt{2}).$$

where $\cosh\psi = (2ka-1)e^{2ka}$. Thus we define new coefficients which denote the amplitudes of $\varphi_1^\dagger$ and $\varphi_2^\dagger$ as

$$\alpha_1\varphi_1 + \alpha_3\varphi_3 = \beta_1\varphi_1^\dagger + \beta_3\varphi_3^\dagger. \tag{7.62}$$

From this relation we obtain

$$\begin{pmatrix} \beta_1 \\ \beta_3 \end{pmatrix} = \frac{2}{\sinh\psi}\begin{pmatrix} e^{\psi} & -1 \\ -1 & e^{\psi} \end{pmatrix}\begin{pmatrix} \alpha_1 \\ \alpha_3 \end{pmatrix}. \tag{7.63}$$

With these new coefficients, we can decouple the diocotron modes, and obtain the following three equations;

$$\mathrm{i}\frac{\mathrm{d}\beta_1}{\mathrm{d}t} = \lambda_1^\dagger\beta_1 - \frac{U}{a\sinh\psi}[e^{-k(a-\mu)}e^{\psi} + e^{-k(a+\mu)}]\alpha_2, \tag{7.64}$$

$$\mathrm{i}\frac{\mathrm{d}\alpha_2}{\mathrm{d}t} = kU\frac{\mu}{a}\alpha_2, \tag{7.65}$$

$$\mathrm{i}\frac{\mathrm{d}\beta_3}{\mathrm{d}t} = \lambda_3^\dagger\beta_3 + \frac{U}{a\sinh\psi}[e^{-k(a-\mu)} + e^{-k(a+\mu)}e^{\psi}]\alpha_2. \tag{7.66}$$

The solution of Eq. (7.65) is given as

$$\alpha_2(t) = \alpha_2(0)\, e^{-\mathrm{i}(kU\mu/a)t}. \tag{7.67}$$

If we assume

$$kU\frac{\mu}{a} = \lambda_1^\dagger \ \text{ or } \ \lambda_3^\dagger, \tag{7.68}$$

then we might have secularity due to the resonance with the simple oscillator $\varphi_2^\dagger$. On the other hand, we *do not* have it, when the eigenvalues $\lambda_{1,3}^\dagger$ are complex or pure imaginary, namely when the system is unstable in a Kelvin-Helmholtz sense.

7.6 Spectral resolution of coupled non-Hermitian generator

In this section, we formulate the vortex dynamics equation (7.12) for a case with a sum of the delta-measure field

$$w(x) = \sum_{j=1}^{N} A_j\delta(x-a_j) \quad (A_j, a_j \in \mathbb{R},\ j=1,\dots,N), \tag{7.69}$$

as an evolution equation in an appropriate Hilbert space, and give a spectral resolution of the generator. The generator reads

$$\begin{aligned}\mathcal{L}\Psi &= kv(x)\Psi + kw(x)\mathcal{K}\Psi \\ &= kv(x)\Psi + \sum_{j=1}^{N} kA_j\delta(x-a_j)\int_{-\infty}^{+\infty} K(x,\xi)\Psi(\xi)\,d\xi,\end{aligned} \tag{7.70}$$

where $kv(x) \in C(\mathbb{R})$, $A_j \in \mathbb{R}$, $a_j \in \mathbb{R}$ $(j = 1, \ldots, N)$, and $K(x, \xi) = e^{-k|x-\xi|}/2k$ is the Green function [see Eq. (7.11)]. In what follows, we assume

$$|v(x)| < c \quad (\forall x)$$

with a finite number c.

It is noted that, since the delta measure $\delta(x-a_j)$ is not a member of the Lebesgue space, we encounter a difficulty in formulating the problem in the conventional L^2 Hilbert space.

7.6.1 Mathematical formulation of the generator

Let us consider a Hilbert space

$$V = \mathbb{C}^N \oplus L^2(\mathbb{R}), \tag{7.71}$$

where $\mathbb{C}^N$ is the unitary space of dimension N, and $L^2(\mathbb{R})$ is the complex Lebesgue space on $\mathbb{R}$ endowed with the standard inner product. The member of V is written as

$$\Psi = \begin{pmatrix} \boldsymbol{\alpha} \\ \tilde{\Psi}(x) \end{pmatrix} \quad [\boldsymbol{\alpha} \in \mathbb{C}^N,\ \tilde{\Psi}(x) \in L^2(\mathbb{R})]. \tag{7.72}$$

The inner product of V is, thus, defined as

$$\begin{aligned} (\Psi \,|\, \Psi^\dagger) &= (\boldsymbol{\alpha}, \boldsymbol{\alpha}^\dagger) + (\tilde{\Psi}, \tilde{\Psi}^\dagger) \\ &= \sum_{j=1}^{N} \bar{\alpha}_j \alpha_j^\dagger + \int_{-\infty}^{+\infty} \bar{\tilde{\Psi}}(x) \tilde{\Psi}^\dagger(x)\, \mathrm{d}x \end{aligned} \tag{7.73}$$

We identify

$$\Psi = \begin{pmatrix} \boldsymbol{\alpha} \\ \tilde{\Psi}(x) \end{pmatrix} \ \Leftrightarrow\ \Psi(x) = \sum_{j=1}^{N} \alpha_j \delta(x - a_j) \ +\ \tilde{\Psi}(x). \tag{7.74}$$

It is essential to decompose the delta-measure part (representing the surface waves) from the total vorticity Ψ. Although the supports (in the sense of distributions) of both components $\delta(x - a_j)$ and $\tilde{\Psi}(x)$ may overlap, we separate them into different degrees of freedom. Because $\mathcal{K}\Psi \in C(\mathbb{R})$ for all $\Psi \in V$, the generator $\mathcal{L}$ is a bounded operator on V.

Following Eq. (7.74), the generator $\mathcal{L}$ of Eq. (7.70) is now written in a matrix form

$$\mathcal{L}\Psi = \begin{pmatrix} \omega_1(a_1) & \cdots & kA_1K(a_1, a_N) & \int kA_1K(a_1, x) \cdot \ \mathrm{d}x \\ \vdots & \ddots & \vdots & \vdots \\ kA_NK(a_N, a_1) & \cdots & \omega_N(a_N) & \int kA_NK(a_N, x) \cdot \ \mathrm{d}x \\ 0 & \cdots & 0 & \omega_{\mathrm{c}}(x) \end{pmatrix} \begin{pmatrix} \alpha_1 \\ \vdots \\ \alpha_N \\ \tilde{\Psi}(x) \end{pmatrix}, \tag{7.75}$$

where we have introduced the notation

$$\omega_j(a_j) = kv(a_j) + \frac{A_j}{2} \quad (j = 1, \ldots, N), \tag{7.76}$$

denoting the Doppler shifted diocotron frequency, and $\omega_{\mathrm{c}}(x) = kv(x)$, respectively.

In the previous section, we dealt delta functions in a formal way and did calculations with $\delta(x-\mu)$ for an arbitrary $\mu \in \mathbb{R}$ [see Eq. (7.15)]. We note that such formal functions are not the member of the Hilbert space V. In this section, however, they are justified as generalized eigenfunctions corresponding to 'continuous spectra.'

7.6.2 Spectral resolution of the generator

First, we consider the simple case of single 'source,' i.e., $w(x) = A\delta(x-a)$ (see Sec. 7.4). The surface wave mode has only one degree of freedom ($N = 1$). Here, the generator $\mathcal{L}$ of Eq. (7.75) simplifies as

$$\mathcal{L} = \begin{pmatrix} \omega_1(a) & \int kAK(a,x)\cdot\ dx \\ 0 & \omega_{\mathrm{c}}(x) \end{pmatrix}. \tag{7.77}$$

As we have shown in Sec. 7.4, there are mainly two different classes of formal eigenfunctions [see Eq. (7.41) and Eq. (7.42)]. According to the notation of Eq. (7.72), the eigenvalues and the corresponding eigenfunctions are shown as

$$\omega_1(a) = kv(a) + \frac{A}{2}, \quad \boldsymbol{U}_1 = \begin{pmatrix} 1 \\ 0 \end{pmatrix} \tag{7.78}$$

$$\omega_{\mathrm{c}}(\mu) = kv(\mu), \quad \tilde{\boldsymbol{U}}_c(\mu) = \begin{pmatrix} \frac{m(\mu)kAK(a,\mu)}{\omega_{\mathrm{c}}(\mu)-\omega_1(a)} \\ \tilde{m}(\mu)\delta(x-\mu) \end{pmatrix}, \tag{7.79}$$

where $\tilde{m}$ is defined in order to unify both the non-resonant and resonant (nilpotent) cases as

$$\tilde{m}(\mu) = \begin{cases} m(\mu) & \text{if } \omega_{\mathrm{c}}(\mu) \neq \omega_1(a) \\ (kAK(a,\mu))^{-1} & \text{if } \omega_{\mathrm{c}}(\mu) = \omega_1(a) \text{ (i.e. } m(\mu) = 0), \end{cases} \tag{7.80}$$

with the normalizer

$$m(\mu) = \left[1 + \left(\frac{kAK(a,\mu)}{\omega_{\mathrm{c}}(\mu) - \omega_1(a)}\right)^2\right]^{-1/2}. \tag{7.81}$$

The first eigenfunction (7.78) represents the surface wave. The second one (7.79) includes an arbitrary real number μ, corresponding to the continuous spectrum, and

a singular function $\delta(x-\mu)$. We must integrate Eq. (7.79) over $\mu \in \mathbb{R}$ to span the complete basis of V. Formally, we can define the non-unitary transform

$$\begin{aligned}\mathcal{T} &= \left(\boldsymbol{U}_1 \int (\delta(x-\mu), \ \cdot\ ) \tilde{\boldsymbol{U}}_c(\mu)\, \mathrm{d}\mu \right) \\ &= \begin{pmatrix} 1 & \int (\delta(x-\mu), \ \cdot\ ) \frac{m(\mu) AK(a,\mu)}{\omega_c(\mu)-\omega_1(a)}\, \mathrm{d}\mu \\ 0 & \int (\delta(x-\mu), \ \cdot\ ) \tilde{m}(\mu)\delta(x-\mu)\, \mathrm{d}\mu \end{pmatrix}. \end{aligned} \tag{7.82}$$

To cast this formal expression in an appropriate mathematical representation, we invoke the resolution of the identity (7.19). The formal correspondence is

$$\int_{-\infty}^{+\infty} (\delta(x-\mu), u(x))\, \delta(x-\mu)\, \mathrm{d}\mu = \int_{-\infty}^{+\infty} \mathrm{d}E(\mu) u = u.$$

We also define

$$F(\mu)u = \int_{-\infty}^{\mu} u(x)\, \mathrm{d}x, \tag{7.83}$$

which gives

$$\mathrm{d}F(\mu)u = u(\mu)\, \mathrm{d}\mu.$$

With this notation, we can write

$$\int f(\mu)\, \mathrm{d}F(\mu)u(x) = \int f(\mu)u(\mu)\, \mathrm{d}\mu = \int f(x)u(x)\, \mathrm{d}x.$$

The operator $\mathcal{T}$ is now written in a rigorous form as

$$\mathcal{T} = \begin{pmatrix} 1 & \int \frac{m(\mu)kAK(a,\mu)}{\omega_c(\mu)-\omega_1(a)} \mathrm{d}F(\mu) \\ 0 & \int \tilde{m}(\mu)\, \mathrm{d}E(\mu) \end{pmatrix} = \begin{pmatrix} 1 & \int \frac{m(x)kAK(a,x)}{\omega_c(x)-\omega_1(a)} \cdot\ \mathrm{d}x \\ 0 & \tilde{m}(x) \end{pmatrix} \tag{7.84}$$

Reflecting the non-Hermitian property of the generator $\mathcal{L}$, the operator $\mathcal{T}$ is not a unitary transform. By combing both non-resonant and resonant (nilpotent) cases, this $\mathcal{T}$ gives a regular transform. The inverse operator is

$$\mathcal{T}^{-1} = \begin{pmatrix} 1 & -\int \left(\frac{m(x)}{\tilde{m}(x)}\right) \left(\frac{kAK(a,x)}{\omega_c(x)-\omega_1(a)}\right) \cdot\ \mathrm{d}x \\ 0 & \tilde{m}(x)^{-1} \end{pmatrix}. \tag{7.85}$$

With the transforms $\mathcal{T}$ and $\mathcal{T}^{-1}$, we obtain the Jordan canonical form of $\mathcal{L}$;

$$\begin{aligned}\mathcal{T}^{-1}\mathcal{L}\mathcal{T} &= \begin{pmatrix} \omega_1 & \int \rho(\mu)\, \mathrm{d}F(\mu) \\ 0 & \int \omega_c(\mu)\, \mathrm{d}E(\mu) \end{pmatrix} \\ &= \begin{pmatrix} \omega_1 & \int \rho(x) \cdot\ \mathrm{d}x \\ 0 & \omega_c(x) \end{pmatrix}, \end{aligned} \tag{7.86}$$

where

$$\rho(x) = \begin{cases} 1 & \text{if } \omega_c(\mu) = \omega_1(a) \\ 0 & \text{if } \omega_c(\mu) \neq \omega_1(a) \end{cases}.$$

The support of $\rho(x)$ may have a finite measure when the resonance condition $\omega_c(\mu) = \omega_1(a)$ holds on a finite interval of x.

7.6.3 Spectral representation of the propagator

The propagator $e^{-\mathrm{i}t\mathcal{L}}$ is defined by solving the initial value problem for Eq. (7.12)

$$\begin{cases} \mathrm{i}\partial_t \Psi = \mathcal{L}\Psi \\ \Psi(0) = \Psi^0 \end{cases}, \tag{7.87}$$

and writing the solution as

$$\Psi(t) = e^{-\mathrm{i}t\mathcal{L}}\Psi^0.$$

By introducing $\Psi = \mathcal{T}\chi$, Eq. (7.87) is transformed into

$$\begin{cases} \mathrm{i}\partial_t \chi = \mathcal{T}^{-1}\mathcal{L}\mathcal{T}\chi \\ \chi(0) = \mathcal{T}^{-1}\Psi^0 \end{cases}. \tag{7.88}$$

Using the spectral resolution (7.86), the solution of Eq. (7.88) is given by

$$\begin{aligned} e^{-\mathrm{i}t\mathcal{T}^{-1}\mathcal{L}\mathcal{T}} &= \begin{pmatrix} e^{-\mathrm{i}t\omega_1} & -\int \mathrm{i}te^{-\mathrm{i}t\omega_1}\rho(\mu)\,\mathrm{d}F(\mu) \\ 0 & \int e^{-\mathrm{i}t\omega_\mathrm{c}(\mu)}\,\mathrm{d}E(\mu) \end{pmatrix} \\ &= \begin{pmatrix} e^{-\mathrm{i}t\omega_1} & -\int \mathrm{i}te^{-\mathrm{i}t\omega_1}\rho(x)\cdot\,\mathrm{d}x \\ 0 & e^{-\mathrm{i}t\omega_\mathrm{c}(x)} \end{pmatrix}. \end{aligned} \tag{7.89}$$

The solution of Eq. (7.87) is given by

$$\Psi(t) = \mathcal{T}\left[e^{-it\mathcal{T}^{-1}\mathcal{L}\mathcal{T}}\right]\mathcal{T}^{-1}\Psi^0.$$

With Eqs. (7.84) and (7.85), we obtain

$$\begin{aligned} e^{-\mathrm{i}t\mathcal{L}} &= \mathcal{T}\begin{pmatrix} e^{-\mathrm{i}t\omega_1} & -\int \mathrm{i}te^{-\mathrm{i}t\omega_1}\rho(x)\cdot\,\mathrm{d}x \\ 0 & e^{-\mathrm{i}t\omega_\mathrm{c}(x)} \end{pmatrix}\mathcal{T}^{-1} \\ &= \begin{pmatrix} e^{-\mathrm{i}t\omega_1} & X \\ 0 & e^{-\mathrm{i}t\omega_\mathrm{c}(x)} \end{pmatrix}, \end{aligned} \tag{7.90}$$

where

$$X = \int \left([1-\rho(x)]\frac{[e^{-\mathrm{i}t\omega_\mathrm{c}(x)} - e^{-\mathrm{i}t\omega_1(a)}]kAK(a,x)}{\omega_\mathrm{c}(x)-\omega_1(a)} - \mathrm{i}te^{-\mathrm{i}t\omega_1}kAK(a,x)\rho(x)\right)\cdot\,\mathrm{d}x,$$

and we have used the relations

$$\begin{cases} \dfrac{m(x)}{\tilde{m}(x)} = 1-\rho(x) \\ \dfrac{\rho(x)}{\tilde{m}(x)} = kAK(a,x)\rho(x) \end{cases}.$$

In the case of multiple sources [see Eq. (7.69)], the first class of formal eigenfunctions are obtained by solving

$$\begin{pmatrix} \omega_1(a_1) & \cdots & kA_1K(a_1,a_N) \\ \vdots & \ddots & \vdots \\ kA_NK(a_N,a_1) & \cdots & \omega_N(a_N) \end{pmatrix}\begin{pmatrix} \alpha_1 \\ \vdots \\ \alpha_N \end{pmatrix} = \omega\begin{pmatrix} \alpha_1 \\ \vdots \\ \alpha_N \end{pmatrix}, \tag{7.91}$$

and the second class by

$$\begin{pmatrix} \omega_1(a_1)-\omega_c(\mu) & \cdots & kA_1K(a_1,a_N) \\ \vdots & \ddots & \vdots \\ kA_NK(a_N,a_1) & \cdots & \omega_N(a_N)-\omega_c(\mu) \end{pmatrix} \begin{pmatrix} \alpha_1 \\ \vdots \\ \alpha_N \end{pmatrix} = -\beta \begin{pmatrix} kA_1K(a_1,\mu) \\ \vdots \\ kA_NK(a_N,\mu) \end{pmatrix}. \tag{7.92}$$

Then we can define the transform as

$$\mathcal{T} = \left(\boldsymbol{U}_1 \ \cdots \ \boldsymbol{U}_N \ \int (\delta(x-\mu), \ \cdot \ ) \tilde{\boldsymbol{U}}_c(\mu) \ \mathrm{d}\mu \right), \tag{7.93}$$

where $\boldsymbol{U}_1, \ldots, \boldsymbol{U}_N$ denote the formal eigenfunctions of the first class, respectively, and $\tilde{\boldsymbol{U}}_c$ denote those of second class which are obtained in the way shown above. Again by combining both non-resonant and resonant (nilpotent) cases, this transform $\mathcal{T}$ is not unitary but regular. Thus, the inverse operator $\mathcal{T}^{-1}$ can be defined and $e^{-\mathrm{i}t\mathcal{T}^{-1}\mathcal{L}\mathcal{T}}$ can be generated.

7.7 Laplace transformation

In this section, we will solve the same initial value problem by means of Laplace transformation which is another method to give a general solution for bounded operators. The Laplace transformation is defined here by

$$\hat{f}(x,s) = \int_0^\infty f(x,t)\, e^{-st} \, \mathrm{d}t, \tag{7.94}$$

where s satisfies the condition that its real part is larger than any temporal singularity of the function $f(x,t)$ for the convergence of the integration. The inversion will be given by

$$f(x,t) = \frac{1}{2\pi\mathrm{i}} \int_{s_0-\mathrm{i}\infty}^{s_0+\mathrm{i}\infty} \hat{f}(x,s)\, e^{st} \, \mathrm{d}s, \tag{7.95}$$

where $s_0 = \mathrm{Re}(s) > 0$. Due to the definition of our Hilbert space (7.71), perturbed vorticity will be transformed as

$$\hat{\Psi}(x,s) = \begin{pmatrix} \hat{\boldsymbol{\alpha}}(s) \\ \hat{\tilde{\Psi}}(x,s) \end{pmatrix} = \begin{pmatrix} \displaystyle\int_0^\infty \boldsymbol{\alpha}(t)\, e^{-st} \, \mathrm{d}t \\ \\ \displaystyle\int_0^\infty \tilde{\Psi}(x,t)\, e^{-st} \, \mathrm{d}t \end{pmatrix}. \tag{7.96}$$

The generalized Rayleigh equation (7.12) will be transformed by multiplying e^{-st} on both sides and integrating with respect to time as

$$[\mathrm{i}s - v(x)]\hat{\Psi} - w(x)\mathcal{K}\hat{\Psi} = i\Psi(0), \tag{7.97}$$

where the integrations with respect to ξ (in the operator $\mathcal{K}$) and t has been commuted.

Let us consider at first the single source case. Plugging

$$w(x) = A\delta(x-a) \tag{7.98}$$

and Eq. (7.96) into Eq. (7.97), we have

$$[s+\mathrm{i}\omega_1(a)]\hat{\alpha}(s) + \mathrm{i}\int_{-\infty}^{\infty} kAK(a,\xi)\hat{\tilde{\Psi}}(\xi,s)\,d\xi = \alpha(0), \tag{7.99}$$

$$[s+\mathrm{i}\omega_c(x)]\hat{\tilde{\Psi}}(x,s) = \tilde{\Psi}(x,0), \tag{7.100}$$

or

$$\begin{pmatrix} s+\mathrm{i}\omega_1(a) & \mathrm{i}\int kAK(a,\xi)\cdot\,\mathrm{d}\xi \\ 0 & s+\mathrm{i}\omega_c(x) \end{pmatrix} \begin{pmatrix} \hat{\alpha} \\ \hat{\tilde{\Psi}} \end{pmatrix} = \begin{pmatrix} \alpha(0) \\ \tilde{\Psi}(0) \end{pmatrix}, \tag{7.101}$$

in the matrix form. Equation (7.100) for the inner vorticity fluctuation will be readily solved for each x as

$$\hat{\tilde{\Psi}}(x,s) = \frac{\tilde{\Psi}(x,0)}{s+\mathrm{i}\omega_c(x)}, \tag{7.102}$$

and its pole at $s=-\mathrm{i}\omega_c(x)$ will give a simple oscillation

$$\tilde{\Psi}(x,t) = \tilde{\Psi}(x,0)\,e^{-\mathrm{i}t\omega_c(x)}, \tag{7.103}$$

which exactly coincides with the result obtained by Case [50]. It is shown for the Couette flow that the continuous spectrum exhibits the phase mixing damping of the velocity field v_{1x} proportional to $1/t$ when integrated.

Equation (7.102) will be substituted into Eq. (7.99), which now reads as

$$\hat{\alpha}(s) = \frac{\alpha(0)}{s+\mathrm{i}\omega_1(a)} - \frac{\mathrm{i}}{s+\mathrm{i}\omega_1(a)}\int_{-\infty}^{+\infty} \frac{kAK(a,\xi)\,\tilde{\Psi}(\xi,0)}{s+\mathrm{i}\omega_c(\xi)}\,\mathrm{d}\xi, \tag{7.104}$$

where the isolated pole in the first term gives again the simple oscillation when inverted. By inverting the Laplace transformation, we formally obtain

$$\alpha(t) = \alpha(0)\,e^{-\mathrm{i}t\omega_1(a)} - \frac{1}{2\pi}\int_{s_0-\mathrm{i}\infty}^{s_0+\mathrm{i}\infty} \frac{e^{st}}{s+\mathrm{i}\omega_1(a)}\int_{-\infty}^{+\infty} \frac{kAK(a,\xi)\,\tilde{\Psi}(\xi,0)}{s+\mathrm{i}\omega_c(\xi)}\,\mathrm{d}\xi\,\mathrm{d}s. \tag{7.105}$$

The second term has two singularities which apparently looks same as the case of kinetic treatment for electrostatic oscillations (see Appendix C). However, since the numerator of the integrand is not an analytic function in all region on the real axis of ξ, the analytic continuation cannot be properly defined. Thus, we have to choose another method here. Fortunately, double integrations in the second term

are commutable since both of them are uniformly converging. Thus, the integration with respect to s can be evaluated by deforming the integration path as

$$\begin{aligned}
&\frac{1}{2\pi}\int_{s_0-\mathrm{i}\infty}^{s_0+\mathrm{i}\infty}\frac{e^{st}}{s+\mathrm{i}\omega_1(a)}\int_{-\infty}^{+\infty}\frac{kAK(a,\xi)\,\tilde{\Psi}(\xi,0)}{s+\mathrm{i}\omega_\mathrm{c}(\xi)}\,\mathrm{d}\xi\,\mathrm{d}s\\
&=\frac{1}{2\pi}\int_{-\infty}^{+\infty}\mathrm{d}\xi\,AK(a,\xi)\,\tilde{\Psi}(\xi,0)\int_{s_0-\mathrm{i}\infty}^{s_0+\mathrm{i}\infty}\frac{e^{st}}{[s+\mathrm{i}\omega_1(a)][s+\mathrm{i}\omega_\mathrm{c}(\xi)]}\,\mathrm{d}s\\
&=\frac{1}{2\pi}\int_{-\infty}^{+\infty}\mathrm{d}\xi\,\frac{kAK(a,\xi)\,\tilde{\Psi}(\xi,0)}{\mathrm{i}\omega_\mathrm{c}(\xi)-\mathrm{i}\omega_1(a)}\int_{s_0-\mathrm{i}\infty}^{s_0+\mathrm{i}\infty}\left(\frac{1}{s+\mathrm{i}\omega_1(a)}-\frac{1}{s+\mathrm{i}\omega_\mathrm{c}(\xi)}\right)e^{st}\,\mathrm{d}s\\
&=\int_{-\infty}^{+\infty}\frac{[e^{-\mathrm{i}t\omega_1(a)}-e^{-\mathrm{i}t\omega_\mathrm{c}(\xi)}]kAK(a,\xi)}{\omega_\mathrm{c}(\xi)-\omega_1(a)}\,\tilde{\Psi}(\xi,0)\,\mathrm{d}\xi. \qquad (7.106)
\end{aligned}$$

Then, the final expression for the surface wave evolution is given by

$$\alpha(t)=\alpha(0)\,e^{-\mathrm{i}t\omega_1(a)}+\int_{-\infty}^{+\infty}\frac{[e^{-\mathrm{i}t\omega_1(a)}-e^{-\mathrm{i}t\omega_\mathrm{c}(\xi)}]kAK(a,\xi)}{\omega_1(a)-\omega_\mathrm{c}(\xi)}\,\tilde{\Psi}(\xi,0)\,\mathrm{d}\xi. \qquad (7.107)$$

By combining Eq. (7.103) with Eq. (7.107), the solution for the initial value problem is expressed in the following matrix form;

$$\begin{pmatrix}\alpha(t)\\ \tilde{\Psi}(x,t)\end{pmatrix}=\begin{pmatrix}e^{-\mathrm{i}t\omega_1(a)} & \int_{-\infty}^{+\infty}\frac{[e^{-\mathrm{i}t\omega_1(a)}-e^{-\mathrm{i}t\omega_\mathrm{c}(x)}]kAK(a,x)}{\omega_1(a)-\omega_\mathrm{c}(x)}\cdot\,\mathrm{d}x\\ 0 & e^{-\mathrm{i}t\omega_\mathrm{c}(x)}\end{pmatrix}\begin{pmatrix}\alpha(0)\\ \tilde{\Psi}(x,0)\end{pmatrix}, \qquad (7.108)$$

which exactly coincides with the previous expression (7.90) obtained by means of the spectral method. It is noted that the value of the function

$$\frac{[e^{-\mathrm{i}t\omega_1(a)}-e^{-\mathrm{i}t\omega_\mathrm{c}(x)}]}{\omega_1(a)-\omega_\mathrm{c}(x)} \qquad (7.109)$$

at zeros of the denominator should be defined by the value $-\mathrm{i}te^{-\mathrm{i}t\omega_1(a)}$ of the limit $\omega_\mathrm{c}(x)\to\omega_1(a)$.

7.8 Summary

We have obtained the spectral resolution of the non-Hermitian operator for the surface wave model of Kelvin-Helmholtz instability. With the aid of dividing the Hilbert space into a finite discrete part and an infinite continuous part, we have shown that the operator of Rayleigh equation is bounded. It is found that the system has a resonance (frequency overlapping) between the inner vorticity fluctuation and the surface wave. When the resonance occurs in a finite measure region which introduces the point spectra in the inner vorticity fluctuation, the resonance gives the energy transfer from the inner vorticity fluctuation to the surface wave. This leads to the secular behavior of the surface wave. However, when the resonance occurs in a zero

measure region, the energy cannot be transferred from the continuous spectrum to the point one. Therefore, the surface wave just represents the asymptotic oscillation.

In the case of kinetic treatment for electrostatic oscillations [95], the multiplication is given by a simple coordinate operator which only contains the continuous spectrum. Therefore, the resonance happens to balance with the phase mixing due to continuum damping, and leads to the stationary asymptotic behavior. Here, the situation of Kelvin-Helmholtz instability is quite similar to the electrostatic oscillations, but the multiplication is given by a function. Thus, the Kelvin-Helmholtz instability may bring about the point spectra and secular behavior of the surface wave. In the physical situation, however, the resonance with finite measure may not be rarely satisfied. In this case, it may not be considered to produce secularity. By modifying the system, resonance may happen between two continuous spectra. Then, a realistic secular behavior is produced [84].

Chapter 8

Concluding remarks

In this thesis, one dimensional linear spectral properties in incompressible single fluid magnetohydrodynamic (MHD) plasma were explored for several cases related to stability problem in magnetically confined plasmas for fusion research.

In Chap. 2, we have discussed the Hermiticity in connection with the norm of the operator in detail. Boundary conditions are well known to affect the spectra of the operators, however, in this chapter, it is explicitly described that the Hermiticity strongly depends on how we take the norm for the operator. If we may prove the Hermiticity of the operator with a certain norm, we can construct a spectral resolution under this norm. We have reviewed the basic spectra of shear Alfvén waves for static plasma (Hermitian generator) in both the slab and cylindrical geometry. Moreover, it is shown that the linearized equation of two dimensional incompressible Euler fluid can be also shown Hermitian if the ambient shear flow does not include any inflection point (Rayleigh's criterion). However, the system which contains any complex eigenvalue is not such a case.

Chapters 3 and 4 are devoted to the analysis of Hermitian operators. In Chap. 3, we have shown the analysis for non-resonant interchange instabilities (point spectra). It has been discussed why the prediction of the Mercier (Suydam) criterion for localized interchange modes does not explain some stable discharges achieved in stellarators. Usually, the destabilizing pressure gradient at the mode resonant surface makes the unstable mode to be localized. However, the local flattening of the pressure profile prohibits the localization of the unstable eigenmode even in the limit of marginal stability. With the numerical computation of the spectral ordinary differential equation, it is shown that the unstable eigenmode tends to have a step like structure at the resonant surface in this case. It is also found that the growth rate of the non-resonant mode decreases to zero without the tail formation near the beta (ratio of plasma pressure to magnetic pressure) limit like the Suydam modes.

The obtained beta limit of the non-resonant mode becomes mostly an order of magnitude higher than that obtained from Suydam criterion for the smooth pressure profile. This may explain the discrepancy of the experimental result that the beta exceeded the Mercier limit. Furthermore, we have shown the situation where the unstable non-resonant mode sets the beta limit which is lower than calculated from Mercier (Suydam) criterion. These perspectives obtained from cylindrical plasma model are also confirmed with a toroidal model for interchange modes.

In Chap. 4, we have calculated the damping of the surface Alfvén wave due to continuous spectra induced by the rapid change of equilibrium density profile in a slab geometry by means of the Laplace transformation method. As is shown in Sec. 2.6, every singular eigenfunction corresponding to the Alfvén continuous spectra has logarithmic singularity originated from the regularity of the singular point in the spectral ordinary differential equation. When we solve the problem by means of the Laplace transformation, it brings about the singularity of the Green's function in the analytically continuated Riemannian surface, which yields the damping rate (exponential damping) of the magnetic fluctuation. The results were compared with experimental observation of the pellet injection in Heliotron-E. The damping rate has a maximum in relation to the sharpness of density gradient, and numerical results show that the damping rate is consistent with experiment for an adequate physical parameters. In the sharp density limit (step function), this damped solution connects to the surface eigenmode.

Chapters 5, 6, and 7 are devoted for the spectral analyses of non-Hermitian (non-selfadjoint) operators. In Chap. 5, the effect of surrounding resistive wall on rigidly flowing plasma has been investigated. Since the whole system is not represented in the form of single evolution equation, it is difficult to construct a spectral representation. However, the detailed property and the behavior of an eigenmode (a point spectrum) are explored. By approximating the system in a slab geometry, we have estimated the effect of the resistive wall with replacing the wall current by a mirror image current. In static plasmas, the external kink mode (surface current driven instability) with surrounding resistive wall carries a smaller image current, which causes the instability in the resistive wall time scale. However, when plasma is rigidly flowing with respect to the wall, the image current is not only weak compared to the plasma surface current, but also becomes phase shifted, which yields another destabilizing mechanism similar to Kelvin-Helmholtz instability in neutral fluids. The combination of the magnitude and relative phase of the image current produces a small hump of the growth rate with respect to the wall position, which is related to the closest limit of wall position for the stabilization of external kink instability due to continuous spectrum. The dispersion relation is analytically

solved by means of the perturbation method, and the wall position of the maximum growth rate is evaluated from the breakdown point of the perturbation expansion. It is predicted that, if the flow velocity is increased, the extremum of the growth rate will become closer to the plasma edge, however, the dependence of growth rate on the flow velocity is very weak (logarithmic).

In Chap. 6, transient and secular behaviors of interchange fluctuations are analyzed in an ambient shear flow by invoking Kelvin's method of shearing modes. The expansion with Kelvin's modes is shown to give general solutions in the case of linear shear flow profile. However, since it is only applicable to the system with infinite domain unfortunately, we cannot study the effect of shear flow on the point spectra. By means of this method, we have first analyzed the incompressible electromagnetic perturbations in the presence of an interchange drive and obtained the ordinary differential equation for the amplitude of the modes. All modes show asymptotic decay proportional to the inverse power of time (non-exponential) without any threshold value. This means that the interchange instabilities are always damped away at sufficiently long time due to the combined effect of the Alfvén wave propagation and the distortion of mode structure by means of the background shear flow; i.e. phase mixing effect. However, the transient behavior is not common for all modes. Fluctuations with particular wave numbers show transient amplifications which are even faster than the growth rate of interchange modes in static plasmas. These amplifications are so prominent that they may lead to the break down of the linearity of the perturbation. On the time evolution for the perturbations with purely perpendicular wave vectors to the ambient magnetic field, which do not excite the Alfvén wave, the flow shear has been also shown to have a stabilizing effect. However, the phase mixing effect alone cannot completely stabilize the interchange instabilities and the algebraic growth of the perturbation still remains. The condition for the boundedness of mode amplitude of the stream function is obtained; however, the conditions of different physical quantities do not coincide. The discrepancies originate from the fact that, in shear flow systems, different perturbations experience algebraic evolutions characterized by different powers of time, while the time evolutions for any fields are expressed in a common exponential form for static systems. This may represent a pathological aspect of the stability problem in shear flow plasmas.

In Chap. 7, the spectral theory of Rayleigh equation is demonstrated with surface wave model by invoking a proper definition of the Hilbert space. When the system is Kelvin-Helmholtz unstable with complex eigenvalues, the generator can be properly diagonalized. The generator turns out to be an infinite dimensional one correspondent to the semi-simple matrix in the finite dimensional linear space. It is shown, however, that the system contains the resonance of point spectra (cor-

responding to diocotron modes) and continuous spectra (corresponding to entropy waves) in the case where the equilibrium is stable to the Kelvin-Helmholtz mode (no complex eigenvalue). Simple resonance among point spectra will cause a secular growth of the mode; however, it is shown that the resonance, which contains the energy flow from continuous spectra to point ones, may not cause secularity of the perturbed quantities. It is noted that, by considering the another model, e.g. parallel dynamics of electrons, such secular behavior will be realized due to the inclusion of the resonance between two continuous spectra. It means that, even if we do not have any unstable eigenvalue, we may have growth of the algebraic type, which may cause an instability of the system.

Appendix A

Equations of state

In this chapter we consider the relation between the Poisson relation in thermodynamics and the adiabatic equation in MHD [10, 12], which are rare to be described simultaneously in references. Moreover, we will show that the incompressibility condition can be derived as a singular limit of the adiabatic equation of state.

We define a fluid element as what occupies a local space surrounded by a certain boundary surfaces. In a plasma, the fluid element consists of innumerable charged particles, however, from macroscopic viewpoint, the fluid element must be sufficiently small in order to treat the macroscopic quantities as a common value. By assuming to take such an element for a plasma, we may define the plasma pressure, volume, and other macroscopic quantities for this element. Rigorously speaking, it is not evident whether the volume for fluid element is well defined. Since the density for the element can be defined, we define the volume in terms of local density of the fluid element. Therefore the volume is considered as a local quantity. Moreover, although the plasma consists of electrons and ions, we do not distinguish the difference and treat as a single fluid within the context of MHD.

Here we assume that each plasma element is at thermodynamical equilibrium in every time and every space. For p, V, n, R, T denoting pressure, volume, mol number of particles in an element, constant of gas, and temperature, respectively, Boyle-Charles' law;

$$pV = nRT \tag{A.1}$$

is assumed valid for a plasma.

For Q, S describing heat and entropy, the specific heat at constant volume C_v and that at constant pressure C_p are represented as

$$C_v = \Big(\frac{\partial Q}{\partial T}\Big)_V = T\Big(\frac{\partial S}{\partial T}\Big)_V, \tag{A.2}$$

$$C_p = \Big(\frac{\partial Q}{\partial T}\Big)_p = T\Big(\frac{\partial S}{\partial T}\Big)_p. \tag{A.3}$$

Here the subscripts for partial derivatives represent the fixed variable explicitly.

For $x = x(y,z)$, $y = y(z,x)$, $z = z(x,y)$ and $t = t(x,y,z)$, there are following relations;

$$\Big(\frac{\partial x}{\partial y}\Big)_z\Big(\frac{\partial y}{\partial z}\Big)_x\Big(\frac{\partial z}{\partial x}\Big)_y = -1, \tag{A.4}$$

$$\Big(\frac{\partial x}{\partial y}\Big)_z = \Big(\frac{\partial x}{\partial y}\Big)_t + \Big(\frac{\partial x}{\partial t}\Big)_y\Big(\frac{\partial t}{\partial y}\Big)_z. \tag{A.5}$$

At first, regarding x, y, z, t as S, T, V, p, respectively, in Eq. (A.5), and using equation of state (A.1) leads straightforwardly to the Mayer's relation;

$$C_p - C_v = nR. \tag{A.6}$$

And next, regarding x, y, z, t as p, V, S, T, respectively, Eq. (A.5) becomes

$$\Big(\frac{\partial p}{\partial V}\Big)_S = \Big(\frac{\partial p}{\partial V}\Big)_T + \Big(\frac{\partial p}{\partial T}\Big)_V\Big(\frac{\partial T}{\partial V}\Big)_S. \tag{A.7}$$

Using Eq. (A.4), we can write the last term as

$$\Big(\frac{\partial T}{\partial V}\Big)_S = -\Big(\frac{\partial T}{\partial S}\Big)_V\Big(\frac{\partial S}{\partial V}\Big)_T = -\frac{T}{C_v}\Big(\frac{\partial p}{\partial T}\Big)_V = -\frac{p}{C_v}. \tag{A.8}$$

In the last form of Eq. (A.8) we used the equation of state (A.1). Substituting this relation into Eq. (A.5) and using Mayer's relation (A.6), we obtain

$$\Big(\frac{\partial p}{\partial V}\Big)_S = -\frac{p}{V}\Big(1 + \frac{nR}{C_v}\Big) = -\frac{p}{V}\frac{C_p}{C_v}, \tag{A.9}$$

and integrating this equation leads to the following relation known as Poisson relation;

$$pV^\gamma = \text{const}, \tag{A.10}$$

where γ denotes the specific heat ratio $\gamma = C_p/C_v$. The relation (A.10) is called adiabatic law, since variation of the system with a fixed S means no heat conduction not only between the system and the outer region, but among all fluid elements. In other words, when the system suffers an adiabatic variation, the Poisson relation is applicable.

For a mass density of particles ρ, the volume is inversely proportional to the mass density, $V \propto \rho^{-1}$. Since the time derivative of Eq. (A.10) vanishes, the Poisson relation can be written as

$$\frac{\mathrm{d}}{\mathrm{d}t}\left(p\rho^{-\gamma}\right) = 0, \tag{A.11}$$

where $\mathrm{d}/\mathrm{d}t = \partial_t + \boldsymbol{v} \cdot \nabla$ and $\boldsymbol{v}$ denotes a fluid velocity. Since we are looking at a certain fluid element, the time derivative should be taken in Lagrangian way. Substituting the continuity equation (2.1);

$$\frac{\mathrm{d}\rho}{\mathrm{d}t} = -\rho \nabla \cdot \boldsymbol{v}, \tag{A.12}$$

into Eq. (A.11), we obtain the pressure evolution equation (2.3);

$$\frac{\mathrm{d}p}{\mathrm{d}t} + \gamma p \nabla \cdot \boldsymbol{v} = 0. \tag{A.13}$$

For the degree of freedom of the macroscopic system N, the specific heat at constant volume is given as $C_v = NR/2$ from equipartition law of energy. Then the Mayer's relation (A.6) yields $\gamma = (N+2)/N$, i.e. for higher N, γ becomes smaller and approaches to unity. It can be interpreted intuitively that for the system with a larger degree of freedom, the fluid element can be deformed in a higher degree of freedom and can escape from the compression when external force is applied. Therefore, the adiabatic compression needs more pressure in the higher N than the lower one in order to decrease the same volume of the fluid element.

Following the above discussion, we can define the incompressibility condition as a singular limit of the adiabatic relation for the ideal gas (A.13). Incompressible fluid is that, the fluid element does not suffer any compression against any strong external pressure, i.e. n/V does not change for any large p. Even if the fluid element is deformed when exposed to an external force, however, it cannot be diverse freely and suffers the tightening from all direction due to its incompressibility, which is connected with the limit $N \to 0$. This gives a singular limit of the adiabatic equation of state $\gamma \to \infty$, which leads to the incompressible equation of state as

$$\nabla \cdot \boldsymbol{v} = 0. \tag{A.14}$$

By replacing the adiabatic equation of state (A.13) by the incompressible one (A.14), we can close the system of MHD equations.

In the same way, we can take the incompressible limit of the solution obtained by means of the compressible equation of state, however, it should be noted that the solution is consistent with the original adiabatic equation only in the limit $\gamma \to \infty$ in the way that

$$\gamma(\nabla \cdot v) \to -\frac{1}{p}\frac{\mathrm{d}p}{\mathrm{d}t}. \tag{A.15}$$

This is the case discussed in Sec. 4.3. The limit $\gamma \to \infty$ corresponds to the situation where the sound wave will be excluded by putting $v_\mathrm{s} \to \infty$. Considering the fact that the phase velocity of the sound wave is much faster in the less compressible water than in the more compressible atmosphere, this result can be acceptable.

It is also noted that the condition of isothermal variation is obtained from Eq. (A.1) as $T = \text{const}$. Sometimes the anisotropic variation is considered. Such a case is discussed in Refs. [10, 12].

Appendix B

Spectral theory

This chapter is devoted to the explanation of mathematical background of the spectral theory. Spectral theory of linear operators is quite widely used in linear stability or linear wave analyses in plasma physics. The mathematical basis is, however, rarely quoted in literatures, which might lead to the improper understanding of the complicated phenomena of plasmas.

The examples described here might be somewhat trivial, at least in mathematics. However, detailed analyses of basic problems may sometimes help the physicists for better understandings. First, we will review the spectral theory of finite dimensional linear matrix operator, which has been completed due to the great works by Jordan. Next, we will treat infinite dimensional differential operator, which is, in any sense, far from complete theory unlike the finite dimensional one. Since whole part of this thesis is devoted to the analyses of such infinite dimensional operators, we will focus on the simple description here and explain the basis of well-known methods widely used in literatures.

B.1 Finite dimensional operators

Let us first describe the complete classification of the finite dimensional operators. The finite dimensional operators can be classified in a suitable way for the spectral theory as follows;

1. Hermitian (selfadjoint) matrix
   All eigenvectors can be taken orthogonal and all eigenvalues are real.

2. Normal matrix (commutable with its adjoint)
   All eigenvectors can be taken orthogonal, but some eigenvalues are complex.

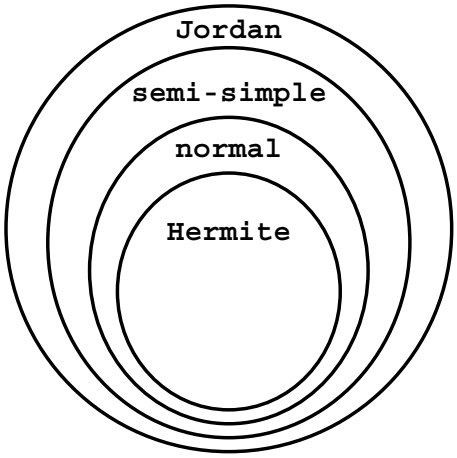

Figure B.1: Classification of finite dimensional linear matrix operators.

3. Semi-simple matrix
   Eigenvectors cannot be taken orthogonal, but linear space is spanned only by eigenvectors.

4. Jordan matrix
   Eigenvectors are not enough to span whole linear space.

The schematic view is shown in Fig. B.1. In general, any finite dimensional matrix operator belongs to one of the above sets. We can recognize how small is the region occupied by the Hermitian operators in the whole linear operators even in the finite dimensional case. In some sense, there may expand rich varieties of unknown sea out of Hermitian operators.

B.1.1 Spectral resolution of Hermitian matrices

Here we will discuss the solution of the abstract Schrödinger type evolution equation

$$\mathrm{i}\partial_t \boldsymbol{\psi} = \mathcal{A}\boldsymbol{\psi}, \tag{B.1}$$

where the generator $\mathcal{A}$ is assumed a Hermitian matrix defined in N ($\in \mathbb{N}$) dimensional vector space $\boldsymbol{V} = \mathbb{C}^N$. The definition of Hermitian matrix will be given later. The scalar product for two elements $\boldsymbol{\phi}, \boldsymbol{\psi} \in \boldsymbol{V}$ is defined as

$$(\boldsymbol{\phi} \,|\, \boldsymbol{\psi}) = \sum_{j=1}^{N} \bar{\phi}_j \psi_j, \tag{B.2}$$

where ϕ_j (ψ_j) denotes the j-th component of the vector $\boldsymbol{\phi}$ ($\boldsymbol{\psi}$). Then the vector space $\boldsymbol{V}$ is found to be an N dimensional Hilbert space. Here, the bar denotes the complex conjugate.

An eigenvector $\boldsymbol{\varphi}$ of the matrix $\mathcal{A}$ is defined by a nonzero element of $\boldsymbol{V}$ which satisfies

$$\mathcal{A}\boldsymbol{\varphi} = \lambda\boldsymbol{\varphi}, \tag{B.3}$$

where $\lambda \in \mathbb{C}$ is called the eigenvalue. Then, the zero vector and the totality of $\boldsymbol{\varphi}$, which belong to the eigenvector corresponding to the eigenvalue λ, are denoted as $\boldsymbol{W}$. This constitutes the $\mathcal{A}$-invariant subspace of $\boldsymbol{V}$. Here $\boldsymbol{W}$ is called an eigenspace corresponding to the eigenvalue λ.

Adjoint matrix $\mathcal{A}^*$ is a matrix which satisfies

$$(\mathcal{A}^*\boldsymbol{\phi} \,|\, \boldsymbol{\psi}) = (\boldsymbol{\phi} \,|\, \mathcal{A}\boldsymbol{\psi}), \tag{B.4}$$

for any $\boldsymbol{\phi}, \boldsymbol{\psi} \in \boldsymbol{V}$. The $\mathcal{A}^*$ is represented by the complex conjugate of the transposed matrix. Hermitian (selfadjoint) matrix is the one which satisfies $\mathcal{A}^* = \mathcal{A}$. It is readily shown that all eigenvalues of the Hermitian matrix are real.[1] Moreover, it is known that all eigenvectors can be taken orthogonal and the totality of eigenspaces span the original vector space:

$$\boldsymbol{V} = \boldsymbol{W}_1 \oplus \boldsymbol{W}_2 \oplus \cdots \oplus \boldsymbol{W}_N, \tag{B.5}$$

where $\oplus$ denotes the direct orthogonal sum of the eigenspaces. It is noted that normal matrices also allow the orthogonal decomposition of the vector space $\boldsymbol{V}$ by their eigenvectors, however, the semi-simple matrices allow the decomposition

$$\boldsymbol{V} = \boldsymbol{W}_1 \dot{+} \boldsymbol{W}_2 \dot{+} \cdots \dot{+} \boldsymbol{W}_N, \tag{B.6}$$

where $\dot{+}$ denotes the simple direct sum in which eigenspaces may not be orthogonal.

The spectral resolution of the Hermitian matrix $\mathcal{A}$ will be described with use of the commutability with its adjoint.[2] Let $\mathcal{P}_n$ be the projection operator from $\boldsymbol{V}$ onto $\boldsymbol{W}_n$, then it will be expressed as

$$\mathcal{P}_n = \boldsymbol{\varphi}_n(\boldsymbol{\varphi}_n| \cdot), \tag{B.7}$$

where $\boldsymbol{\varphi}_n \in \boldsymbol{V}$ denotes the normalized eigenvector of the operator $\mathcal{A}$ which corresponds to the eigenvalue λ_n. Here the dimension of the eigenspace $\boldsymbol{W}_n$ is assumed as unity for simplicity. It is noted that Eq. (B.7) is sometimes expressed as $\mathcal{P}_n = |\boldsymbol{\varphi}_n)(\boldsymbol{\varphi}_n|$ in the quantum mechanics context by following Dirac [8]. It is shown that any Hermitian operator $\mathcal{A}$ will be expressed in terms of the projector as

$$\mathcal{A} = \sum_{n=1}^{N} \lambda_n \mathcal{P}_n, \tag{B.8}$$

[1] For any eigenvalue λ and the corresponding eigenvector $\boldsymbol{\varphi}$, $(\boldsymbol{\varphi} \,|\, \mathcal{A}\boldsymbol{\varphi}) = \lambda(\boldsymbol{\varphi} \,|\, \boldsymbol{\varphi})$ holds. On the other hand, $(\boldsymbol{\varphi} \,|\, \mathcal{A}\boldsymbol{\varphi}) = (\mathcal{A}\boldsymbol{\varphi} \,|\, \boldsymbol{\varphi}) = \bar{\lambda}(\boldsymbol{\varphi} \,|\, \boldsymbol{\varphi})$ also holds, which supports $\lambda = \bar{\lambda}$.

[2] Therefore, the following orthogonal spectral resolution is applicable to more general normal matrix which satisfies $\mathcal{A}^*\mathcal{A} = \mathcal{A}\mathcal{A}^*$.

which is called a spectral resolution of the Hermitian matrix operator $\mathcal{A}$. Here the resolution of identity can be produced as

$$\sum_{n=1}^{N} \mathcal{P}_n = \mathcal{I}, \tag{B.9}$$

where $\mathcal{I}$ denotes the identity matrix, and the orthogonality of the projector

$$\mathcal{P}_i \mathcal{P}_j = 0 \quad (i \neq j) \tag{B.10}$$

holds due to the orthogonality of the eigenvectors.

Based on the above knowledges, we can solve Eq. (B.1) by means of spectral resolution method. Substituting the spectral resolution (B.8) into original Schrödinger type equation (B.1) leads to

$$\begin{aligned} \mathrm{i}\partial_t \boldsymbol{\psi} &= \sum_{n=1}^{N} \lambda_n \mathcal{P}_n \boldsymbol{\psi} \\ &= \sum_{n=1}^{N} \lambda_n \boldsymbol{\varphi}_n (\boldsymbol{\varphi}_n \,|\, \boldsymbol{\psi}). \end{aligned} \tag{B.11}$$

Taking the scalar product of both sides with $\boldsymbol{\varphi}_i$ ($i \in \mathbb{N}$) gives

$$\mathrm{i}\partial_t (\boldsymbol{\varphi}_i |\, \boldsymbol{\psi}) = \lambda_i (\boldsymbol{\varphi}_i |\, \boldsymbol{\psi}), \tag{B.12}$$

due to the orthogonality of eigenvectors. Equation (B.12) is readily solved and we obtain the time evolution of each 'mode' as

$$(\boldsymbol{\varphi}_i |\, \boldsymbol{\psi})(t) = e^{-\mathrm{i}\lambda_i t} (\boldsymbol{\varphi}_i |\, \boldsymbol{\psi})(0) \tag{B.13}$$

Substituting it into resolution of $\boldsymbol{\psi}(t)$

$$\begin{aligned} \boldsymbol{\psi}(t) &= \sum_{n=1}^{N} \mathcal{P}_n \boldsymbol{\psi}(t) \\ &= \sum_{n=1}^{N} \boldsymbol{\varphi}_n (\boldsymbol{\varphi}_n |\, \boldsymbol{\psi})(t), \end{aligned} \tag{B.14}$$

we obtain the general solution as

$$\boldsymbol{\psi}(t) = \sum_{n=1}^{N} \boldsymbol{\varphi}_n e^{-\mathrm{i}\lambda_i t} (\boldsymbol{\varphi}_i |\, \boldsymbol{\psi})(0). \tag{B.15}$$

Since the whole linear vector space $\boldsymbol{V}$ is spanned by only eigenfunctions with real eigenvalues for the Hermitian matrix $\mathcal{A}$, the time evolution is written in the form of the superposition of simple harmonic oscillators (eigenmodes).

It is noted that, up to semi-simple matrix, this method works with slight modifications. The time evolution of the whole system is determined by the exponential function with eigenvalues of the operator as its exponent, even though the orthogonality of eigenmodes may not follow in the case of semi-simple matrix.

B.1.2 Algebraic instability of Jordan matrices

In this section, the pathology of applying the spectral resolution for Jordan matrices is shown. We will invoke here a different method from the previous section. Since finite dimensional matrix operator is a bounded one, we can define the exponential function of the operator as

$$e^{\mathcal{A}} = \mathcal{I} + \mathcal{A} + \frac{1}{2!}\mathcal{A}^2 + \cdots, \tag{B.16}$$

where $\mathcal{I}$ denotes the identity matrix. It is shown that this expression gives a convergent series. Using the exponential function of the matrix, we can write the solution of the original Schrödinger equation (B.1) as

$$\boldsymbol{\psi}(t) = e^{-\mathrm{i}t\mathcal{A}}\boldsymbol{\psi}(0). \tag{B.17}$$

If $\mathcal{A}$ were a Hermitian (semi-simple) matrix, the linear space $\boldsymbol{V}$ would be spanned by eigenvectors. Therefore, the expansion

$$\begin{aligned} e^{-\mathrm{i}t\mathcal{A}} &= e^{-\mathrm{i}\lambda t}e^{-\mathrm{i}t(\mathcal{A}-\lambda\mathcal{I})} \\ &= e^{-\mathrm{i}\lambda t}\Big[\mathcal{I} - \mathrm{i}t(\mathcal{A}-\lambda\mathcal{I}) - \frac{t^2}{2}(\mathcal{A}-\lambda\mathcal{I})^2 + \cdots\Big], \end{aligned} \tag{B.18}$$

applied for the component of the eigenspace corresponding to the eigenvalue λ, would give no contribution except for the first term in the square bracket. It made the problem possible to represent the whole dynamics of the system by the superposition of exponential time evolution.

However, the eigenvectors are not enough, in general, to span the whole linear space $\boldsymbol{V}$ for the Jordan matrix. Let $\boldsymbol{\varphi}$ be one of eigenvectors in a wider sense belonging to the eigenvalue λ, and $(\mathcal{A}-\lambda\mathcal{I})^n\boldsymbol{\varphi}$ vanishes at first for $n \in \mathbb{N}$ $(n > 1)$. That is shown as

$$(\mathcal{A}-\lambda\mathcal{I})^j\boldsymbol{\varphi}\begin{cases} \neq 0 & \text{for} \quad j < n \\ = 0 & \text{for} \quad j \geq n \end{cases}. \tag{B.19}$$

Suppose that the initial condition is taken as $\boldsymbol{\varphi}$. From the expressions shown in Eqs. (B.17) and (B.18), we have

$$\begin{aligned} \boldsymbol{\psi}(t) &= e^{-\mathrm{i}\lambda t}e^{-\mathrm{i}t(\mathcal{A}-\lambda\mathcal{I})}\boldsymbol{\varphi} \\ &= e^{-\mathrm{i}\lambda t}\sum_{j=0}^{n-1}\frac{(-\mathrm{i}t)^j}{j!}(\mathcal{A}-\lambda\mathcal{I})^j\boldsymbol{\varphi}. \end{aligned}$$

Thus, the fastest growing mode of the eigenvector in a wider sense belonging to the eigenvalue λ shows divergence of the dependence $t^{(n-1)}e^{-\mathrm{i}\lambda t}$, which corresponds to an instability even if the eigenvalue λ is real. The algebraic growth of amplitudes is called 'secularity.'

B.2 Differential operator

In this section, we will show an example of spectral resolution for the differential operator corresponding to Schrödinger equation, and compare two widely used methods for the spectral analysis, i.e. Fourier transformation and Laplace transformation. Difficulties of constructing the complete spectral theory for differential operators are coming from the infinity of their dimensions, which leads to the appearance of continuous spectra, and unboundedness of their spectra. However, we will not discuss such difficulties in this section. For readers who are interested in such profound problems, several mathematical books are useful [28, 11, 6]. It is also noted that the following discussions may not follow with the terminology of modern mathematics.

B.2.1 Spectral resolution

First, we will consider the one dimensional Laplacian operator

$$\mathcal{A} = \partial_x^2, \tag{B.20}$$

defined in the Sobolev space $H_0^1[0,1]$. Here, $H_0^1[0,1]$ denotes the set of the once differentiable functions $f(x)$ defined in the region $x \in [0,1]$ which satisfies the boundary condition $f(0) = f(1) = 0$. The scalar product in this functional space is defined by

$$(u \,|\, v) = \int_0^1 \bar{u} v \, \mathrm{d}x, \tag{B.21}$$

for the elements $u, v \in H_0^1[0,1]$, where the bar denotes the complex conjugate. It is readily shown that the operator $\mathcal{A}$ is Hermitian (selfadjoint) in this functional space.

Since

$$\frac{\mathrm{d}^2}{\mathrm{d}x^2} \sin(n\pi x) = -(n\pi)^2 \sin(n\pi x) \tag{B.22}$$

holds, the eigenvalues of the operator $\mathcal{A}$ are

$$\lambda_n = -(n\pi)^2 \quad (n \in \mathbb{N}), \tag{B.23}$$

and the corresponding normalized eigenfunctions are

$$u_n = \sqrt{2} \sin(n\pi x). \tag{B.24}$$

It is known that this set of eigenfunctions u_n constitutes a complete orthogonal basis in $H_0^1[0,1]$ with the scalar product (B.21). Therefore, an arbitrary function $\phi \in H_0^1[0,1]$ will be expanded as

$$\phi(x) = \sum_{n=1}^{\infty} a_n u_n(x), \tag{B.25}$$

where a_n is given by

$$a_n = (u_n \,|\, \phi). \tag{B.26}$$

It is noted here that the operator

$$\mathcal{P}_n = |u_n)(u_n| = u_n(x) \int_0^1 u_n(x) \ \cdot \ \mathrm{d}x \tag{B.27}$$

describes the projection from $H_0^1[0,1]$ onto the subspace spanned by $|u_n)$ and the spectral resolution of $\mathcal{A}$ is denoted as

$$\mathcal{A} = \sum_{n=1}^{\infty} \lambda_n \mathcal{P}_n, \tag{B.28}$$

which shows the formal equivalence between the matrix representation and the differential one in quantum mechanics [8, 22]. Furthermore,

$$\sum_{n=1}^{\infty} \mathcal{P}_n = 1 \tag{B.29}$$

is called the resolution of identity for the operator $\mathcal{A}$, which is obtained from the Parseval's equality

$$\|\phi\|^2 = \sum_{n=1}^{\infty} |(u_n \,|\, \phi)|^2, \tag{B.30}$$

where $\|\phi\| = (\phi \,|\, \phi)$ denotes the norm of the element ϕ. The possibility of constructing the resolution of identity by means of eigenfunctions is guaranteed only for Hermitian operators (von Neumann theorem). Although this resolution is not always expressed by the summation — in general, the Hermitian operator of the Hilbert space contains the continuous spectra, we have taken such a space for simplicity. In the extension of the previous sections, it is quite natural to consider that non-Hermitian operators may include eigenfunctions in a wider sense.

Based on the above knowledges, we can solve the following time evolution equation (Schrödinger equation for a free particle);

$$\mathrm{i}\partial_t \psi = \partial_x^2 \psi, \tag{B.31}$$

by means of the spectral resolution of the operator $\mathcal{A}$. Expanding ψ by the eigenfunctions u_n of the operator $\mathcal{A}$ as

$$\psi(x,t) = \sum_{n=1}^{\infty} a_n(t) u_n(x), \tag{B.32}$$

and substituting it into Eq. (B.31), we have

$$\sum_{n=1}^{\infty} (\mathrm{i}\partial_t a_n - \lambda_n a_n) u_n = 0. \tag{B.33}$$

Since u_n is orthogonal for different n, the equation can be decomposed into the one for each 'mode' to give

$$\mathrm{i}\partial_t a_n = \lambda_n a_n, \tag{B.34}$$

which leads to the solution of each mode as

$$a_n(t) = a_n(0)e^{-\mathrm{i}\lambda_n t}. \tag{B.35}$$

Thus, the general solution for an arbitrary initial perturbation $\psi(x,0)$ can be obtained as

$$\psi(x,t) = \sum_{n=1}^{\infty} \sqrt{2} a_n(0) e^{\mathrm{i}n^2\pi^2 t} \sin(n\pi x), \tag{B.36}$$

where $a_n(0)$ is obtained by

$$a_n(0) = (u_n \,|\, \psi(x,0)). \tag{B.37}$$

B.2.2 Fourier transformation

Let us solve the Schrödinger equation (B.31) by means of the Fourier transformation. This method is intrinsically parallel to the spectral resolution.

Fourier transformation is formally defined as

$$\hat{\psi}(k,\omega) = \int_0^1 \int_{-\infty}^{\infty} \psi(x,t)\, e^{-\mathrm{i}(kx-\omega t)}\, \mathrm{d}t\, \mathrm{d}x, \tag{B.38}$$

where the inversion will be given by

$$\psi(x,t) = \frac{1}{2\pi} \sum_k \int_{-\infty}^{\infty} \hat{\psi}(k,\omega)\, e^{\mathrm{i}(kx-\omega t)}\, \mathrm{d}\omega, \tag{B.39}$$

where the inversion with respect to k is expressed by the discrete summation since we have taken the finite domain [0,1]. The wave number k is chosen as

$$k = n\pi \quad (n \in \mathbb{N}). \tag{B.40}$$

We will apply the Fourier transformation to the Schrödinger equation and obtain

$$(\omega + k^2)\hat{\psi}(k,\omega) = 0, \tag{B.41}$$

which is readily solved for $\hat{\psi}$ to give

$$\hat{\psi}(k,\omega) = \delta(\omega + k^2). \tag{B.42}$$

The relation

$$\omega = -k^2, \tag{B.43}$$

denoting the singularity of $\hat{\psi}$, is called the 'dispersion relation' since only these values which satisfy Eq. (B.43) will give the contribution when inverted.

The way of solving the initial value problem is described as follows. Since an initial perturbation can be spatially Fourier transformed as

$$\hat{a}(k) = \int_0^1 \psi(x,0)\, e^{-\mathrm{i}kx}\, \mathrm{d}x, \tag{B.44}$$

the solution will be given by the superposition of singular eigenfunction $\hat{\psi}(k,\omega)$ multiplied by $\hat{a}(k)$, which leads to

$$\begin{aligned}\psi(x,t) &= \sum_k \int_\infty^{-\infty} \hat{a}(k)\delta(\omega + k^2)\, e^{\mathrm{i}(kx-\omega t)}\, \mathrm{d}\omega \\ &= \sum_{n=1}^{\infty} \hat{a}_n \, \exp[\mathrm{i}(n\pi x + n^2\pi^2 t)],\end{aligned} \tag{B.45}$$

where we have defined $\hat{a}_n = \hat{a}(k)$ with the relation (B.40). This expression exactly coincides with the solution obtained by the spectral resolution (B.36) by taking the real part of Eq. (B.45).

It should be noted that the Fourier transformation in time corresponds to the expression with whole superposition *on* the spectra, which now has a discrete sum of projections onto point eigenvalues.

B.2.3 Laplace transformation

Here we will solve the same Schrödinger equation (B.31) with an another method, i.e. Fourier transformation in space and Laplace transformation in time.

Fourier-Laplace transformation of the perturbed field is defined as

$$\tilde{\psi}(k,s) = \int_0^1 \int_0^\infty \psi(x,t)\, e^{-\mathrm{i}kx - st}\, \mathrm{d}t\, \mathrm{d}x, \tag{B.46}$$

where the real part of s is chosen to be larger than any temporal singularity of the function $\psi(t)$ for the convergence of the integration. The inversion will be given by

$$\psi(x,t) = \frac{1}{2\pi\mathrm{i}} \sum_k \int_{s_0-\mathrm{i}\infty}^{s_0+\mathrm{i}\infty} \tilde{\psi}(k,s)\, e^{\mathrm{i}kx+st}\, \mathrm{d}s, \tag{B.47}$$

where $s_0 = \mathrm{Re}(s) > 0$ and k satisfies the condition (B.40).

The Fourier-Laplace transformation of the Schrödinger equation (B.31) gives

$$\mathrm{i}s\tilde{\psi} = -k^2\tilde{\psi} + \mathrm{i}\bar{\psi}(k,0), \tag{B.48}$$

which leads to

$$\tilde{\psi}(k,s) = \frac{\bar{\psi}(k,0)}{s - \mathrm{i}k^2}. \tag{B.49}$$

Here $\bar{\psi}(k,0)$ denotes the spatially Fourier transformed initial value

$$\bar{\psi}(k,0) = \int_0^1 \psi(x,0)\, e^{-\mathrm{i}kx}\, \mathrm{d}x. \tag{B.50}$$

By inverting Eq. (B.49), we obtain

$$\begin{aligned} \psi(x,t) &= \frac{1}{2\pi\mathrm{i}} \sum_k \int_{s_0-\mathrm{i}\infty}^{s_0+\mathrm{i}\infty} \frac{\bar{\psi}(k,0)}{s - \mathrm{i}k^2}\, e^{\mathrm{i}kx+st}\, \mathrm{d}s, \\ &= \sum_{n=1}^{\infty} \bar{\psi}(k,0)\, \exp[\mathrm{i}(n\pi x + n^2\pi^2 t)], \end{aligned} \tag{B.51}$$

which again coincides with the previous two methods.

It is noted that the Laplace transformation method in time corresponds to the expression with whole integration *around* the spectra, which is now rewritten by the discrete sum of independent eigenmodes due to Cauchy's integral theorem.

Appendix C

Electrostatic oscillations in an unmagnetized plasma

C.1 Langmuir oscillation

Let us first derive the dispersion relation of plasma oscillations by means of the fluid description. The governing equations for describing the one dimensional electrostatic oscillation (electron plasma oscillation) in an cold unmagnetized plasma are

$$\partial_t n + \partial_x (nv) = 0, \tag{C.1}$$

$$mn(\partial_t v + v\partial_x v) = qnE, \tag{C.2}$$

$$\epsilon_0 \partial_x E = qn. \tag{C.3}$$

Assuming the static homogeneous background plasma and linearizing Eqs. (C.1)-(C.3) for a plane wave with the dependence $e^{\mathrm{i}(kx-\omega t)}$ yields

$$-\mathrm{i}\omega n_1 + \mathrm{i}k n_0 v_1 = 0, \tag{C.4}$$

$$-\mathrm{i}\omega m v_1 = qE_1, \tag{C.5}$$

$$\mathrm{i}k\epsilon_0 E_1 = qn_1. \tag{C.6}$$

Combining Eqs. (C.5) and (C.6), we obtain

$$v_1 = \frac{q^2}{\epsilon_0 m\omega k} n_1. \tag{C.7}$$

Substituting Eq. (C.7) into Eq. (C.4) leads to the dispersion relation

$$\omega = \pm\omega_\mathrm{p} = \pm\sqrt{\frac{n_0 q^2}{\epsilon_0 m}}, \tag{C.8}$$

which is called a plasma oscillation.

It is known that the dispersion effect appears due to the finite electron pressure. Here we modify the equation of motion (C.2) as

$$mn(\partial_t v + v\partial_x v) = qnE - \partial_x p, \tag{C.9}$$

and add the adiabatic pressure equation

$$\partial_t p + v\partial_x p + \gamma p \partial_x v = 0, \tag{C.10}$$

as a closure of the fluid model. Linearizing these equations with the same plane wave dependence $e^{\mathrm{i}(kx-\omega t)}$, we have

$$-\mathrm{i}\omega m n_0 v_1 = q n_0 E_1 - \mathrm{i}k p_1, \tag{C.11}$$

$$-\mathrm{i}\omega p_1 + \mathrm{i}k\gamma p_0 v_1 = 0. \tag{C.12}$$

Substituting Eq. (C.12) into Eq. (C.11) and using Eq. (C.6) leads to

$$v_1 = \frac{\omega n_0 q^2}{k\epsilon_0(\omega^2 m n_0 - k^2\gamma p_0)} n_1. \tag{C.13}$$

Plugging Eq. (C.13) into (C.4) yields the dispersion relation

$$\begin{aligned}\omega^2 &= \omega_\mathrm{p}^2 + k^2\frac{\gamma p_0}{m n_0}, \\ &= \omega_\mathrm{p}^2 + k^2\frac{\gamma T_0}{m},\end{aligned} \tag{C.14}$$

where we have used the fact that the electron pressure can be expressed by $p = nT$. Equation (C.14) explicitly shows the dispersion effect coming from the ∇p term in the equation of motion coupled with the adiabatic pressure equation.

C.2 Vlasov-Poisson system

The governing equations for describing Landau damping of one dimensional electrostatic oscillation (electron plasma oscillation) are

$$\partial_t f + v\partial_x f + \frac{qE}{m}\partial_v f = 0, \tag{C.15}$$

$$\epsilon_0 \partial_x E = q\int_{-\infty}^{+\infty} f \,\mathrm{d}v, \tag{C.16}$$

where f denotes the particle distribution function defined in the phase space, E the electric field, q and m the electric charge and mass of a particle (electron), ϵ_0 the vacuum susceptibility, respectively. Here x (v) denotes the coordinate space (velocity space) variable. Let us assume here that the background plasma is spatially

homogeneous and electrically neutral ($E = 0$). For linearizing Eqs. (C.15) and (C.16), we can define a wave number k in the x direction. Combining these two equations with eliminating electric field yields

$$\partial_t f_1 + \mathrm{i}kv f_1 - \frac{\mathrm{i}q^2}{\epsilon_0 mk}(\partial_v f_0)\int_{-\infty}^{+\infty} f_1 \,\mathrm{d}v = 0, \tag{C.17}$$

where the subscripts 0 and 1 denote the equilibrium and the perturbation of distribution function, respectively. The distribution function f_1 belongs to $L^1(\mathbb{R})$ in the velocity space. Hereafter, we will omit the subscript 1 for simplicity.

Defining the Laplace transformation of the perturbed fields as

$$\tilde{\psi}(s) = \int_0^{\infty} \psi(t)\, e^{-st}\,\mathrm{d}t, \tag{C.18}$$

where the real part of s is chosen to be larger than any temporal singularity of the function $\psi(t)$ for the convergence of the integration. The inversion will be given by

$$\psi(t) = \frac{1}{2\pi\mathrm{i}}\int_{s_0-\mathrm{i}\infty}^{s_0+\mathrm{i}\infty} \tilde{\psi}(s)\, e^{st}\,\mathrm{d}s, \tag{C.19}$$

where $s_0 = \mathrm{Re}(s) > 0$.

Transforming Eq. (C.17) by multiplying e^{-st} and integrating with respect to time, we obtain

$$(s + \mathrm{i}kv)\tilde{f} - \frac{\mathrm{i}q^2}{\epsilon_0 mk}(\partial_v f_0)\int_{-\infty}^{+\infty} \tilde{f}\,\mathrm{d}v = f(v, t=0). \tag{C.20}$$

Let us try an another calculation for comparison which can be seen in the literature [12]. Transforming Eqs. (C.15) and (C.16) by multiplying e^{-st} and integrating with respect to time yield

$$(s + \mathrm{i}kv)\tilde{f} + \frac{q}{m}\tilde{E}\partial_v f_0 = f(0), \tag{C.21}$$

$$\mathrm{i}k\epsilon_0\tilde{E} = q\int_{-\infty}^{+\infty} \tilde{f}\,\mathrm{d}v, \tag{C.22}$$

where the subscript 0 denotes the equilibrium field. The perturbations are Laplace transformed here. The initial condition for the electric field should be related with the distribution function through Poisson equation at $t = 0$ as

$$\mathrm{i}k\epsilon_0 E(0) = q\int_{-\infty}^{+\infty} f(v, 0)\,\mathrm{d}v. \tag{C.23}$$

Dividing Eq. (C.21) by $(s - \mathrm{i}kv)$ and plugging it into Eq. (C.22) lead to

$$\left[1 + \frac{q^2}{\epsilon_0 mk}\int_{-\infty}^{+\infty} \frac{\partial_v f_0}{\mathrm{i}s - kv}\,\mathrm{d}v\right]\tilde{E} = \frac{q}{\epsilon_0 k}\int_{-\infty}^{+\infty} \frac{f(0)}{\mathrm{i}s - kv}\,\mathrm{d}v. \tag{C.24}$$

The time evolution of the electric field can be obtained by inverting the Laplace transformation expressed in Eq. (C.19). From Eq. (C.24), we formally obtain

$$E(t) = \frac{1}{2\pi \mathrm{i}} \int_{s_0-\mathrm{i}\infty}^{s_0+\mathrm{i}\infty} \frac{\dfrac{q}{\epsilon_0 k} \displaystyle\int_{-\infty}^{+\infty} \frac{f(0)}{\mathrm{i}s - kv}\,\mathrm{d}v}{1 + \dfrac{q^2}{\epsilon_0 m k} \displaystyle\int_{-\infty}^{+\infty} \frac{\partial_v f_0}{\mathrm{i}s - kv}\,\mathrm{d}v} e^{st}\,\mathrm{d}s. \tag{C.25}$$

C.3 Spectrum of operators in Vlasov-Poisson system

The operator in the evolution equation (C.17) consists of two parts. In this subsection, we will discuss the properties of each part separately. The evolution equation for the perturbed distribution function is written as

$$\mathrm{i}\partial_t f = kvf - \frac{\omega_\mathrm{p}^2}{k}(\partial_v f_0) \int_{-\infty}^{+\infty} f\,\mathrm{d}v, \tag{C.26}$$

where we have normalized the equilibrium distribution function as

$$f_0(v) \to n_0 f_0(v). \tag{C.27}$$

C.3.1 Ballistic response

The first operator kv is the multiplication operator which gives rise to continuous spectrum on the whole real axis of λ, where λ is the spectrum of the operator defined by

$$\lambda f = kvf. \tag{C.28}$$

The spectra given by this multiplication operator are continuous ones and their generalized eigenfunctions are

$$f = \delta(v - \lambda/k), \tag{C.29}$$

where corresponding eigenvalues are

$$\lambda = kv. \tag{C.30}$$

The initial value problem of the multiplication operator is readily solved as

$$f(v,t) = e^{-\mathrm{i}kvt} f(v,0), \tag{C.31}$$

which is called the ballistic response of the plasma, since it describes the free streaming of particles with keeping their memory of initial disturbances [19]. The distribution function does not lose the initial memory $f(v,0)$, however, if we observe the integrated physical quantities such as density, there appears continuum damping given by

$$n(t) = \int_{-\infty}^{\infty} f(v,t)\,\mathrm{d}v \overset{t\to\infty}{\to} 0, \tag{C.32}$$

due to Riemann-Lebesgue theorem [28].

C.3.2 Operator $(\partial_v f_0)\int\cdot\,\mathrm{d}v$

Let us consider here the spectrum of the second operator $(\partial_v f_0)\int\cdot\,\mathrm{d}v$ in Eq. (C.26), which denotes the combination of linear functional and multiplication. Since the definite integral with respect to v and the multiplication of the function $(\partial_v f_0)(v)$ does not commute, this operator is non-Hermitian. The spectral problem is written as

$$\lambda f = -\frac{\omega_\mathrm{p}^2}{k} h(v) \int_{-\infty}^{\infty} f\,\mathrm{d}v, \tag{C.33}$$

where we have introduced $h(v) = \partial_v f_0$. Since the definite integral gives just a constant, it is clear that the eigenfunction is written as

$$f = ah(v), \tag{C.34}$$

where a is assumed as a constant coefficient. The eigenvalue is proportional to the integral of f. Suppose

$$\int_{-\infty}^{\infty} h(v)\,\mathrm{d}v = c \tag{C.35}$$

with a real number c, then we have the eigenvalue

$$\lambda = -\frac{\omega_\mathrm{p}^2}{k} ac. \tag{C.36}$$

For an equilibrium distribution function f_0 which gives a finite c (positive or negative), the spectrum of this operator continuously occupies the whole real axis, and all eigenfunctions are parallel and integrable. It is clear that such eigenfunctions will not span any physical linear space. However, to complete it is so difficult that we do not discuss how to solve this problem.

It seems strange that the eigenvalue depends on the magnitude of eigenfunction itself. In a realistic situation, however, we have to choose $f_0(v)$ as a member of a certain linear functional space, e.g. $L^1(\mathbb{R})$, thus

$$\int_{-\infty}^{\infty} h(v)\,\mathrm{d}v = \int_{-\infty}^{\infty} \partial_v f_0\,\mathrm{d}v \tag{C.37}$$

$$= [f_0(v)]_{-\infty}^{\infty} \tag{C.38}$$

holds. Consequently, the eigenvalue becomes zero if we take integrable $f_0(v)$.

C.4 Cold plasma with $f_0(v) = n_0\delta(v)$

Let us consider the cold electron plasma in this section by assuming

$$f_0(v) = n_0\delta(v). \tag{C.39}$$

In order to formulate the Hilbert space with following the discussion of Sec. 7.6, we have to include $\delta'(v)$ term in $f(v,t)$ as

$$f(v,t) = \alpha(t)\delta(v) + \beta(t)\delta'(v) \ + \ \varphi(v,t). \tag{C.40}$$

Here prime denotes the derivative with respect to its argument and $\varphi(v,t)$ denotes the continuous part of the perturbed distribution function, respectively. Then, the Laplace transformed equation (C.20) will give for the continuous part,

$$(s + \mathrm{i}kv)\tilde{\varphi}(v,s) = \varphi(v,0). \tag{C.41}$$

There appear couplings between singular surface wave parts. Using the formula $v\delta'(v) = -\delta(v)$, we obtain

$$s\tilde{\alpha}(s) - \mathrm{i}k\tilde{\beta}(s) = \alpha(0) \tag{C.42}$$

for the $\delta(v)$ component and

$$s\tilde{\beta}(s) - \frac{\mathrm{i}\omega_\mathrm{p}^2}{k}\tilde{\alpha}(s) - \frac{\mathrm{i}\omega_\mathrm{p}^2}{k}\int_{-\infty}^{\infty}\tilde{\varphi}(v,s)\,\mathrm{d}v = \beta(0) \tag{C.43}$$

for the $\delta'(v)$ component, respectively. Multiplying $(\mathrm{i}\omega_\mathrm{p}^2/k)$ on Eq. (C.42) and s on Eq. (C.43), and adding each other, we obtain

$$(s^2 + \omega_\mathrm{p}^2)\tilde{\beta}(s) - \frac{\mathrm{i}s\omega_\mathrm{p}^2}{k}\int_{-\infty}^{\infty}\tilde{\varphi}(v,s)\,\mathrm{d}v = \frac{\mathrm{i}\omega_\mathrm{p}^2}{k}\alpha(0) + s\beta(0). \tag{C.44}$$

From this equation,

$$\tilde{\beta}(s) = \frac{1}{(s - \mathrm{i}\omega_\mathrm{p})(s + \mathrm{i}\omega_\mathrm{p})}\left[\frac{\mathrm{i}\omega_\mathrm{p}^2}{k}\alpha(0) + s\beta(0) + \frac{\mathrm{i}s\omega_\mathrm{p}^2}{k}\int_{-\infty}^{\infty}\frac{\varphi(v,0)}{s + \mathrm{i}kv}\,\mathrm{d}v\right], \tag{C.45}$$

is given, where we have used Eq. (C.41). It is noted that this system also contains the resonance where the energy is transferred from the continuous spectrum to the point spectrum (surface wave). Inverting this expression, we obtain

$$\begin{aligned}\beta(t) = {} & \frac{\mathrm{i}\omega_\mathrm{p}}{k}\alpha(0)\sin(\omega_\mathrm{p}t) + \beta(0)\cos(\omega_\mathrm{p}t) \\ & + \frac{1}{2\pi\mathrm{i}}\int_{s_0-\mathrm{i}\infty}^{s_0+\mathrm{i}\infty}\frac{\mathrm{i}s\omega_\mathrm{p}^2/k}{(s - \mathrm{i}\omega_\mathrm{p})(s + \mathrm{i}\omega_\mathrm{p})}\int_{-\infty}^{\infty}\frac{\varphi(v,0)}{s + \mathrm{i}kv}\,\mathrm{d}v\,\mathrm{d}s.\end{aligned} \tag{C.46}$$

On the other hand, if we partially integrate the denominator of Eq. (C.25) as

$$\begin{aligned}\int \frac{\partial_v f_0}{\mathrm{i}s - kv}\,\mathrm{d}v &= \frac{n_0}{k}\int \frac{\delta'(v)}{v - (\mathrm{i}s/k)}\,\mathrm{d}v \\ &= \frac{n_0}{k}\left[\frac{\delta(v)}{v-(\mathrm{i}s/k)}\right]_{-\infty}^{+\infty} + \frac{n_0}{k}\int \frac{\delta(v)}{[v-(\mathrm{i}s/k)]^2}\,\mathrm{d}v \\ &= -\frac{n_0 k}{s^2}, \end{aligned} \tag{C.47}$$

then the denominator of Eq. (C.25) will have zeros for

$$1 + \frac{q^2}{\epsilon_0 m k}\int_{-\infty}^{+\infty} \frac{\partial_v f_0}{\mathrm{i}s - kv}\,\mathrm{d}v = 0. \tag{C.48}$$

This gives

$$s_\pm = \pm \mathrm{i}\omega_\mathrm{p} \tag{C.49}$$

in the complex s-plane. In this case, we can formally rewrite $E(t)$ by substituting Eq. (C.47) into Eq. (C.25) as

$$E(t) = \frac{1}{2\pi}\int_{s_0-\mathrm{i}\infty}^{s_0+\mathrm{i}\infty} \frac{s^2 e^{st}}{(s-\mathrm{i}\omega_\mathrm{p})(s+\mathrm{i}\omega_\mathrm{p})}\frac{q}{\epsilon_0 k}\int_{-\infty}^{+\infty}\frac{f(0)}{s+\mathrm{i}kv}\,\mathrm{d}v\,\mathrm{d}s. \tag{C.50}$$

We consider the completely cold plasma by assuming

$$f(x,v,0) = \hat{n}_1 e^{\mathrm{i}kx}\delta(v), \tag{C.51}$$

where $\hat{n}_1$ denotes the real number expressing the amplitude of the initial disturbance. Then, the integration with respect to v is easily carried out,

$$E(t) = \frac{\hat{n}_1 e^{\mathrm{i}kx}}{2\pi}\frac{q}{\epsilon_0 k}\int_{s_0-\mathrm{i}\infty}^{s_0+\mathrm{i}\infty}\frac{s e^{st}}{(s-\mathrm{i}\omega_\mathrm{p})(s+\mathrm{i}\omega_\mathrm{p})}\,\mathrm{d}s. \tag{C.52}$$

This expression gives the simple oscillation

$$E(t) = \frac{\mathrm{i}q}{\epsilon_0 k}\hat{n}_1 e^{\mathrm{i}kx}\cos(\omega_\mathrm{p} t) \tag{C.53}$$

which exactly coincides with the analysis based on the fluid description.

On the other hand, if we introduce a finite temperature in the initial perturbation as

$$f(x,v,0) = \hat{n}_1 e^{\mathrm{i}kx}F(v), \tag{C.54}$$

where $F(v)$ denotes arbitrary analytic function. In this case, we can commute the integration with respect to v and s in Eqs. (C.46) and (C.50), and obtain the formal resonance which corresponds to the second order pole where

$$v = \pm\frac{\omega_\mathrm{p}}{k}, \tag{C.55}$$

is satisfied. By performing the integration with respect to s, we may be able to write the explicit form which only contains the integration with respect to v.

C.5 General continuous profile $f_0(v)$

In the case where $f_0(v)$ is a continuous function, van Kampen [90] and Case [49] have found the complete set of eigenfunctions. According to these references, all eigenvalues are real continuous ones in the case of Maxwellian equilibrium distribution, although the system may contain some complex point spectra in general. Construction of the propagator semi-group for the Vlasov-Poisson generator including such general distribution functions is discussed in Ref. [58]. Since the non-Hermitian operator $(\partial_v f_0) \int \cdot \, \mathrm{d}v$ gives fairly close effect to the inhomogeneous terms with its rank unity, they could have found those eigenfunctions by introducing the normalization of f in a tricky way. It is concluded that Landau's exponential damping for Maxwellian distribution function $f_0(v)$ does not denote a spectra of the operator, but just a consequence of the phase mixing damping due to the superposition of the continuous spectra.

It is pointed out by Weitzner [148, 149] that the Landau's prescription of taking a detour at the pole is not appropriate in general even though phase mixing will surely cause sometimes *non-exponential* Landau damping [in the sense of Eq. (C.32)]. However, it is experimentally confirmed to be *exponential* [102]. There might be something which we do not understand yet. It is also noted that a spatially inhomogeneous density profile will give rise to another continuous spectra in the coordinate space [39, 117].

Vector Relations

$$\mathbf{A}\cdot(\mathbf{B}\times\mathbf{C})=\mathbf{B}\cdot(\mathbf{C}\times\mathbf{A})=\mathbf{C}\cdot(\mathbf{A}\times\mathbf{B})=(\mathbf{ABC}) \tag{1}$$

$$\mathbf{A}\times(\mathbf{B}\times\mathbf{C})=\mathbf{B}(\mathbf{A}\cdot\mathbf{C})-\mathbf{C}(\mathbf{A}\cdot\mathbf{B}) \tag{2}$$

$$(\mathbf{A}\times\mathbf{B})\cdot(\mathbf{C}\times\mathbf{D})=(\mathbf{A}\cdot\mathbf{C})(\mathbf{B}\cdot\mathbf{D})-(\mathbf{A}\cdot\mathbf{D})(\mathbf{B}\cdot\mathbf{C}) \tag{3}$$

$$(\mathbf{A}\times\mathbf{B})\times(\mathbf{C}\times\mathbf{D})=(\mathbf{ABD})\mathbf{C}-(\mathbf{ABC})\mathbf{D}=(\mathbf{ACD})\mathbf{B}-(\mathbf{BCD})\mathbf{A} \tag{4}$$

$$\nabla\cdot(f\mathbf{A})=\mathbf{A}\cdot\nabla f+f\nabla\cdot\mathbf{A} \tag{5}$$

$$\nabla\times(f\mathbf{A})=\nabla f\times\mathbf{A}+f\nabla\times\mathbf{A} \tag{6}$$

$$\nabla(\mathbf{A}\cdot\mathbf{B})=\mathbf{A}\times(\nabla\times\mathbf{B})+\mathbf{B}\times(\nabla\times\mathbf{A})+\mathbf{A}\cdot\nabla\mathbf{B}+\mathbf{B}\cdot\nabla\mathbf{A} \tag{7}$$

$$\nabla\cdot(\mathbf{A}\times\mathbf{B})=\mathbf{B}\cdot(\nabla\times\mathbf{A})-\mathbf{A}\cdot(\nabla\times\mathbf{B}) \tag{8}$$

$$\nabla\times(\mathbf{A}\times\mathbf{B})=\mathbf{A}(\nabla\cdot\mathbf{B})-\mathbf{B}(\nabla\cdot\mathbf{A})+\mathbf{B}\cdot\nabla\mathbf{A}-\mathbf{A}\cdot\nabla\mathbf{B} \tag{9}$$

$$\nabla\times\nabla\times\mathbf{A}=\nabla(\nabla\cdot\mathbf{A})-\nabla^2\mathbf{A} \tag{10}$$

$$\nabla\times\nabla f=0 \tag{11}$$

$$\nabla\cdot(\nabla\times\mathbf{A})=0 \tag{12}$$

$$\mathbf{A}\cdot\nabla\mathbf{A}=\nabla\left(\frac{1}{2}A^2\right)-\mathbf{A}\times(\nabla\times\mathbf{A}) \tag{13}$$

$$\nabla\times(\mathbf{A}\cdot\nabla\mathbf{A})=\mathbf{A}\cdot\nabla(\nabla\times\mathbf{A})+\nabla\cdot\mathbf{A}(\nabla\times\mathbf{A})-\{(\nabla\times\mathbf{A})\cdot\nabla\}\mathbf{A} \tag{14}$$

$$\mathbf{A}\cdot\{\mathbf{B}\cdot\nabla(\nabla f)\}=\mathbf{B}\cdot\{\mathbf{A}\cdot\nabla(\nabla f)\} \tag{15}$$

$$\mathbf{A}\cdot(\mathbf{B}\cdot\nabla\mathbf{C})=\mathbf{B}\cdot(\mathbf{A}\cdot\nabla\mathbf{C})-(\mathbf{A}\times\mathbf{B})\cdot(\nabla\times\mathbf{C}) \tag{16}$$

$$\mathbf{A}\cdot\nabla(\mathbf{B}\cdot\nabla f)=(\mathbf{A}\cdot\nabla\mathbf{B})\cdot\nabla f+(\mathbf{AB}:\nabla\nabla)f \tag{17}$$

$$\mathbf{A}\cdot\nabla(\mathbf{B}\cdot\nabla\mathbf{C})=(\mathbf{A}\cdot\nabla\mathbf{B})\cdot\nabla\mathbf{C}+(\mathbf{AB}:\nabla\nabla)\mathbf{C} \tag{18}$$

$$[(\mathbf{A}\times\mathbf{B})\times\nabla]\times\mathbf{C}=\mathbf{B}\times(\mathbf{A}\cdot\nabla\mathbf{C})-\mathbf{A}\times(\mathbf{B}\cdot\nabla\mathbf{C}) \tag{19}$$

$$(\mathbf{A}\times\nabla)\times\mathbf{B}=(\nabla\mathbf{B})\cdot\mathbf{A}-\mathbf{A}(\nabla\cdot\mathbf{B}) \tag{20}$$

Quasi-toroidal Coordinates

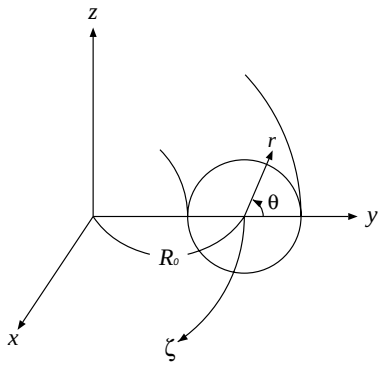

Definition

$$\begin{cases} x = (R_0 + r\cos\theta)\sin\phi \\ y = (R_0 + r\cos\theta)\cos\phi \\ z = r\sin\theta \end{cases} \tag{1}$$

Unit vectors

$$\begin{cases} \boldsymbol{e}_r = \boldsymbol{e}_x\cos\theta\sin\phi + \boldsymbol{e}_y\cos\theta\cos\phi + \boldsymbol{e}_z\sin\theta \\ \boldsymbol{e}_\theta = -\boldsymbol{e}_x\sin\theta\sin\phi - \boldsymbol{e}_y\sin\theta\cos\phi + \boldsymbol{e}_z\cos\theta \\ \boldsymbol{e}_\phi = \boldsymbol{e}_x\cos\phi - \boldsymbol{e}_y\sin\phi \end{cases} \tag{2}$$

Metric

$$d\ell^2 = dr^2 + r^2 d\theta^2 + (R_0 + r\cos\theta)^2 d\phi^2 \tag{3}$$

Jacobian matrix

$$\frac{\partial(r,\theta,\phi)}{\partial(x,y,z)} = \begin{pmatrix} \cos\theta\sin\phi & \cos\theta\cos\phi & \sin\theta \\ -\dfrac{1}{r}\sin\theta\sin\phi & -\dfrac{1}{r}\sin\theta\cos\phi & \dfrac{1}{r}\cos\theta \\ \dfrac{\cos\phi}{R_0 + r\cos\theta} & -\dfrac{\sin\phi}{R_0 + r\cos\theta} & 0 \end{pmatrix} \tag{4}$$

$$\left|\frac{\partial(r,\theta,\phi)}{\partial(x,y,z)}\right| = \frac{1}{r(R_0 + r\cos\theta)} \tag{5}$$

Gradient operator

$$\nabla = \boldsymbol{e}_r\frac{\partial}{\partial r} + \boldsymbol{e}_\theta\frac{1}{r}\frac{\partial}{\partial\theta} + \boldsymbol{e}_\phi\frac{1}{R_0 + r\cos\theta}\frac{\partial}{\partial\phi} \tag{6}$$

Acknowledgements

First of all, I would like to express my sincerest gratitude to my forever teacher, Professor Masahiro Wakatani. He had given me many interesting subjects in spite of my strange way of expressing my own interests. He has very wide knowledge including plasma physics and fusion technology, and accurate physical intuition. He had often pointed out the incompleteness of my works and helped me to improve my understandings on each problem. Moreover, he had been continuously encouraging and guiding me as a great teacher. I admire his gentle, kind, and patient personality. Without his careful and proper guidance, I could not have completed this work.

The next person whom I would like to thank is Professor Zensho Yoshida in the University of Tokyo. He had been patient of my doing PhD work for two and a half years, in spite of the fact that I was hired as a research associate of his laboratory. Even before that, he had visited Kyoto University several times for giving some lectures as a visiting professor, and his talk attracted me very much. Many parts of this thesis also owe to his profound and interesting understandings of the World.

Professor Hideki Zushi in Kyushu University is the first person who had lead me into the domain of plasma physics at the time of entrance examination for graduate school of nuclear engineering. Without his kind invitation to plasma physics, I had not known this very profound and interesting subject. He had guided me in my master course on the data analysis of Heliotron-E experiment.

Professor Vazha Berezhiani in Georgian Academy of Science was the visiting professor in the University of Tokyo for a year. He taught me how widely and how interestingly the plasma physics is related to other domains. I was surprised at his manifold knowledge, which affects me to love plasma physics much more than before. Moreover, he taught me that the easiest way to learn foreign language is to just try to communicate with foreigners.

Professors Swadesh Mahajan and Mikhail Pekker in the University of Texas, Professor Katsuji Ichiguchi in National Institute for Fusion Science, Professor Benjamin Carreras in Oak Ridge National Laboratory, Doctors Francesco Volponi, Shigeo Kondoh, Akira Yoshioka, and Makoto Hirota are coauthors of my papers published in scientific journals. I have learned a lot of things from them, and they have been very kind and patient to allow my slow progress.

Professors Y. Nakamura and S. Hamaguchi in Kyoto University, Professors Y. Ogawa, N. Shatashvili, H. Himura, S. Kado and J. Morikawa in the University of Tokyo have been very kindly teaching me a lot of interesting topics in plasma physics through seminars.

Professor M. Yagi in Kyushu University, Professors H. Sugama, K. Watanabe, M. Yokoyama and A. Takayama in National Institute for Fusion Science, and Doctors Y. Ishii, T. Matsumoto, Y. Idomura, and M. Furukawa in Japan Atomic Energy Research Institute are the great honorable seniors of Wakatani's laboratory. I feel that they have done excellent works and I will never quit trying to do my best in my forthcoming days as a researcher in order to follow them.

Doctors S. Tokuda, Y. Kishimoto, M. Kikuchi, and S. Takeji in Japan Atomic Energy Research Institute, Professors S. Kida, N. Nakajima, K. Yamazaki, K. Ida and H. Yamada in National Institute for Fusion Science, Professor A. Ishida in Niigata University, Professors J. Van Dam, P. Valanju, and F. Waelbroeck in the University of Texas, Professor R. Dewar in Australian National University, Professors E. Hameiri and H. Strauss in New York University, and Doctor K. Noguchi in Los Alamos National Laboratory are the researchers I have met in the conference or my visit to their institutions. Although I have also met other many scientists in the world, I would like to express my gratitude especially to them whom I have discussed and learned a lot of things related to this thesis.

Finally, I would like to express my gratitude to all members at Graduate School of Energy Science and Institute of Advanced Energy, Kyoto University, those at Graduate School of Frontier Sciences, the University of Tokyo, and all my friends and parents who supported me during my long term studies.

Bibliography

[1] A. I. Akhiezer, I. A. Akhiezer, R. V. Polovin, A. G. Sitenko and K. N. Stepanov, *Plasma Electrodynamics* (Pergamon, New York, 1975).

[2] G. B. Arfken and H. J. Weber, *Mathematical Methods for Physicists*, 5th ed. (Academic, San Diego, 2001).

[3] R. Balescu, *Transport Processes in Plasmas, 1. Classical transport theory* (Elsevier, Amsterdam, 1988).

[4] D. Biskamp, *Magnetic Reconnection in Plasmas* (Cambridge Univ., Cambridge, 2000).

[5] D. Biskamp, *Nonlinear Magnetohydrodynamics* (Cambridge Univ., Cambridge, 1993).

[6] M. S. Brodskiĭ, *Triangular and Jordan Representations of Linear Operators* (Amer. Math. Soc., Providence, 1971).

[7] S. Chandrasekhar, *Hydrodynamic and Hydromagnetic Stability* (Clarendon, Oxford, 1961).

[8] P. A. M. Dirac, *The Principles of Quantum Mechanics*, 4th ed. (Clarendon, Oxford, 1995).

[9] P. G. Drazin and W. H. Reid, *Hydrodynamic stability*, (Cambridge Univ., Cambridge, 1981).

[10] J. P. Freidberg, *Ideal Magnetohydrodynamics* (Plenum, New York, 1987).

[11] I. C. Gohberg and M. G. Kreĭn, *Introduction to the Theory of Linear Nonselfadjoint Operators* (Amer. Math. Soc., Providence, 1969).

[12] R. J. Goldston and P. H. Rutherford, *Introduction to Plasma Physics* (IOP, London, 1995).

[13] *Guinness World Records* (`http://www.guinnessworldrecords.com/`).

[14] A. Hasegawa, *Plasma Instabilities and Nonlinear Effects* (Springer, Berlin, 1975).

[15] I. Imai, *Applied Hyperfunction Theory* (Kluwer, Dordrecht, 1992).

[16] E. L. Ince, *Ordinary Differential Equations* (Dover, New York, 1956).

[17] J. D. Jackson, *Classical Electrodynamics*, 3rd ed. (Wiley, New York, 1999).

[18] T. Kato, *Perturbation Theory for Linear Operators*, (Springer, Berlin, 1995).

[19] N. A. Krall and A. W. Trivelpiece, *Principles of Plasma Physics* (McGraw-Hill, New York, 1973).

[20] L. D. Landau and E. M. Lifshitz, *The Classical Theory of Fields*, 4th ed. (Pergamon, New York, 1975).

[21] A. E. Lifschitz, *Magnetohydrodynamics and Spectral Theory* (Kluwer, Dordrecht, 1989).

[22] J. von Neumann, *Mathematical Foundation of Quantum Mechanics* (Princeton Univ., Princeton, 1996).

[23] K. Nishikawa and M. Wakatani, *Plasma Physics*, 3rd ed. (Springer, Berlin, 2000).

[24] E. Priest and T. Forbes, *Magnetic Reconnection* (Cambridge Univ., Cambridge, 2000).

[25] B. F. Schutz, *A First Course in General Relativity* (Cambridge Univ., Cambridge, 1988).

[26] T. H. Stix, *Waves in Plasmas* (AIP, New York, 1992).

[27] M. Wakatani, *Stellarator and Heliotron Devices* (Oxford Univ., New York, 1998).

[28] K. Yosida, *Functional Analysis*, 6th ed. (Springer, Berlin, 1995).

[29] Z. Yoshida, *Mathematical physics of collective phenomena* (Iwanami, Tokyo, 1995, in Japanese).

[30] A. Hasegawa and C. Uberoi, *The Alfvén Wave*, DOE Critical Review DOE/TIC-11197 (1982).

[31] M. Furukawa, *Localized pressure-driven MHD instabilities in reversed-magnetic-shear tokamaks*, Ph.D. thesis, Kyoto Univ. (2001).

[32] K. Ichiguchi, *Numerical Studies of Three-Dimensional Equilibrium and Stability for Stellarator/Heliotron Configurations*, Ph.D. thesis, Kyoto Univ. (1989).

[33] F. Volponi, *Non-hermitian Properties of Shear-flow Systems*, Ph.D. thesis, Univ. Tokyo (2001).

[34] B. Alpher *et al.*, Plasma Phys. Contrl. Fusion **31**, 205 (1989).

[35] K. Appert, R. Gruber, F. Troyon, and J. Vaclavik, Plasma Phys. **24**, 1147 (1982).

[36] K. Appert, R. Gruber, and J. Vaclavik, Phys. Fluids **17**, 1471 (1974).

[37] N. J. Balmforth and P. J. Morrison, Stud. Appl. Math. **102**, 309 (1999).

[38] N. J. Balmforth and P. J. Morrison, *Hamiltonian description of shear flow*, IFS Report, University of Texas, IFSR-903 (`http://hagar.ph.utexas.edu:80/ifs/`).

[39] E. M. Barston, Ann. Phys. **29**, 282 (1964).

[40] I. B. Bernstein *et al.*, Proc. R. Soc. London, Ser. A **244**, 17 (1958).

[41] R. Betti and J. P. Freidberg, Phys. Rev. Lett. **74**, 2949 (1995).

[42] S. N. Bhattacharyya and A. Bhattacharjee, Phys. Plasmas **4**, 3744 (1997).

[43] A. Bondeson, R. Iacono, and A. Battacharjee, Phys. Fluids **30**, 2167 (1987).

[44] A. Bondeson and D. J. Ward, Phys. Rev. Lett. **72**, 2709 (1994).

[45] B. A. Carreras, V. E. Lynch, K. Ichiguchi, T. Tatsuno, and M. Wakatani, Plasma Phys. Rep. **25**, 958 (1999).

[46] B. A. Carreras, V. E. Lynch, K. Ichiguchi, M. Wakatani, and T. Tatsuno, 18th IAEA Fusion Energy Conf. (Sorrento, 2000) IAEA-CN-77/THP2/03.

[47] B. A. Carreras, V. E. Lynch, K. Ichiguchi, M. Wakatani, and T. Tatsuno, Phys. Plasmas **8**, 990 (2001).

[48] B. A. Carreras, V. E. Lynch, H. Zushi, K. Ichiguchi, and M. Wakatani, Phys. Plasmas **5**, 3700 (1998).

[49] K. M. Case, Ann. Phys. **7**, 349 (1959).

[50] K. M. Case, Phys. Fluids **3**, 143 (1960).

[51] M. Cekic, B. A. Nelson, and F. L. Ribe, Phys. Fluids B **4**, 392 (1992).

[52] G. D. Chagelishvili, T. S. Hristov, R. G. Chanishvili, and J. G. Lominadze, Phys. Rev. E **47**, 366 (1993).

[53] G. D. Chagelishvili, A. D. Rogava, and I. N. Segal, Phys. Rev. E **50**, 4283 (1994).

[54] L. Chen and A. Hasegawa, J. Geophys. Res. **79**, 1033 (1974).

[55] L. Chen and A. Hasegawa, Phys. Fluids **17**, 1399 (1974).

[56] J. W. Connor, R. J. Hastie, and J. B. Taylor, Phys. Rev. Lett. **40**, 396 (1978); Proc. R. Soc. London, Ser A **365**, 1 (1979).

[57] W. O. Criminale and P. G. Drazin, Stud. Appl. Math. **83**, 123 (1990).

[58] P. Degond, Trans. Amer. Math. Soc. **294**, 435 (1986).

[59] R. L. Dewar, P. Cuthbert, and R. Ball, Phys. Rev. Lett. **86**, 2321 (2001).

[60] C. F. Driscoll and K. S. Fine, Phys. Fluids B **2**, 1359 (1990).

[61] B. F. Farrell and P. J. Ioannou, J. Atomos. Sci. **53**, 2025 (1996).

[62] J. M. Finn, Phys. Plasmas **2**, 198 (1995); *ibid* **2**, 3782 (1995).

[63] J. M. Finn and C. R. Sovinec, Phys. Plasmas **5**, 461 (1998).

[64] R. Fitzpatrick and A. Aydemir, Nucl. Fusion **36**, 11 (1996).

[65] S. Friedlander and M. Vishik, Chaos **5**, 416 (1995).

[66] E. Frieman and M. Rotenberg, Rev. Mod. Phys. **32**, 898 (1960).

[67] G. Y. Fu, *et al.*, Phys Fluids B **4**, 1401 (1992).

[68] H. P. Furth, J. Killeen, and M. N. Rosenbluth, Phys. Fluids **6**, 459 (1963).

[69] J. P. Goedbloed, Phys. Plasmas **5**, 3143 (1998).

[70] J. P. Goedbloed and D. A. D'Ippolito, Phys. Fluids B **2**, 2366 (1990).

[71] J. P. Goedbloed, D. Pfirsch, and H. Tasso, Nucl. Fusion **12**, 649 (1972).

[72] J. P. Goedbloed and P. H. Sakanaka, Phys. Fluids **17**, 908 (1974).

[73] S. Goldstein, Proc. Roy. Soc. London A **132**, 524 (1931).

[74] H. Grad, Proc. Natl. Acad. Sci. **70**, 3377 (1973).

[75] W. Grossmann and J. A. Tataronis, Z. Phys. **261**, 217 (1973).

[76] K. Hain and R. Lüst, Z. Naturforsch. **13a**, 936 (1958).

[77] E. Hameiri, Phys. Fluids **26**, 230 (1983).

[78] E. Hameiri, Phys. Plasmas **5**, 3270 (1998).

[79] E. Hameiri and S.-T. Chun, Phys. Rev. A **41**, 1186 (1990).

[80] S. W. Haney and J. P. Freidberg, Phys. Fluids B **1**, 1637 (1989).

[81] A. Hasegawa and L. Chen, Phys. Fluids **19**, 1924 (1976).

[82] A. Hasegawa and M. Wakatani, Phys. Rev. Lett. **59**, 1581 (1987).

[83] H. Helmholtz, Philos. Mag., Ser. 4, **36**, 337 (1868).

[84] M. Hirota, T. Tatsuno, S. Kondoh, and Z. Yoshida, submitted to Phys. Plasmas.

[85] K. Ichiguchi, N. Nakajima, M. Okamoto, N. Ohyabu, T. Tatsuno, M. Wakatani and B. A. Carreras, Proc. 9th Intern. Toki Conf. (Toki, 1998) ITC-9/P-Ⅱ-17.

[86] K. Ichiguchi, Y. Nakamura, and M. Wakatani, Nucl. Fusion **31**, 2073 (1991).

[87] K. Ichiguchi, M. Wakatani, T. Unemura, T. Tatsuno, and B. A. Carreras, 18th IAEA Fusion Energy Conf. (Sorrento, 2000) IAEA-CN-77/THP2/08.

[88] K. Ichiguchi, M. Wakatani, T. Unemura, T. Tatsuno, and B. A. Carreras, Nucl. Fusion **41**, 181 (2001).

[89] T. H. Jensen and R. Fitzpatrick, Phys. Plasmas **4**, 2997 (1997).

[90] N. G. van Kampen, Physica **21**, 949 (1955).

[91] S. Kondoh, T. Tatsuno, and Z. Yoshida, Phys. Plasmas **8**, 2635 (2001).

[92] D. Koppel, Phys. Fluids **8**, 1467 (1965).

[93] B. T. Kress and D. C. Montgomery, J. Plasma Phys. **64**, 371 (2000).

[94] M. D. Kruskal, J. L. Johnson, M. B. Gottlieb, and L. M. Goldman, Phys. Fluids **1**, 421 (1958).

[95] L. D. Landau, J. Phys. U.S.S.R. **10**, 25 (1946).

[96] G. Laval, C. Mercier, and R. M. Pellat, Nucl. Fusion **5**, 156 (1965).

[97] B. Lehnert, Phys. Fluids **9**, 1367 (1966).

[98] A. Lifschitz, Phys. Fluids **9**, 2864 (1997).

[99] Z. Lin, T. S. Hahm, W. W. Lee, W. M. Tang, and R. B. White, Science **281**, 1835 (1998).

[100] S. M. Mahajan and A. D. Rogava, Astrophys. J. **518**, 814 (1999).

[101] S. M. Mahajan and Z. Yoshida, Phys. Rev. Lett. **81**, 4863 (1998).

[102] J. H. Malmberg and C. B. Wharton, Phys. Rev. Lett. **13**, 184 (1964).

[103] C. Mercier, Nucl. Fusion **1**, 47 (1960).

[104] Y. Nakamura, *et al.*, Fusion Technol. **19**, 217 (1991).

[105] Y. Nakamura, M. Wakatani, C. C. Hegna, and A. Bhattacharjee, Phys. Fluids B **2**, 2528 (1990).

[106] J. Nührenberg and R. Zille, Phys. Lett. A **114**, 129 (1986).

[107] S. Okamura, *et al.*, Nucl. Fusion **35**, 283 (1995).

[108] S. Okamura, *et al.*, Nucl. Fusion **39**, 1337 (1999).

[109] D. Pfirsch and H. Tasso, Nucl. Fusion **11**, 259 (1971).

[110] D. C. Pridmore-Brown, Phys. Fluids **9**, 1290 (1966).

[111] J. W. S. Rayleigh, Proc. London Math. Soc. **9**, 57 (1880).

[112] A. D. Rogava and S. M. Mahajan, Phys. Rev. E **55**, 1185 (1997).

[113] M. N. Rosenbluth, R. Y. Dagazian, and P. H. Rutherford, Phys. Fluids **16**, 1894 (1973).

[114] A. M. Savill, Ann. Rev. Fluid Mech. **19**, 531 (1987).

[115] P. J. Schmid, Phys. Plasmas **7**, 1788 (2000).

[116] P. Secchi, J. Math. Fluid Mech. **2**, 107 (2000).

[117] Z. Sedláček, J. Plasma Phys. **5**, 239 (1971).

[118] V. D. Shafranov, Phys. Fluids **26**, 357 (1983).

[119] V. D. Shafranov and E. I. Yurchenko, Zh. Eksp. Teor. Fiz. **53**, 1157 (1967) [Sov. Phys. JETP **26**, 682 (1968)].

[120] R. A. Smith and M. N. Rosenbluth, Phys. Rev. Lett. **64**, 649 (1990).

[121] E. J. Strait *et al.*, in Contrl. Fusion Plasma Phys. (Proc. 18th Eur. Conf. Berlin, 1991) **15C** II-105 (1991).

[122] E. J. Strait *et al.*, Phys. Rev. Lett. **74**, 2483 (1995).

[123] H. R. Strauss, Phys. Fluids **19**, 134 (1976).

[124] H. R. Strauss, Phys. Fluids **20**, 1354 (1977).

[125] H. R. Strauss, Plasma Phys. **22**, 733 (1980).

[126] H. Sugama and M. Wakatani, J. Phys. Soc. Jpn. **58**, 1128 (1989).

[127] B. R. Suydam, in *Proc. of the second United Nations Intern. Conf. on the Peaceful Uses of Atomic Energy*, United Nations, Genova, Vol. 31, p. 157 (1958).

[128] T. Tamano *et al.*, Phys. Rev. Lett. **59**, 1444 (1987).

[129] J. A. Tataronis and W. Grossmann, Z. Phys. **261**, 203 (1973).

[130] T. Tatsuno, V. I. Berezhiani, and S. M. Mahajan, Phys. Rev. E **63**, 046403 (2001) [`http://arXiv.org/abs/astro-ph/0008212`].

[131] T. Tatsuno, F. Volponi, and Z. Yoshida, Phys. Plasmas **8**, 399 (2001).

[132] T. Tatsuno and M. Wakatani, J. Phys. Soc. of Jpn. **67**, 2322 (1998).

[133] T. Tatsuno, M. Wakatani, and K. Ichiguchi, Nucl. Fusion **39**, 1391 (1999).

[134] G. I. Taylor, Proc. Roy. Soc. London A **132**, 499 (1931).

[135] T. S. Taylor *et al.*, in Plasma Phys. Contrl. Nucl. Fusion Res. (Proc. 13th Int. Conf. Washington, DC 1990), **1**, 177 (1991).

[136] P. W. Terry, Rev. Mod. Phys. **72**, 109 (2000).

[137] A. G. Tevzadze, Phys. Plasmas **5**, 1557 (1998).

[138] W. Thomson (Lord Kelvin), Philos. Mag., Ser. 4, **42**, 362 (1871).

[139] W. Thomson (Lord Kelvin), Philos. Mag., Ser. 5, **24**, 188 (1887).

[140] L. N. Trefethen, A. E. Trefethen, S. C. Reddy, and T. A. Driscoll, Science **261**, 578 (1993).

[141] C. Uberoi, Phys. Fluids **15**, 1673 (1972).

[142] V. A. Vladimirov and K. I. Ilin, Phys. Plasmas **5**, 4199 (1998).

[143] F. Volponi, Z. Yoshida, and T. Tatsuno, Phys. Plasmas **7**, 2314 (2000).

[144] M. Wakatani, *et al.*, Proc. 9th Int. Toki Conf. on Plasma Phys. and Contrl. Nucl. Fusion (Toki, Japan, 1998), paper OP-5.

[145] M. Wakatani, T. Tatsuno, K. Ichiguchi, and K. Watanabe, J. Accel. Plasma Res. **5**, 43 (2000).

[146] M. Wakatani, A. Yoshioka and T. Tatsuno, Proc. GA of APFA '98 and APPTC '98 (Beijing, 1998) OS/A-4.

[147] D. J. Ward and A. Bondeson, Phys. Plasmas **2**, 1570 (1995).

[148] H. Weitzner, Phys. Fluids **6**, 1123 (1963).

[149] H. Weitzner, Comm. Pure and Appl. Math. **13**, 307 (1965).

[150] Z. Yoshida, Phys. Rev. Lett. **68**, 3168 (1992).

[151] Z. Yoshida and S. M. Mahajan, Intern. J. Mod. Phys. B **9**, 2857 (1995).

[152] Z. Yoshida and T. Tatsuno, in preparation.

[153] A. Yoshioka, T. Tatsuno, and M. Wakatani, J. Phys. Soc. Jpn. **67**, 3794 (1998).

[154] P. Zanca, *et al.*, Phys. Plasmas **8**, 516 (2001).

[155] H. Zushi *et al.*, TCM on Pellet Injection, IAEA (1993).

[156] H. Zushi, *et al.*, Proc. 16th IAEA Fusion Energy Conf. (Montreal, 1996) vol. 2, p. 143.